ANKARA YILDIRIM BEYAZIT UNIVERSITY

GRADUATE SCHOOL OF NATURAL AND APPLIED SCIENCES

SIMULATION-BASED PERFORMANCE AND COST OPTIMIZATION OF ALKALINE ELECTROLYSERS

M.Sc. Thesis by

Sami Şaban DEMİREZEN

Department of Mechanical Engineering

February, 2025

ANKARA

SIMULATION-BASED PERFORMANCE AND COST OPTIMIZATION OF ALKALINE ELECTROLYSERS

A Thesis Submitted to

The Graduate School of Natural and Applied Sciences of

Ankara Yıldırım Beyazıt University

In Partial Fulfillment of the Requirements for the Degree of Master of Science in Mechanical Engineering, Department of Mechanical Engineering

by

Sami Şaban DEMİREZEN

February, 2025

ANKARA

M.Sc. THESIS EXAMINATION RESULT FORM

We have read the thesis entitled **"SIMULATION-BASED PERFORMANCE AND COST OPTIMIZATION OF ALKALINE ELECTROLYSERS"** completed by **SAMİ ŞABAN DEMİREZEN** under the supervision of **PROF. DR. HASAN ÖZCAN** and we certify that in our opinion it is fully adequate, in scope and in quality, as a thesis for the degree of Master of Science.

Prof. Dr. Hasan ÖZCAN

Supervisor

Prof. Dr. Kamil ARSLAN

Jury Member

Prof. Dr. Selahattin ÇELİK

Jury Member

Prof. Dr. İlyas ÇANKAYA

Director

Graduate School of Natural and Applied Sciences

ETHICAL DECLARATION

I hereby declare that, in this thesis which has been prepared in accordance with the Thesis Writing Manual of Graduate School of Natural and Applied Sciences,

- All data, information and documents are obtained in the framework of academic and ethical rules,
- All information, documents and assessments are presented in accordance with scientific ethics and morals,
- All the materials that have been utilized are fully cited and referenced,
- No change has been made on the utilized materials,
- All the works presented are original,

and in any contrary case of above statements, I accept to renounce all my legal rights.

Date: 04.02.2025 **Signature:……..**

Name & Surname:…….

ACKNOWLEDGMENTS

I would like to express my deepest gratitude to my supervisor, Professor Hasan Özcan, for his invaluable guidance, support, and encouragement throughout this journey. His expertise, insightful feedback, and dedication have been instrumental in shaping this thesis and my academic growth. Professor Özcan's unwavering commitment to excellence and his genuine interest in my progress have been a source of inspiration. His ability to challenge me intellectually while fostering an environment of trust and collaboration has made this experience both rewarding and enriching.

I am also profoundly thankful for the unwavering love and support of my family. To my beloved wife, Gizem, your patience, understanding, and encouragement have been my greatest strength during this journey. Your belief in me has kept me motivated and focused through every challenge. To my wonderful son, Ahlas Batu, your joy and laughter have been a constant reminder of what truly matters, and you have been my light in even the most demanding moments.

To my parents and siblings, your unconditional love and endless support have been the foundation of everything I have achieved. Your sacrifices and belief in my potential have been a driving force in my life, and I cannot thank you enough for always being there for me.

2025, 04 February **Sami Şaban DEMİREZEN**

SIMULATION-BASED PERFORMANCE AND COST OPTIMIZATION OF ALKALINE ELECTROLYSERS

ABSTRACT

This study focuses on the optimization of alkaline water electrolyzers to develop a cost-effective and efficient approach for hydrogen production. A one-dimensional electrochemical modeling was performed using the COMSOL Multiphysics software to analyze the impact of varying model parameters on system performance. The current and voltage data obtained from COMSOL were integrated into the Engineering Equation Solver (EES) program for detailed cost analysis.

The modeling systematically investigated key operational parameters, including current density, voltage, electrolyte concentration, temperature, distance between electrode and separator, and porosity, to evaluate their effects on system performance and economic feasibility. The results demonstrated that low electricity costs and optimal current densities significantly reduced the Levelized Cost of Hydrogen (LCOH). Furthermore, larger systems were observed to achieve lower costs through economies of scale.

This study highlights the critical interactions between operational parameters and cost optimization, providing actionable insights for the development of alkaline electrolyzer technologies. The findings contribute to the advancement of more sustainable and cost-effective solutions for hydrogen production.

Keywords: Alkaline water electrolysis, hydrogen production, cost optimization, performance optimization, electrolyzer, COMSOL, LCOH, EES, LCOE.

COMSOL İLE ALKALİ ELEKTROLİZERLERİN PERFORMANS VE MALİYET OPTİMİZASYONU

ÖZ

Bu çalışma, hidrojen üretiminde maliyet etkin ve verimli bir yaklaşım geliştirmek amacıyla alkalin su elektrolizörlerinin optimizasyonuna odaklanmıştır. Çalışmada, COMSOL Multiphysics programı kullanılarak bir boyutlu elektrokimyasal modelleme gerçekleştirilmiş ve model parametrelerindeki değişikliklerin performans üzerindeki etkileri detaylı bir şekilde incelenmiştir. COMSOL ile elde edilen akım ve voltaj verileri, Engineering Equation Solver (EES) programına entegre edilerek detaylı bir maliyet analizi yapılmıştır.

Modelleme kapsamında, akım yoğunluğu, voltaj, elektrolit konsantrasyonu, sıcaklık, elektrotlar ve separator arası mesafe ve porozite gibi temel operasyonel parametreler, sistem performansı ve ekonomik fizibilite üzerindeki etkilerinin belirlenmesi amacıyla sistematik olarak incelenmiştir. Elde edilen sonuçlar, düşük elektrik maliyetlerinin ve optimum akım yoğunluklarının hidrojenin seviyelendirilmiş maliyetini (LCOH) önemli ölçüde azalttığını ortaya koymuştur. Ayrıca, daha büyük sistemlerin ölçek ekonomisi sayesinde maliyetleri düşürdüğü gözlemlenmiştir.

Bu çalışma, operasyonel parametreler ile maliyet optimizasyonu arasındaki kritik etkileşimleri vurgulayarak alkalin elektrolizör teknolojilerinin gelişimine yönelik uygulanabilir öneriler sunmaktadır. Elde edilen bulgular, hidrojen üretiminde daha sürdürülebilir ve maliyet etkin çözümler geliştirilmesi adına önemli bir katkı sağlamaktadır.

Anahtar Kelimeler: Alkali su elektrolizi, hidrojen üretimi, maliyet optimizasyonu, performans optimizasyonu, elektrolizör, COMSOL, LCOH, EES, LCOE

CONTENTS

NOMENCLATURE

Roman Letter Symbols

C	Molarity, mol/L
d	Distance, m
E	Potential, V
F	Faraday constant, C/mol
K,L	Coefficients for KOH and NaOH
M	Concentration, mol/L
M_w	Molar mass, g/mol
n,y,z	Parameter for overpotential
R	Universal gas constant, J/K/mol
r,t,s	Empirical coefficients for overpotential
S	Siemens
T	Absolute temperature, K or °C
U	Cell potential, V
Y_K,Y_N	Mass fraction of KOH and NaOH

Greek Letter Symbols

ϵ_s	Separator porosity
τ_s	Separator tortuosity
η	Efficiency, %
ρ	Density, kg/m3
σ	Conductivity, S/m
Ω	Electrical resistance unit, Ohm
Δ	change or difference

Subscripts

Ox	Oxidized
Red	Reduced

Acronyms

AEM	Anion Exchange Membrane
AWE	Alkaline Water Electrolysis
CapEx	Capital Expenditure
DC	Direct Current
HER	Hydrogen Evolution Reaction
HHV	Higher Heating Value
kW_el	Kilowatt Electrical
LCOE	Levelized Cost of Electricity
LCOH	Levelized Cost of Hydrogen
LHV	Lower Heating Value
OER	Oxygen Evolution Reaction
OpEx	Operating Expenditure
PEM	Proton Exchange Membrane
PV	Photovoltaic
RE	Renewable Energy
SMR	Steam Methane Reforming
SOE	Solid Oxide Electrolysis

LIST OF TABLES

LIST OF FIGURES

CHAPTER 1- INTRODUCTION

1.1. Introduction to and General Review of Hydrogen Production and Electrolysis

The global demand for primary energy is projected to increase at an average annual rate of 1.3% through 2040, primarily driven by the growing need for energy services due to sustained economic growth, population growth, and advancements in technology [1]. Despite efforts to diversify energy sources, fossil fuels such as oil, natural gas, and coal are expected to remain the dominant sources of energy supply until at least 2050 [2]. However, the continued reliance on fossil fuels for energy production and chemical processes contributes significantly to environmental challenges by releasing greenhouse gases—including carbon dioxide, nitrogen oxides, volatile organic compounds, and particulate matter—into the atmosphere, thereby accelerating global climate change [3].

The growing demand for energy, particularly for fuel, coupled with the finite availability of fossil resources such as petroleum and natural gas, emphasizes the urgent need for the development of clean and environmentally friendly alternatives [4]. In response, numerous studies have focused on hydrogen technology as a promising solution, recognizing its advantageous properties and potential to serve as a sustainable alternative to conventional fossil fuels [5]. Specifically, hydrogen exhibits the highest energy content per unit mass, with a higher heating value (HHV) of 3.54 kWh/Nm³ (39.42 kWh/kg), rendering it approximately 2.5 times more energetic than methane and nearly three times more than gasoline [6].

The two main categories most commonly used in hydrogen production are conventional methods and water electrolysis. Conventional hydrogen production techniques include steam methane reforming (SMR), oil/naphtha reforming and coal gasification [7]. These processes rely heavily on fossil fuels and contribute to greenhouse gas emissions, so similarly seriously affects ecosystem like other utilizations [8]. Currently, the majority of global hydrogen production fromfossil

fuels is achieved through steam methane reforming (SMR), a process that involves reacting natural gas or coal with steam under high temperatures and pressure [9].

An alternative method of hydrogen production is water electrolysis. In contrast, water electrolysis offers a cleaner alternative by splitting water into hydrogen and oxygen using electricity. The three most appealing and proven technologies of water electrolysis are solid oxide electrolysis (SOE), alkaline water electrolysis (AWE), and proton exchange membrane (PEM) electrolysis [10]. Another water electrolysis technology that is Anion exchange membrane electrolysis (AEM) has been recently introduced in the literature as a solution to overcome the limitations associated with both alkaline and PEM electrolyzers [11].

1.1.1 General Review of Water Electrolysis

Electrolysis is an electrochemical process in which electrical energy drives chemical reactions. In this process, an electric current passes through a solution, decomposing substances within the solution.[12].

Water electroylsis, also referred to as electrochemical water splitting, has been utilized since around 1800 [13]. In 1800, Alessandro Volta invented the voltaic pile, and just weeks afterward, William Nicholson and Anthony Carlisle employed it to perform the electrolytic splitting of water [14]. The development of Faraday's law in 1833 established a quantitative link between the amount of hydrogen produced and the electrical energy used, laying the scientific foundation for water electrolysis. In 1869, Zénobe Gramme invented a dynamo capable of generating continuous electricity, making water electrolysis a practical method for hydrogen production. Dmitry Lachinov advanced the field further in 1888 by developing a method for industrial-scale synthesis of hydrogen and oxygen through electrolysis. By 1902, over 400 industrial electrolyzers were operational. A significant boost in hydrogen demand during the early 20th century was driven by ammonia fertilizer production and the availability of inexpensive hydroelectricity. However, with the rise of hydrocarbon-based energy, coal gasification, and natural gas reforming, water electrolysis became less economically competitive due to the lower costs of these alternative methods for large-scale hydrogen production [15]. The years from the

1920s to the 1970s marked the "golden age" for advancements in water electrolysis technology, during which most of the conventional designs were established. Industrial demand for hydrogen and oxygen facilitated the application of foundational knowledge to the industrialization of water electrolysis technologies. In 1939, the first large-scale water electrolysis plant was commissioned, followed by the production of the first pressurized industrial electrolyzer in 1948. The commercial electrolysis systems developed during this period incorporated several technological components that remain foundational in current designs. From the 1970s onward, the introduction of advanced materials has further enhanced electrolyzer efficiency and durability [16].

Water electrolysis process involves the decomposition of water by applying direct current (DC) between two electrodes immersed in water. The electrodes are separated by a non-conductive aqueous or solid electrolyte, which facilitates ion transport and completes the electrical circuit [17]. When employed electricity (electro) which is emission-free technology, water molecules break down (-lysis) into their elemental components, resulting in dissolved oxygen and hydrogen [9]. In this study, alkaline water electrolysis will be studied.

Regardless of the electrolyte type and electrolysis method, the fundamental reaction of water electrolysis is represented by the following equation [9,18,19].

$$H_2O_{(l)} + Electricity + Heat \rightarrow H_{2(g)} + {}^{1}/_{2}\, O_{2(g)} \quad (1.1)$$

The energy requirements for this chemical reaction, along with a detailed discussion of the associated process, will be provided in subsequent sections.

Figure 1.1 summarizes the key characteristics and performance metrics of different types of water electrolyzers. Alkaline, PEM, SOM, and AEM electrolyzers are compared in terms of operating temperature, pressure, current density, the electrolytes used, and catalyst materials. While alkaline electrolyzers are the most commercially mature technology, they exhibit relatively low efficiency. In contrast, PEM and SOM electrolyzers offer higher efficiency but face limitations due to their cost and material requirements. Specific energy consumption, hydrogen purity, and

expected stack lifetime are critical metrics that play a significant role in determining their suitability for various applications [20].

Technology readiness level (TRL)	Mature/commercialised			R & D
Electrolysis technology	Alkaline electrolysis (AE)	Proton exchange membrane (PEM) electrolysis	Solid oxide membrane (SOM) electrolysis	Anion exchange membrane (AEM) electrolysis
Schematic diagram and operating principle	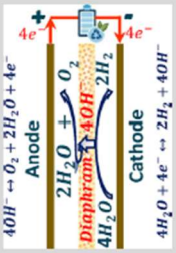	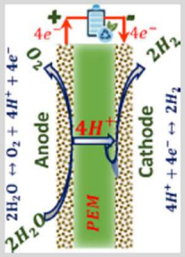	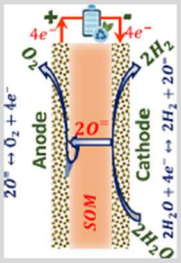	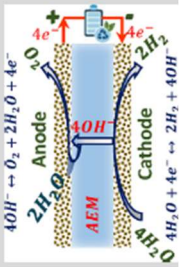
Operating temperature, °C	70–90	50–80	600–1000	40–60
Operating pressure, bar	~Atmospheric	<40	<5	<35
Nominal voltage, V	1.8–2.4	1.8–2.2	0.80–1.6	1.4–2.0
Nominal current density, A/cm^2	0.2–0.5	0.6–3.0	0.1–3.9	0.2–2.0
Type of Electrolyte/ membrane	KOH solution (25–30 wt.%)	Generic PEMs (PFSA)	Yttria-Stabilised zirconia (YSZ) or gadolinium-doped ceria (GDC)	Generic AEMs (DVB polymers)
Commercial separator	Zirfon™, polysulfone, and polyphenylene sulphide polymers	Nafion™	YSZ/GDC Pellets	Fumatech™
Common types of cathode/ anode electrocatalysts	Nickel-coated perforated stainless steel	Iridium/platinum	Nickel-YSZ/LSM (lanthanum strontium manganite)-YSZ	Nickel foam or carbon cloth
Cell nominal efficiency (HHV), %	50–80	50–83	80–100	52–67
Specific energy consumption, kWh/Nm^3	5.0–5.9	5.0–6.5	3.7–3.9	Unknown
Hydrogen purity, %	99.5–99.9998	99.9–99.9999	99.9	99.9–99.9999
Stack lifetime, h	<90,000	<20,000	<20,000	<5000
Stack cost, USD/kW)	270	400	>2000	Unknown

Figure 1.1 Key Characteristics and Performance Metrics of Water Electrolyzers

1.1.1 General Aspects of Hydrogen Production from Alkaline Water Electrolysis and Thermodynamic Modelling

Hydrogen, the most abundant element in the universe, is often seen as the energy carrier of the future, especially for storing renewable energy (RE) from intermittent sources like solar and wind [21]. Hydrogen can be used with fuel cell technology to produce energy with no carbon emission and minimal emission of other pollutants. It has the advantage of having the highest energy density among other fuels (120 MJ/kg) which is more than twice the energy density of other fossil fuels [22]. Among the various methods for producing green hydrogen, water electrolysis stands out as a

prominent option, particularly when the electrical input is derived from RE sources [23].

Among the various available options, alkaline electrolysis stands out as the most established and widely used water electrolysis technology in industrial applications. [24]. The major components of the electrolyzer include the cell frame, electrolyte, anode and cathode electrodes, and a separating diaphragm, which together facilitate the electrolysis process. Its durability, technological maturity, and the use of materials free from platinum-group metals make it a cost-effective choice for large-scale hydrogen production [25]. A typical alkaline electrolysis cell consists of two Ni-based electrodes in an aqueous KOH solution, separated by a porous separator, operating at 60-90°C and below 30 bar pressure [26].

The schematic of an alkaline electrolyzer is illustrated in Figure 1.2; while the chemical reactions as a semi reactions at a cathod and anode side for 25 ºC and 1 bar are given in Equations (1.2a and 1.2b). At the anode side, hydroxide ions are oxidized, producing oxygen and water while releasing electrons. Here, the anodic (oxygen evolution reaction) (OER) reactions occurs. Conversely, at the cathode side, water molecules are reduced by electrons to hydrogen and negatively charged hydroxide ions and cathodic (hydrogen evolution reaction) (HER) reactions takes place. In summary, the water-splitting reaction yields hydrogen and oxygen in a 2:1 molar ratio. [27].

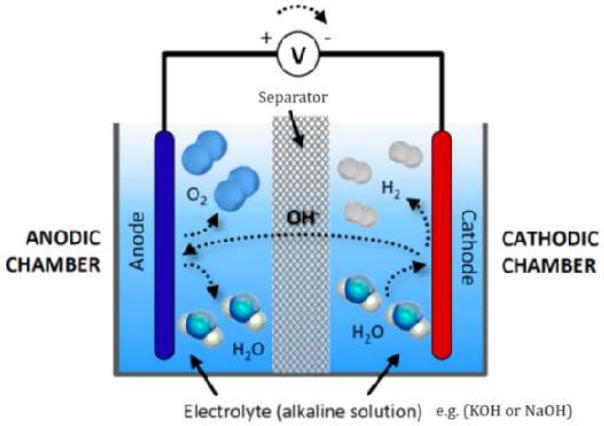

Figure 1.2 General scheme and principle of an alkaline electrolysis cell

$$Cathode\ side:\ 2\,H_2O_{(l)} + 2\,e^- \rightarrow H_{2(g)} + 2\,OH^-_{(aq)} \quad (1.2a)$$

$$Anode\ side:\ 2\,OH^-_{(aq)} \rightarrow {}^1/_2\,O_{2(g)} + H_2O_{(l)} + 2\,e^- \quad (1.2b)$$

Thus, net reaction in the electrolysis is;

$$H_2O_{\ (l)} \rightarrow H_{2(g)} + {}^1/_2\,O_{2(g)} \quad (1.3)$$

To perform electrolysis, it's essential to determine the amount of potential required. This potential has to at least overcome *equilibrium cell voltage* to occur the electrolysis. The equilibrium cell voltage, also known as reversible voltage (U^0_{rev}), is achieved when the electrochemical reactions at the electrodes exhibit reversibility, and no net current flows through the cell. It represents the potential difference between the anode and cathode at equilibrium conditions. This voltage, which reflects the balance between the two half-cell reactions, is mathematically expressed by Equation (1.4) [28].

$$E^0 = E_{OER} - E_{HER} \quad (1.4)$$

For OER in Eq (1.2a) required potential is E^0_{OER} =+0.401 V and for HER in Eq.(1.2b) required potential is E^0_{HER} = -0.829 V [29]. Overall required net reaction potential at standart conditions ($E^0 = U^0_{rev}$) is 1.229 V. This reversible voltage under different operating conditions can be calculated using the Nernst equation [30], which accounts for factors such as operating temperature, the partial pressures of the

reaction products (P_{O2}, P_{H2}), and the activity of water in the electrolyte, which is approximately close to unity in a first approximation, is expressed in Eq.(1.5),

$$U_{rev} = U^{o}_{rev} + \frac{R\times(T+273,15)}{z\times F} \times \ln(\frac{P_{O_2}^{1/2}\times P_{H_2}}{\propto_{H_2O}}) \quad (1.5)$$

where P_{O2} and P_{H2} are the partial pressure of the reaction products, α_{H2O} is the water activity and R is the absolute gas constant (8.314 J/K/mol).

In thermodynamic modeling, several assumptions can simplify the analysis: hydrogen and oxygen behave as ideal gases, water is treated as an incompressible fluid, and the gas and liquid phases remain distinct. Using these assumptions, the enthalpy (ΔH), entropy (ΔS), and Gibbs free energy (ΔG) changes associated with water splitting can be calculated. These values are referenced against the standard states of pure hydrogen (H_2), oxygen (O_2), and water (H_2O) at 25°C and 1 bar. The total enthalpy change for the reaction reflects the difference between the enthalpies of the products (H_2 and O_2) and the reactant (H_2O) [16]. For the change in Gibbs energy is described as below,

$$\Delta G = \Delta H - T \times \Delta S \quad (1.6)$$

In standard conditions, these parameters take the values of ΔH^0 =286 kJ/mol, and T x ΔS^0 = 48.7 kJ/mol [31]. The standard Gibbs energy for water splitting is ΔG^0=237 kJ/mol.

Under standard conditions , water splitting is a non-spontaneous reaction, indicated by a positive Gibbs free energy change (ΔG). In electrochemical systems operating at constant temperature and pressure, the maximum theoretical work (reversible work) corresponds directly to the Gibbs free energy change. According to Faraday's law, the electrical energy required to drive water electrolysis is proportional to the molar conversion of chemical species. For a reversible electrochemical process, the reversible cell voltage is described by Eq.(1.7) [32],

$$U_{rev} = \frac{\Delta G}{z\times F} \quad (1.7)$$

Here, z is the number of electrons transferred in water electrolysis ($2e^-$), and F is the Faraday constant (96,500 C/mol).

The total energy required for water electrolysis corresponds to the change in enthalpy (ΔH). According to Eq. (1.6), the Gibbs free energy change (ΔG) incorporates the thermal irreversibility term (TxΔS), which in a reversible process matches the heat requirement. For water splitting, the standard enthalpy change is ΔH^0=286 kJ/mol [19]. The total energy requirement (ΔH) is linked to the thermoneutral cell voltage (U_{tn}) through the given equation (1.8),

$$U_{tn} = \frac{\Delta H}{z \times F} \tag{1.8}$$

Although the thermoneutral cell voltage (U_{tn}) varies with temperature and pressure, it is measured as 1.48 V under standard conditions.

In addition to the general overview of hydrogen production through alkaline water electrolysis provided in this section, detailed calculations, electrochemical modelling and further technical information will be addressed in the subsequent sections.

1.2 Literature Review on performance improvement efforts in Alkaline Water Electrolysis

Alkaline water electrolysis is regarded as the principal method for facilitating water-splitting reactions because it is a mature and economic technology. The development of this technology was notably accelerated by military applications involving hydrogen isotopes. Norway established the earliest plants focused on the electrolysis of heavy water and the production of deuterium. Currently, several companies are producing alkaline electrolyzers to generate hydrogen of electrolytic grade, supporting a wide range of industrial applications fueled by the increasing demand for hydrogen. Key sectors utilizing hydrogen include power generation, semiconductor manufacturing, flat panel display production, heat treatment plants, and analytical laboratories. Additionally, hydrogen is being investigated as a potential replacement for helium in gas analyzers and as a fuel source for flame

detectors, with further applications extending to glass manufacturing, food processing, meteorology, and welding industries [33].

Large-scale atmospheric alkaline water electrolyzers (AWEs) have been in use since the early 20th century, while designs specifically optimized for pressurized operation only became widespread during the latter half of the century [34].

Since the late 20th century, numerous studies have been conducted on alkaline water electrolysis. In these studies, photovoltaic and wind energy systems are the most compatible sources for integration with hydrogen generators, offering a range of configurations and applications that make them highly suitable for coupling with electrolysis-based hydrogen production systems [6].

Hug et al. in 1993 examined the performance of alkaline water electrolyzers under intermittent operating conditions, developing a simulation model called SIMELINT for this purpose. The study analyzed parameters such as thermal behavior, cell voltage, gas purity, and current efficiency, with the model's accuracy tested against actual operational data [35].

Hug et al. in 1993 also developed a mathematical model based on experimental data obtained from the PHOEBUS facility to examine the performance of alkaline water electrolyzers under intermittent operation. The study analyzed parameters such as heat transfer, cell voltage, and gas purity of an electrolyzer operating at 80°C and 7 bar pressure. The model, validated with data from the 10 kW-capacity HYSOLAR facility, revealed the relationship between efficiency and Faraday efficiency. This study provides an important reference for optimizing the performance of electrolyzers integrated with renewable energy sources [36].

In 1997, Ulleberg and Mørner conducted a study using the TRNSYS simulation model to investigate different system configurations for energy-independent structures. The study focused on the performance of alkaline electrolyzers, hydrogen production, and energy storage. The objective was to optimize system components to enhance the efficiency of solar-hydrogen integration, particularly at high latitudes [37].

In 2003, Ulleberg et al. conducted a comprehensive study to model the performance of advanced alkaline electrolyzers. Thermodynamic, heat transfer theory, and empirical relationships were combined to model the electrochemical and thermal dynamics. Ulleberg et al. focused on optimizing control strategies for hydrogen production systems integrated with renewable energy sources like PV and wind energy. During model validation, experimental data from the HYSOLAR project and the PHOEBUS facility in Jülich, Germany, were used. These projects served as a basis for testing how accurately the model could predict parameters such as cell voltage, hydrogen production, and efficiency under real conditions. The model was developed to integrate with simulation software like TRNSYS, allowing dynamic system analyses and optimization studies [19]. This model has garnered significant attention and is widely used for dynamic simulations of renewable energy-hydrogen (RE-H2) systems due to its precision and adaptability to various types of electrolyzers.

In 2005, Kothari et al. examined the effect of electrolyte temperature on the rate of hydrogen production in alkaline water electrolysis, analyzing the role of temperature on hydrogen efficiency. Experiments were conducted with electrolyte temperatures ranging from 10°C to 80°C, using carbon electrodes and a 12V DC power supply. Findings showed that the hydrogen production rate increased with temperature, but efficiency remained nearly constant after 50°C; efficiency rose from 6.67% to 14.91%, but no additional efficiency gains were observed beyond this temperature. The study suggests that maintaining the electrolyte temperature at an optimum level, approximately 50°C, can enhance efficiency [38].

Roy et al. in 2006 developed a detailed thermodynamic model using MATLAB-Simulink to compare the energy efficiency of atmospheric and high-pressure alkaline water electrolyzers. The study indicated that high-pressure electrolyzers aim to increase efficiency without the need for a mechanical compressor; however, it was observed that electrolysis voltage and heat losses increase with pressure. The results show that atmospheric electrolyzers consume less energy at all pressure levels, and a high-pressure electrolyzer operating at 700 atm consumes 16% more energy compared to an atmospheric system. Therefore, atmospheric electrolyzers are

suggested to be more efficient and economical, especially for integration with intermittent renewable energy sources [39].

Gandía et al. in 2007 investigated the performance of a commercial alkaline water electrolyzer powered by renewable energy sources. In the study, a 5 kW HySTAT electrolyzer was used, and the efficiency, cell temperature, and purity of produced gases were analyzed under dynamic conditions with a power emulator simulating wind conditions. A power profile from real wind data was applied to the electrolyzer, and the temporal changes in parameters such as cell voltage, temperature, and gas purity were monitored. The electrolyzer demonstrated an ohmic behavior by responding quickly to variable currents, maintaining efficiency between 74-83% even under fluctuating power conditions. The purity of the produced hydrogen remained above 99.8%, and the system operated safely even at low current conditions. This study provides significant insights into optimizing the dynamic performance of wind-powered electrolyzers and suggests a reliable solution for hydrogen production compatible with renewable energy systems [40].

In 2008, Dieguez et al. conducted experimental studies and mathematical modeling to investigate the thermal performance of a commercial alkaline water electrolyzer. Modeling conducted using ANSYS software analyzed temperature changes under different current conditions and developed strategies to minimize heat losses. Experimental data, monitored with IR cameras and thermocouples, showed that heat losses could be reduced by 50-67% with converters providing a stable DC current. This study makes a substantial contribution to optimizing electrolyzer performance in systems integrated with renewable energy [41].

In a 2011 study by Artuso et al., the performance of a 36 kW capacity alkaline electrolyzer was analyzed in relation to temperature and pressure. In tests beginning at maximum power, increases in current and hydrogen production were observed as the temperature rose, and pressure levels directly influenced the system's efficiency. Hydrogen production was optimized by maintaining stable temperature and pressure at balanced power levels. A discrepancy of 2% in voltage and 0.89% in hydrogen production between model predictions and actual data supported the model's validity. The study demonstrated that temperature and pressure management are critical for

electrolyzer performance and that insulation and thermal management can enhance energy efficiency [42].

Ursúa and Sanchis (2012) developed a comprehensive model to analyze the static and dynamic electrical behavior of a commercial advanced alkaline water electrolyzer. The study detailed the fundamental physical phenomena, including thermodynamic, activation, double-layer, and ohmic effects, occurring in the electrolysis process, and the model was validated using MATLAB-Simulink. Experimental results confirmed values for cell-specific resistance and double-layer capacitance under static operating conditions and showed the model's accuracy in predicting behavior under various current profiles [43].

In a 2012 study, Hammoudi et al. investigated how the performance of alkaline electrolyzers is affected by changes in operating conditions. Parameters such as temperature, pressure, electrolyte concentration, and current density were evaluated for their impact on energy efficiency and hydrogen production rate. The study found that increasing temperature improved efficiency; for instance, Faraday efficiency rose from approximately 59% at 25°C to 63% at 70°C, while thermal efficiency increased from 71% to 83% at the same temperature. High-pressure conditions were observed to improve hydrogen storage efficiency but reduce thermal efficiency; thermal efficiency decreased from 83% at 1 atm to 75% at 30 atm. Additionally, the study concluded that the optimal KOH concentration range is between 30-50%, with ohmic losses of up to 30% occurring outside this range [44].

Marini et al. in 2012 analyzed the performance of alkaline water electrolyzers powered by renewable energy sources to assess their potential in sustainable hydrogen production. In the study, an electrolyzer with a capacity of 1 Nm^3/h was tested under current, temperature, and pressure conditions ranging from 40-120 A, 35-65°C, and 5-25 bar, respectively. Experiments were conducted in standalone scenarios with wind and PV energy emulations. The electrolyzer demonstrated energy efficiency between 77% and 78.6% in PV and wind energy emulations [45].

Mori et al. in 2013 analyzed the efficiency of a commercial alkaline water electrolyzer, examining the effects of parameters such as electrolyte temperature,

current density, and operating pressure on cell efficiency through an empirical model. The study found that electrolyzer efficiency ranged between 73% and 83%, while energy efficiency was between 50% and 60%. The empirical model was developed based on the current-voltage relationship and was used to analyze voltage characteristics as a function of current density. Additionally, it was determined that hydrogen losses in the system ranged from 10% to 25%, with these losses increasing as pressure increased [46].

Manabe et al. in 2013 investigated the development of new cell technologies to improve the efficiency of alkaline water electrolysis. Aiming to develop cost-effective and durable electrolysis systems for large-scale hydrogen production, this study focused on enhancing efficiency using a zero-gap cell system. It was found that the zero-gap system offered advantages by reducing cell voltage; however, challenges such as anode degradation and membrane lifespan were observed. The study examined the effects of various separator materials, considering factors like porosity, thickness, and material type, on cell voltage and gas crossover. It was observed that cell voltage ranged from 1.7 V to 2.2 V, depending on the chosen separator material. By selecting an optimal separator, both cell voltage was reduced, and system efficiency improved. The study analyzed parameters such as temperature, current density, and electrode composition to provide solutions for enhancing the applicability of electrolyzers in hydrogen production [47].

The zero-gap design is an innovative approach that minimizes the distance between electrodes and the separator, thereby reducing ohmic losses. This design accelerates ion transport, lowers energy consumption, and enhances cell efficiency. Widely applied in alkaline electrolyzers, zero-gap technology offers both economic and performance advantages.

Figure 1.3 compares the voltage-current density relationship between an alkaline electrolyzer with a zero-gap design and a conventional alkaline electrolyzer. It is evident that the zero-gap design achieves lower cell voltages at all current density levels. These results highlight the effectiveness of zero-gap technology in improving energy efficiency and reducing hydrogen production costs.

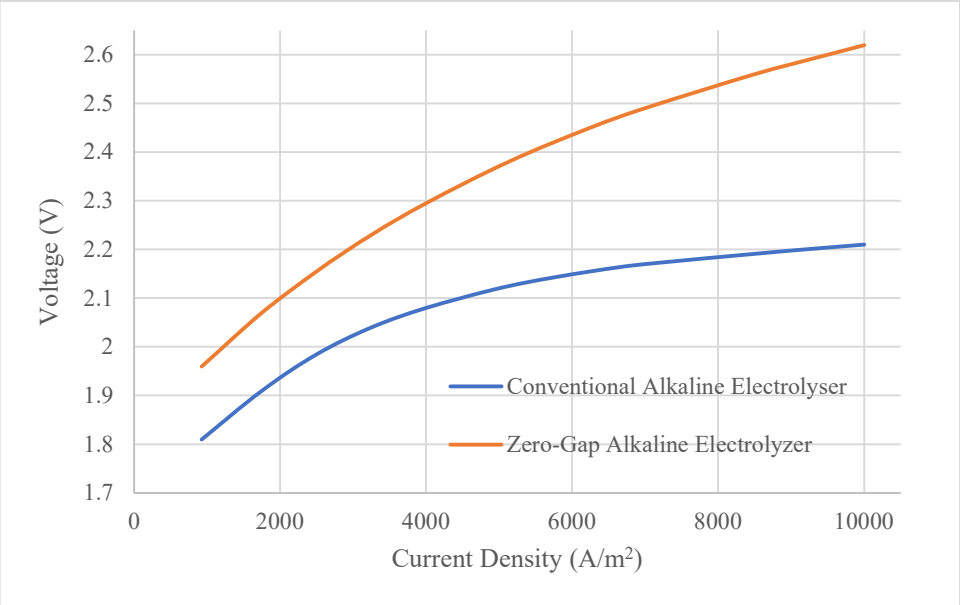

Figure 1.3 Comparison of I-U Curve for Conventional and Zero-Gap Alkaline Electrolyzers

Table 1.3 compares the key features of conventional alkaline electrolyzers and zero-gap alkaline electrolyzers. The zero-gap design offers significant advantages, including higher efficiency (65–80%) and a wider current density range (5000–20,000 A/m²) compared to conventional designs. Additionally, zero-gap systems operate within a lower voltage range (1.45–2.0 V), leading to reduced energy consumption. In terms of gas purity, zero-gap technology demonstrates superior performance, making it suitable for modern, high-efficiency projects. On the other hand, conventional systems, with their simple design and moderate efficiency, are typically utilized in legacy or less demanding applications [10,48].

Table 1.1 Comparison of Key Features Between Conventional and Zero-Gap Alkaline Electrolyzers

Feature	Conventional Alkaline	Zero-Gap Alkaline
Design Complexity	Simple	Advanced
Efficiency	Moderate (~ 50-60%)	High (~ 65-80%)
Voltage Range	1.8-2.4 V	1.45-2.0 V
Current Density (A/m^2)	2,000-5,000	5,000-20,000
Gas Purity	Moderate	High
Applications	Legacy Systems	Modern high-efficiency projects
Advantages	Low cost, simple design	Higher efficiency, compatible with renewable energy
Disadvantages	Higher energy consumption, limited efficiency	More complex design, higher initial investment cost

Douglas et al. in 2013 examined the use of alkaline water electrolyzers operated at ambient temperature when integrated with renewable energy sources. The study found that electrolyzers operating at ambient temperature reduce operational costs by minimizing the need for auxiliary equipment, offering a broader operating range and faster response times compared to systems operating at conventional temperatures. Experimental results indicated that voltage efficiency in ambient-temperature-operated electrolyzers increased by up to 12%, while electrode corrosion rates were approximately 6.3 times lower. The researchers recommended operating electrolyzers at ambient, low temperatures and using electrocatalysts that reduce corrosion rates to enhance energy efficiency and extend the lifespan of the electrolyzers [49].

In a 2014 study by Amores et al., the effects of parameters such as temperature, electrolyte concentration, and electrode/diaphragm distance were numerically analyzed in an alkaline electrolyzer model developed to enhance eco-friendly hydrogen production. The study is based on the model previously proposed by Ulleberg, which only considers temperature; however, Amores et al. expanded this

model by incorporating the effects of electrode distance and electrolyte concentration. According to the simulation results, as the temperature increases from 20°C to 80°C, the required voltage at a given current density decreases due to improved reaction kinetics and a reduction in reversible voltage. For electrolyte concentration, optimal conductivity of the KOH solution was observed in the range of 34-38%; outside this range, energy requirements increased. Maintaining the electrode/diaphragm distance around 0.4 mm resulted in the lowest voltage at a current density of 350 mA/cm² and a gas rise rate of 4-6 cm/s, while this distance could be extended to 1 mm at lower flow rates [50].

Tijani et al. in 2014 evaluated the hydrogen production efficiency of an advanced alkaline water electrolyzer through mathematical modeling and simulation. Using MATLAB, the model developed by Tijani et al. analyzed relationships involving overpotential due to activation energy, ohmic losses, and cell voltage for electrochemical reactions. In the study, cell voltage was found to be 2.395 V at 40°C and 2.359 V at 80°C, while at a current density of 300 mA/cm², the activation overpotential was 1.12 V, and ohmic losses were 0.022 V. The activation overpotential was found to be 80% higher than the ohmic losses, and cell voltage decreased at higher temperatures. Faraday efficiency rapidly increased from 70% to 96% at low current densities. The results highlight the need to optimize temperature and current density to improve energy efficiency, providing strategies for integration with renewable energy systems [51].

In a 2016 study by Zouhri and Lee, the effects of ohmic polarization on exergy efficiency in alkaline water electrolysis were analyzed, focusing on optimizing key parameters to improve efficiency. Factors such as electrode material resistance, distance between electrodes, electrolyte concentration, and temperature were identified as primary factors affecting efficiency, along with the coverage of electrode surfaces by hydrogen and oxygen bubbles, which also reduce efficiency. For example, increasing anode resistance from 0.0002 Ω m to 0.001 Ω m decreases exergy efficiency by 0.06%. Additionally, increasing the distance between electrodes from 0.05 m to 0.1 m reduces exergy efficiency from 0.6855 to 0.6846. An electrolyte molarity of 8 mol/L maximizes ionic conductivity at 2.5 S/cm, enhancing

efficiency. Raising the temperature from 298 K to 360 K further increases ionic conductivity from 0.7 S/cm to 2.5 S/cm, thereby improving efficiency. This study aims to reduce energy losses and enhance hydrogen production efficiency in water electrolysis through such numerical optimizations [52].

Chen et al. in 2017 conducted experimental and analytical modeling to analyze the performance of a commercial alkaline water electrolyzer under different current densities and electrode distances. Using electrode distances of 1 cm and 2 cm in a 0.4 M KOH solution, thermal, kinetic, ohmic, and mass transfer-related voltage losses were evaluated. According to experimental results, when the electrode distance increased from 1 cm to 2 cm, cell voltage and ion transfer resistance also increased. Analytical modeling, using the Butler-Volmer equation, examined the effect of hydrogen and oxygen bubbles on the surface, showing that bubble coverage stabilized when current density exceeded 0.1 A/cm^2. Results indicate that OH^- ion conductivity increased up to 95.8%, suggesting that optimizing electrode distance and current density is essential to enhance electrolyzer efficiency [53].

In a 2018 study by Sanchez et al., a semi-empirical mathematical model was developed to evaluate the performance of a 15 kW capacity alkaline water electrolyzer. The study examined the effects of parameters such as temperature, pressure, and current density on the thermodynamic and electrochemical processes of electrolysis, with key performance indicators like efficiency and Faraday efficiency considered during the modeling process. Electrochemical performance was analyzed through the current-voltage curve, and the model, based on Ulleberg's 2003 model, was extended to include the effects of temperature and pressure. For modeling Faraday efficiency, two different models—one with four parameters and the other with five—were employed, both showing that high temperatures reduce efficiency. The results indicate that while increased temperature lowers cell voltage and reduces the energy required for electrolysis, the efficiency is negatively impacted by parasitic currents that arise at higher temperatures. Pressure was found to have a more limited effect on cell voltage, with increases within a certain range causing only a slight rise in total voltage. This study presents a detailed model aimed at optimizing alkaline

electrolyzer performance and comprehensively addresses the impact of different operating conditions on the system [25].

In a December 2019 study by Sánchez et al., an alkaline water electrolysis system model was developed using Aspen Plus for hydrogen production. The system was operated within a temperature range of 50-80°C and pressure range of 5-9 bar. Raising the temperature from 50°C to 80°C lowered cell voltage, reducing the required power, although higher temperatures also reduced hydrogen purity. Increasing pressure caused gas bubbles to shrink, reducing ohmic resistance; however, high pressure could negatively affect hydrogen and oxygen purity. Under operating conditions of 75°C and 7 bar, with a current density of 0.42 A/cm², 10 kW of power consumption resulted in hydrogen production of 1.95 Nm³/hour (approximately 0.17 kg/hour), with cell efficiency calculated at 58% and system efficiency at 53.3%. Optimizing temperature and pressure to enhance efficiency showed that the optimal condition was achieved at 80°C and 5 bar pressure, with a current density of 0.25 A/cm², yielding approximately 58% efficiency [26].

In a 2020 study by Rodríguez and Amores, numerical data was presented to optimize the performance of an alkaline water electrolysis cell. Experiments varied the temperature from 30°C to 70°C and the electrolyte concentration from 22% to 42% KOH, with 32% KOH concentration at 50°C providing optimal performance with a conductivity of 94.54 S/m. Current densities ranging from 50 to 400 mA/cm² were applied in the cell, and the error rate in polarization curves remained below 0.51%, indicating strong alignment of the model with experimental data. At low current densities, voltage remained low, but efficiency decreased during the activation phase due to limitations. The gas production and distribution profile varied with current density, with gas bubbles accumulating along the electrode surface, creating a gas volume ratio between 1% and 4%. Additionally, the effects of varying the distance between the electrode and separator from 1.5 mm to 10 mm were investigated. Reducing the separator distance lowered ohmic losses and improved cell performance, though it was noted that very narrow cell configurations could increase the gas phase ratio, potentially raising ohmic losses. These findings support the

model's applicability for enhancing efficiency in electrolysis cell operating conditions [29].

In a 2022 study by Gambou et al., the focus was on modeling and optimizing the performance of alkaline electrolyzers, emphasizing their potential as a sustainable alternative to fossil fuel-based hydrogen production when integrated with renewable energy sources. The study examined how parameters such as electrolyte conductivity, operating temperature, and electrolyte concentration affect the performance of alkaline electrolyzers, which offer advantages like low cost, long lifespan, and high-purity gas production. A potassium hydroxide (KOH) solution in the 25-30% range was found to enhance efficiency by providing high specific conductivity within a 50-80°C temperature range, highlighting the high hydrogen production capacity of alkaline electrolyzers. The study concludes that optimizing alkaline electrolyzer modeling is crucial for effective integration with renewable energy sources [11].

In 2023, S. Niroula et al. conducted parametric modeling and analysis to optimize the performance of alkaline water electrolyzers. The study examined the effects of temperature, pressure, and KOH concentration on electrolyzer performance and developed a mathematical model of the voltage-current density curve using MATLAB/SIMULINK. Findings indicate that increasing temperature reduces cell voltage and enhances electrolysis efficiency; higher temperatures improved electrode performance, reduced membrane resistance, and decreased bubble formation, thereby increasing current density. Furthermore, low-pressure conditions positively impacted efficiency by reducing cell voltage, and a 30% KOH solution was identified as optimal for conductivity, minimizing ohmic resistance losses. In addition to these parameters, the study allowed analysis of the effects of other factors such as electrode thickness and porosity on performance [22].

After reviewing modeling studies on alkaline water electrolyzers, examining the thermoeconomic performance as another key criterion offers a comprehensive assessment of alkaline water electrolyzers in terms of both energy efficiency and cost-effectiveness. In this context, it is crucial to review the literature on thermoeconomic analyses to provide a thorough understanding.

In the study conducted by Ursúa et al. in 2012, it was noted that the cost of hydrogen production in alkaline water electrolysis varies between 3 and 15 Euros per kilogram, depending on electricity consumption, with an average energy consumption of around 4-7 kWh/Nm^3. It was emphasized that developing electrolyzers with low energy intensity is critical to reducing production costs. Additionally, investment costs were reported to range between 1000 and 5000 USD/kW depending on capacity, with additional costs incurred during installation for auxiliary equipment such as cooling, purification, and compression. Large systems generally require water cooling, whereas smaller systems are typically equipped with air cooling. The study also highlighted that the average durability of alkaline electrolyzers, reaching up to 15 years, reduces maintenance and spare parts requirements, thereby lowering lifetime costs. In this regard, it was concluded that electrode designs capable of operating at high current densities and thermal recovery techniques are essential for optimizing both installation and operational costs [6].

Douglas et al. in 2013 analyzed the techno-economic advantages of ambient temperature alkaline electrolysers. The study highlights how, compared to traditional high-temperature electrolysers, lower operating temperatures reduce both electricity consumption and corrosion, achieving cost-effectiveness. Specifically, the cost of hydrogen production at ambient temperature drops from $13.61 to $11.13 per kilogram, while electrode corrosion rates decrease by a factor of 2 to 6 [49].

In the 2018 study by Kuckshinrichs and Koj, hydrogen production costs in alkaline water electrolysis were analyzed from both private and social perspectives. For a 6 MW capacity facility, investment costs were reported as €1020/kW in Germany, €1010/kW in Austria, and €990/kW in Spain. Electricity consumption was calculated to be 53.9 kWh per kilogram of hydrogen produced. In Germany, the levelized cost from a private perspective (pLCH) was approximately €3.64/kg of hydrogen, which increased to €4.39/kg (pLCHe) when environmental costs were included. From a social perspective, the cost (sLCH) was calculated to be €6.24/kg in Germany, €6.34/kg in Austria, and €6.73/kg in Spain. These figures illustrate the cost structure of alkaline water electrolysis and the impact of environmental costs across different countries in detail [54].

In their 2019 study on the economic analysis of alkaline electrolysis technology, El-Emam and Özcan highlighted that this technology has lower installation costs compared to other types of electrolysis and stands out as a cost-effective solution for industrial hydrogen production. Average investment costs range from 600 to 1200 USD/kW, while hydrogen production costs vary between 4.5 and 6 USD/kg depending on the energy source used. This makes alkaline electrolyzers suitable for medium-scale hydrogen production projects. Additionally, due to their long lifespan (approximately 20-30 years) and robust structure, alkaline electrolyzers offer low maintenance costs, providing a thermoeconomic advantage. Over the long term, this durability positively impacts the payback period of the initial investment, enhancing its economic appeal [10].

In the 2019 study by Lee et al., various economic parameters, such as unit electricity price, learning rate, and automation level, were evaluated through scenario analyses to enhance the cost-effectiveness of hydrogen production via alkaline water electrolysis. In the baseline scenario, characterized by high electricity costs, no learning effect, and low automation, hydrogen costs were significantly high (8.41 USD/kg). When medium electricity costs and an 18% learning rate were considered, though maintaining a low automation level, costs decreased to 4.07 USD/kg, but still did not meet the target cost level. Scenarios involving zero-cost electricity from renewable sources, medium or high automation levels, and an 18% learning rate (Scenarios 5 and 6) notably reduced costs, with the best-case scenario yielding a hydrogen cost of 0.29 USD/kg. Ultimately, the combination of low electricity costs, learning effects, and high automation levels demonstrated that the hydrogen cost produced through alkaline water electrolysis could fall below the U.S. Department of Energy's 2030 target of 1.25 USD/kg [55].

In a 2022 analysis by Reksten et al., it was found that the capital expenditure (CapEx) for Alkaline Water Electrolyzers could stabilize between $320 and $400/kW by 2030 for large-scale facilities (100 MW and above). As facility size increases, a significant reduction in costs is achieved; however, higher unit costs are observed in smaller facilities (1-2 MW) due to the fixed costs of auxiliary equipment. The learning rate for AWE technology is estimated at approximately 25%, meaning a

25% cost reduction is expected each time capacity doubles. This trend provides substantial cost advantages, particularly for large-scale projects, further promoting AWE as a more sustainable option [56].

In their 2023 study, Zun and McLellan projected that, due to economies of scale and the technology learning effect, alkaline electrolyzer costs could decrease by up to 77%, with investment costs estimated to range between 397 and 940 USD/kW by 2030. The learning rate for this technology was noted as 18.8%, with a scale factor that provides a marked advantage for capacities below 0.5 MW but gradually decreases to 0.69% as capacity increases. Projections suggest that the size of alkaline electrolyzer systems could grow annually by 6%, reaching approximately 70 MW by 2050, while installed capacity, boosted by technological learning, is anticipated to expand by 10% to reach 7 GW_el. In terms of current density, values for alkaline electrolyzers vary within a range of 0.2–0.6 A/cm² [57].

In a separate 2023 study by Sadiq et al., numerical data on AWE systems clearly highlighted the cost and performance advantages of this technology. Capital expenditures (CapEx) for AWE electrolyzers vary between 500 and 1331 USD/kW_el, depending on the components involved. These costs include subcategories such as electrolyzer structure and mechanical and electrical balance-of-system elements. Operating expenses (OpEx) are estimated at 2% of annual CapEx and cover logistics, labor, and maintenance costs. AWE systems are economically favorable due to their high efficiency (around 80%) and low energy consumption (4.1 kWh/Nm³). In terms of the levelized cost of hydrogen (LCOH), costs range from 2.09 to 2.66 USD/kg, depending on the facility's location and configuration, with costs as low as 2.09 USD/kg observed in setups using bi-face modules. For the electrolysis process, a 20-30% concentration KOH solution is used, resulting in a cost of approximately 2.8119 USD/kg of hydrogen. These data form a solid foundation for the cost and performance analysis of AWE technology, underscoring its economic advantages [58].

Alkaline water electrolyzers are widely utilized in hydrogen production and are recognized as a cost-effective technology. Globally, several manufacturers have developed systems offering high efficiencies (ranging between 60–80%, HHV) and

large-scale production capacities (90 kg/h and above). For instance, McPhy reports that its 16 MW system produces 288 kg/h of hydrogen [59]. Similarly, Sunfire states that its system produces 200 kg of hydrogen per hour with 64% efficiency (LHV) and has the capability to install systems exceeding 100 MW [60]. Another manufacturer, Hygreen Energy, offers systems up to 15 MW, with its model producing 90 kg/h of hydrogen at 82% efficiency and another model producing 180 kg/h at 80% efficiency [61]. Thyssenkrupp has announced that its 20 MW system is capable of producing 360 kg/h of hydrogen [62]. These data underscore the critical role of alkaline electrolyzers in industrial hydrogen production, demonstrating their scalability and energy efficiency in meeting the demands of large-scale applications.

1.3 Motivation and Objectives

The primary motivation behind this thesis work is to efficiently provide an easy method to integrate simulation based performance assessment to economics of hydrogen production focusing on alkaline water electrolysis technology.

Single to multi-dimensional simulations are more available with accurate estimations on cell and stack performances bringing ease of analysis of complex electrochemical systems, making it possible for researchers to make error free modeling work by taking into account complex details such as material characteristics.

The aims of the thesis can be listed as follows:

- Conduct one dimensional simulation to investigate effects of such as current density, electrode porosity, membrane tortuosity, material thickness and type, electrolyte molarity etc. on cell performance via I-U curves.

- Optimize cell conditions, geometry and material choice for increased efficiency

- Perform cost optimization by analyzing key economic parameters such as capital expenditure (CapEx), operational expenditure (OpEx), and levelized cost of hydrogen (LCOH).

- Investigate optimal size and conditions for cost-effective operation at scale.

- Use existing quotes on AWE technology to provide correlations for module and system factors at scale.

Overall, this thesis provides an integrated approach from basic modeling work to economic aspects of alkaline water electrolysis cells, stacks and systems and provides an insight into true cost of hydrogen production. The simplistic approach here opens a door to retrieve hydrogen costs from systems based on simplified correlations taking into account basic cell variables.

CHAPTER 2- MODELLING

2.1. Electrochemical Modelling

Electrochemical modeling serves as a crucial tool in understanding the reaction mechanisms, kinetics, and mass transport phenomena within alkaline water electrolysis systems. By simulating parameters such as current density, electrode potentials, and overpotentials, electrochemical models allow for the precise evaluation of cell performance and the identification of factors that can enhance efficiency and reduce energy consumption. Analyzing the behavior of electrodes under various operational conditions is fundamental to advancing the understanding of electrolyzer cell performance and efficiency.

The electrode kinetics of an electrolyzer cell can be modeled using empirical current–voltage (I–U) relationships. In practice, the cell voltage is always higher than the reversible voltage due to inherent irreversibilities in the system. Therefore, the cell voltage can be expressed as the sum of the reversible voltage and various overpotentials in Eq (2.1) which will be detailed furthermore. The basic form of the I–U curve used in this study is, for a given temperature from Ulleberg in Eq (2.2) [21],

$$U_{cell} = U_{rev} + \sum U_{op} \tag{2.1}$$

$$U_{cell} = U_{rev} + \frac{r}{A} * i + s \log(\frac{t}{A} * i + 1) \tag{2.2}$$

Overpotentials (U_{op}) can be described as ohmic overpotentials, activation overpotentials and concentration overpotentials.

$$U_{op} = U_{ohm} + U_{act} + U_{conc} \tag{2.3}$$

- Ohmic overpotentials stem from the sum of electrical resistance from various components, such as electrodes, current collectors, and bipolar plates, as well as transport resistance associated with gas bubbles, ionic transfer in the electrolyte, pressure and the resistivity of the membrane/separator [28].

- Activation overpotentials is required energy to overcome activation energies of hydrogen and oxygen formation reactions on the cathode and anode surfaces [50]. This can be estimated using the Butler-Volmer equation, which provides a fairly accurate prediction of electrochemical reaction kinetics[50].

- Concentration overpotentials arises from mass-transport limitations at the electrode surfaces, particularly at high current densities, due to changes in the surface concentrations of reactants and products. It can be defined as the additional activation energy required to facilitate mass transfer at a rate sufficient to sustain the current [29].

For ohmic potentials, the following equation can be written as

$$U_{ohm} = r * i \tag{2.4}$$

Activation potentials can be calculated in below,

$$U_{act} = s * \log(t * i + 1) \tag{2.5}$$

The influence of these overpotentials (U_{ohm} and U_{act}) is accounted for by presenting the coefficients "r" ($\Omega \cdot m^2$), "t" ($m^2 \cdot A^{-1}$), and "s" (V). The coefficients "t" and "s" are associated with activation overpotentials and the parameter "r" relates to ohmic overpotentials.

To model the polarization curve of an electrolyzer precisely it is essential to consider three key aspects: thermodynamics, described by the Nernst equation; kinetics, captured by the Butler-Volmer equation; and resistive effects, which are analyzed using Ohm's Law [63].

When simplified Eq (2.2), it provides a basic form of the polarization curve for a described operation temperature,

$$U_{cell} = U_{rev} + r * i + s * \log(t * i + 1) \tag{2.6}$$

To simulate the temperature (T) dependence of overvoltages, Ulleberg [21] proposed a modification to the Eq. (2.6), incorporating the influence of temperature on the parameters "r" and "t":

$$r = r_1 + r_2 * T \tag{2.7}$$

$$t = t_1 + \frac{t_2}{T} + \frac{t_3}{T^2} \tag{2.8}$$

According to Eq. (2.7) and Eq. (2.8), the ohmic resistance coefficient "r" exhibits a linear temperature dependence, while the coefficient "t", related to activation overpotentials, demonstrates a quadratic behavior. Ulleberg's proposal allows for the modeling of electrolyzer performance with high accuracy using just six parameters [21].

The mathematical model proposed by Ulleberg [21] considers temperature as the sole operational variable, assuming that other parameters remain constant. In this study, a new mathematical model is introduced that accounts for the influence of electrolyte concentration, the distance between electrodes/seperator, electrolyte solution, pressure and separator porosity. This model incorporates four additional parameters: "n" ($\Omega x m^2$), "q" ($\Omega x m^2$), “y” ($\Omega x m^2$) and “z” ($\Omega x m^2$). The parameter "n" reflects the variation in system resistance with electrolyte concentration (C), while "q" accounts for the change in resistance with the electrode/seperator distance (electrolyte gap) (d), "x" represents the change in ohmic resistance due to the change in electrolytic solution, “y” expresses the change in resistance with pressure and the "z" parameter reflects the change in the resistance of the ohmic system depending on the separator porosity. Since these parameters impact ohmic overpotentials, they are included in the resistive term. Consequently, the following equation Eq. (2.9) is proposed.

$$U_{cell} = U_{rev} + (r + n + q + x + y + z) \times i + s \log(t \times i + 1) \tag{2.9}$$

In this model, "n" and "z" are not independent parameters but are influenced by "q" and "x".While, "n" depends on both the electrolyte concentration, the electrode-separator distance “q” and the electrolyte solution “x” , "z" is also affected by separator porosity and “q” and "x." Therefore, instead of adding "q" and "x" separately to the main equation, they are included within the terms of "n" and "z," enhancing the model's ability to represent resistive effects on ohmic overpotentials.

Thus, the simplified final form of the equation presented in Eq. (2.9) is given in Eq. (2.10).

$$U_{cell} = U_{rev} + (r + n + y + z) * i + s * \log(t * i + 1) \quad (2.10)$$

where "s" is a constant, and "r" and "t" are expressions which mentioned before that was introduced by Ulleberg in Eq. (2.7) and Eq. (2.8), respectively. Additionally, "n", “y”and "z" are defined by Eq. (2.16) ,Eq (2.17) and Eq.(2.19), respectively.

- For the effects of the electrolyte concentration;

In an electrolysis cell, the movement and concentration of hydroxide ions (OH^-) within the electrolyte determine the conductivity (or resistivity) of the medium. Consequently, potassium hydroxide (KOH) or sodium hydroxide (NaOH) solutions are commonly used as electrolytes for alkaline water electrolysis due to their effective ion conductivity. Various studies have investigated the effects of electrolyte concentration on alkaline water electrolysis, specifically analyzing how electrolyte conductivity (σ) changes with concentration (C) and operating temperature (T).

In the literature, concentration effects and distance effects have also been evaluated using different empirical formulas [50]. However, in the commonly used empirical model for concentration, the mass fraction of the electrolyte is assumed to be independent of temperature and density. This assumption may be limiting for analyses that require a more dynamic calculation approach. Therefore, using a formulation that accounts for the influence of temperature and density on concentration would provide a more accurate and comprehensive model, allowing for more realistic modeling of the electrolyte solution and improving the overall accuracy of the results.

In this context, See and White [64] and Gilliam et al. [65] proposed an empirical model for KOH that correlates conductivity with both temperature and KOH concentration. La Bideau et al [66] developed an equation for correlation with minimized error from [64] and [65]. Similarly, for NaOH Zaytsev gives an experimental data with no correlation but La Bideau et al [66] developed a correlation and gives an empirical model for NaOH, establishing a relationship

between conductivity, temperature, and NaOH concentration. Many authors have investigated the effects of concentration on electrical conductivity for different temperatures along with these empirical modeling. The empirical model for KOH and NaOH is given in the Eq.(2.11) and (2.12), respectively.

$$\sigma_{KOH} = K_1 + K_2 * T + K_3 * Y^2{}_K + K_4 * Y^3{}_K + K_5 * T * Y_K \quad (2.11)$$

$$\sigma_{NaOH} = L_1 + L_2 * T + L_3 * Y^3{}_N + L_4 * Y^2{}_N + L_5 * Y_N \quad (2.12)$$

σ is the electrical conductivity of the electrolyte in $S*m^{-1}$. T is the temperature in C, Y_K is the mass fraction of KOH, Y_N is the mass fraction of NaOH and K and L is the coefficients for KOH and NaOH, respectively.

When analyzing the effect of electrolyte concentration on overpotential in COMSOL, it was determined that current data and the previously mentioned formulation were used for KOH, while for NaOH, data were derived from an outdated list containing temperature, concentration, and conductivity values. While performing analysis, no adjustments were made in COMSOL for KOH; however, calculations for NaOH were performed using Eq. 2.12.

In reporting specific conductivity values, two commonly used concentration units are weight percent (Y) (wt% electrolyte) and molarity (M). To convert between these units, the following equation is given by [65]:

$$C = Y/100 * \rho * M_w{}^{-1} \quad (2.13)$$

Y is the mass fraction of solution (wt%) in the electrolyte, ρ is the solution density of the electrolyte in $kg*m^{-3}$, M_w is the molar mass $g*mol^{-1}$ and C is the molarity in $mol*L^{-1}$ or M.

To determine the density of an electrolyte at specific temperatures and concentrations, empirical correlations have been established that link the electrolyte's mass fraction and molarity to its density.

For determining the density of KOH and NaOH, various authors have developed empirical equations. For KOH and NaOH, Zaytsev uses the same correlation

equation, mentioned in [66], for density as a function of temperature and mass fraction,

$$\rho_K = (P_1 + P_2 * T + P_3 * T^2) * 10\hat{}((P_4 + P_5 * T) * Y_K) \quad (2.14)$$

where ρ_K is the density of KOH, T is temperature in C, Y_K is the mass fraction of KOH.

The same equation for the NaOH,

$$\rho_N = (R_1 + R_2 * T + R_3 * T^2) * 10\hat{}((R_4 + R_5 * T) * Y_N) \quad (2.15)$$

where ρ_N is the density of NaOH, T is temperature in C, Y_N is the mass fraction of KOH.

For general equation for effects of electrolyte concentration ise ;

$$n = {\sigma_o}^{-1} * (d_1 + d_2) \quad (2.16)$$

"n" parameter is here in Ω*m^2 accounts for effects of the electrolyte according to density, temperature, concentration and distance. "d_1" and "d_2" is the distance in m, between electrode and separator for anode and cathode side, respectively. Since $d_1 = d_2 = 2d$ for most cases, equation can be given:

$$n = 2d * {\sigma_o}^{-1} \quad (2.17)$$

- For the effects of pressure;

In this model, for determining the change in resistance with pressure (p) has been added to equation for more comprehensive model. For this purpose, "y" parameter added to ohmic overpotential equation and has been incorporated in the model. This parameter expresses the linear variation in the ohmic overpotentials according to the pressure, equation obtained from [25], given in Eq. (2.17):

$$y = y_1 + y_2 * p \quad (2.18)$$

"y" parameter in Ω*m^2 accounts for the effects of pressure, "y_1" and "y_2" is the coefficients and "p" reflects the pressure in bar.

- For the effects of the seperator porosity;

The conductivity of the separator (σ_s, in S/m) is defined as a function of the conductivity of the electrolyte (σ_o) and geometric parameters such as porosity (ε_s) and tortuosity (τ_s), according to [29]:

$$\sigma_s = \sigma_0 * \varepsilon_s * {\tau_s}^{-1} \tag{2.19}$$

From this equation, higher porosity generally increases conductivity, while higher tortuosity (a more complex path for ions) reduces it.

$$z = {\sigma_s}^{-1} * d_s \tag{2.20}$$

"z" parameter in also Ω*m^2 accounts for the effects of separator porosity and thickness, d_s is the thickness of separator in m.

The Bruggeman equation describes the impact of the gas phase volume fraction $\emptyset_g$ on the effective conductivity σ_e of an electrolyte. This relationship models the effective conductivity as a power function of the intrinsic conductivity of the gas-free electrolyte σ_0 and the gas phase fraction:

$$\sigma_e = \sigma_0 * (1 - \emptyset_g)^{1,5} \tag{2.21}$$

In this equation, σ_0 represents the baseline conductivity of the electrolyte without gas, $\emptyset_g$ denotes the volume fraction of gas within the electrolyte, and value of 1.5 is an empirical exponent, that accounts for structural properties such as porosity. As $\emptyset_g$ increases, conductivity decreases due to the non-conductive nature of the gas phase, which obstructs ionic pathways, reducing effective conductivity. In the present study, however, no gas phase is present, and ionic transfer occurs without obstruction from gas bubbles; thus, $\emptyset_g$ is taken as zero $\emptyset_g$= 0. This assumption simplifies the Bruggeman equation to $\sigma_e = \sigma_0$, reflecting an environment where only ionic conduction occurs within the liquid phase of the electrolyte.

When the parameters constituting Eq. (2.10) are detailed, the following formula is obtained:

$$U_{cell} = U_{rev} + ((r_1 + r_2 * T) + ((d_1 + d_2) * {\sigma_o}^{-1}) + (y_1 + y_2 * p) + ({\sigma_s}^{-1} * d_s)) * i + s * \log\left((t_1 + \frac{t_2}{T} + \frac{t_3}{T^2}) * i + 1\right) \quad (2.22)$$

2.2. COMSOL Modelling and Simulation Approaches

2.2.1 Equations and Computational Approaches

In here, for the modeling and analysis studies, the COMSOL Multiphysics software was utilized. This program is a highly suitable for our studies, offering extensive capabilities in both modeling and analysis through its multiphysics approach. In this study, version 6.2 of the software was employed. The software and its licensing were accessed through Niğde University, and I would like to express my gratitude to Niğde University for their support in providing access to COMSOL.

In the program for the alkaline water electrolysis, the water electrolyzer interface is used in the model, which defines a current distribution model using Butler–Volmer kinetics on both electrodes [67].

In the analysis performed, it is observed that equations accounting for the conservation of current density and surface reactions are used, with the assumptions that mass transport and heat transfer are absent, and there are no time-dependent or two-phase effects. Additionally, it is noted that the equilibrium potential is calculated using the Nernst equation, and the Butler-Volmer electrode kinetics are applied. Due to the consideration of activation and ohmic overpotentials, it is understood that this calculation is performed as a Secondary Current Distribution, and the model is solved within this framework [68] .

In the Secondary Current Distribution model, the current density in the electrolyte is calculated based on the electric field and is defined by the relationship between conductivity (σ) and the potential gradient (∇∅):

$$i_l = -\sigma_l * \nabla \emptyset_l \quad (2.23)$$

where i_l represents the current density vector in the electrolyte, σ_l denotes the effective conductivity of the electrolyte, and $\nabla\emptyset_l$ is the potential gradient within the electrolyte.

This expression describes the current density within the electrolyte according to Ohm's law and only considers the electrical potential difference.

At the electrode-electrolyte interface, charge transfer is defined by the Butler-Volmer equation, which incorporates the activation energy associated with the overpotential:

$$\frac{i_{loc}}{i_0} = e^{\alpha_a \frac{F\eta}{RT}} - e^{\alpha_c \frac{F\eta}{RT}} \tag{2.24}$$

where, i_{loc} is the local current density at the interface, i_0 epresents the exchange current density, α_a and α_c are the anodic and cathodic transfer coefficients, respectively, F is the Faraday constant, η denotes the overpotential, R is the universal gas constant, and T is the temperature.

The use of this equation enables a more realistic modeling of the system by accounting for activation energy in the current density distribution.

In this model, the equilibrium potential is typically calculated using the Nernst equation:

$$E = E^o + \frac{RT}{nF} * \ln\left(\frac{[Ox]}{[Red]}\right) \tag{2.25}$$

where, E is the equilibrium potential, E^o the standard electrode potential, R is the universal gas constant, T represents the temperature, n is the number of electrons transferred in the reaction, F is the Faraday constant, and [Ox] and [Red] represent the concentrations of the oxidized and reduced species, respectively.

This equation provides equilibrium conditions in terms of concentrations for electrode reactions and is often used in conjunction with Butler-Volmer kinetics.

2.2.2 Modeling Process

In the CFD modeling process, the electrolyzer cell was created in 2D using the multiphysics program COMSOL 6.1. The cell geometry was simplified to define boundary conditions effectively. As shown in Figure 2.1, the inner parts of the electrodes were designated as the boundaries (4 and 8), while the oxygen and hydrogen compartments were separated by a rectangular separator (2, 6, 9, 10). The electrodes appear as lines in the model, whereas the separator is represented by one rectangle, and each compartment by two rectangles. The lower and upper sides of these compartments were defined as the electrolyte inlet (1 and 3) and the biphasic mixture outlet (5 and 7), respectively.

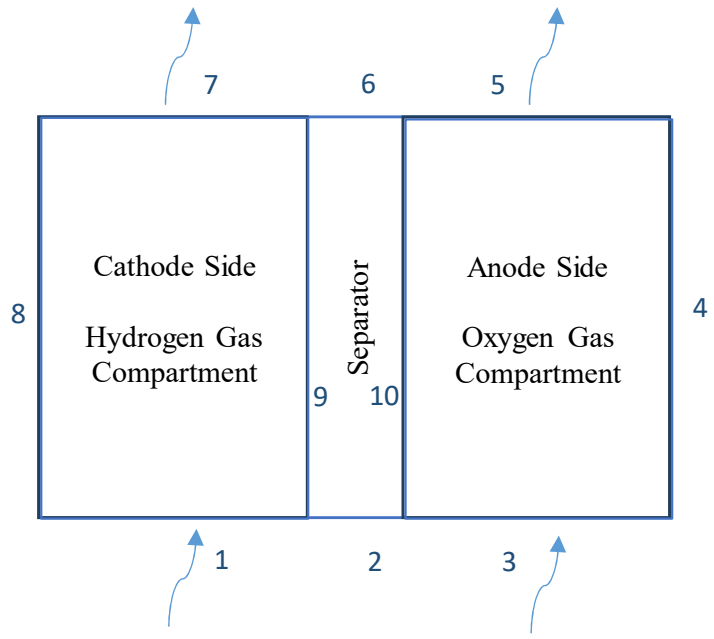

Figure 2.1 Schematic view of electrolysis cell

The parameters used in the COMSOL simulation are provided in the table below.

Table 2.1 Parameters used for modeling

Parameter	**Value**	**Unit**
Cathode Side Electrode-Separator Distance Range	2-4	mm
Anode Side Electrode-Separator Distance Range	2-4	mm
Separator Width	1	mm
Cell Height	10	mm
Operating Temperature Range	25-75	ºC
Exchange Current Density for Anode Side	100	$A*m^2$
Exchange Current Density for Cathode Side	1	$A*m^2$
Separator Porosity	0.3-0.4	-
Electrolyte Concentration	6-10	mol/L
Electrolyte Solution	KOH-NaOH	-
Operating Voltage Range	1.2-2.4	V

In order to simplify the model and focus on the key factors influencing the electrolysis process, certain assumptions have been made. These assumptions help streamline the calculations and reduce the complexity of the system, allowing for a more efficient analysis of the core parameters. In light of these considerations, the following assumptions have been made to facilitate the modeling process:

1. The fluids are assumed to be Newtonian, viscous, and incompressible.
2. Physical properties are considered constant throughout the analysis.
3. The electrolyte is assumed to be uniformly distributed since the distribution of ions has minimal impact on the overall results.
4. The flow is modeled as isothermal; thus, heat exchange and energy equations are excluded from the analysis.
5. Surface tension effects are considered negligible.
6. Hydrogen and oxygen crossover through the separator is negligible.
7. The gas density is negligible compared to the liquid density.

Five different parameters with varying numerical values were used in the analysis to systematically investigate their effects on the electrolysis process. These are temperature, concentration, distance between electrodes and separator, electrolyte solution and separator porosity.

Temperature was analyzed between 25 and 75°C and electrode distance from 2 to 4 mm. Separator porosity was varied between 0.3 and 0.4, the electrolyte solution was selected as either KOH or NaOH, and concentration ranged from 6 mol/L to 12 mol/L. In each analysis, one of the five parameters was varied while the remaining four parameters were kept constant.

The list of analyses, along with the varying parameters, is provided below.

Table 2.2 List of Analysis Cases with Varying Parameters

Analysis Nu.	**Temperature (C)**	**Electrolyte Concentration (1000mol/liter)**	**Electrode-Separator Distance (mm)**	**Seperator Porosity**	**Electrolyte**
1	25	6	2	0.3	KOH
2	25	10	2	0.3	KOH
3	25	6	4	0.3	KOH
4	25	10	4	0.3	KOH
5	25	6	4	0.4	KOH
6	50	6	2	0.3	KOH
7	50	10	2	0.3	KOH
8	50	6	4	0.3	KOH
9	50	10	4	0.3	KOH
10	75	6	2	0.3	KOH
11	75	6	4	0.3	KOH
12	25	6	2	0.4	KOH
13	75	6	2	0.4	KOH
14	50	6	2	0.4	KOH
15	25	6	2	0.3	NaOH
16	25	6	4	0.3	NaOH
17	50	6	2	0.3	NaOH
18	50	6	4	0.3	NaOH
19	75	6	2	0.3	NaOH
20	25	6	4	0.4	NaOH

The table above outlines 20 different analysis cases, each designed to assess the influence of a specific parameter on the electrolysis process. In each case, an I-U curve was generated to obtain the cell voltage and the corresponding average current density values. Voltages ranging from 1.23 to 1.98 V were applied to the cell, and the corresponding average current density data were obtained. By systematically varying one parameter at a time while keeping the others constant, the aim is to isolate the effects of each factor and its relationship to the overall efficiency and performance of the electrolysis system. This methodology enables a detailed understanding of how each variable impacts the electrolysis process.

Temperature variations were examined between 25°C and 75°C to understand their impact on the electrochemical reaction kinetics and the ionic conductivity of the electrolyte. The temperature range is essential for optimizing electrolyzer performance under different operational conditions, as it influences both the cell voltage and the corresponding current density observed in the I-U curve. Concentration changes between 6 mol/L and 12 mol/L were analyzed to assess how varying concentration impacts the electrolyte's conductivity and electrolysis efficiency. Electrode-separator distance variations between 2 mm and 4 mm were studied to determine how changes in this gap affect the system's ohmic resistance and voltage requirements. This parameter is key for understanding how electrode-separator spacing influences the I-U curve, specifically regarding the voltage needed for a given current density. The separator porosity was varied between 0.3 and 0.4 to explore its effects on ion transport efficiency and system performance. Changes in porosity can influence the current density values on the I-U curve, with higher porosity potentially improving ion mobility, though it may introduce other mechanical challenges. The choice of electrolyte solution, either KOH or NaOH, was tested to assess how different electrolytes affect the conductivity and efficiency of the electrolysis process. These different electrolytes lead to distinct I-U curve behaviors, with each influencing the voltage-current density relationship in unique ways under various operational conditions. The combinations in the table provide a comprehensive analysis of the key operational parameters, helping to identify the optimal conditions for enhancing electrolysis performance. Each parameter's

individual and combined effects will be discussed in the following sections to draw conclusions about their relative importance in achieving efficient electrolysis.

2.3. Cost Optimization Modelling

This study utilizes the EES program to calculate and optimize costs associated with alkaline water electrolyzers. The cost of alkaline water electrolyzers was determined based on real-world market data at the end of 2024, as provided in Table 2.3, which includes stack, module, and system costs for various system sizes. Using these data, the cost per square meter of active area was calculated. This calculation yielded a single-cell cost of $19,200 per m², incorporating factors such as material costs, labor, and other project-related expenses.

Table 2.3 Cost and Scaling Factors for Alkaline Electrolysis Systems at Different Sizes

System Size (kWh)	Stack ($)	Mod ($)	Systems ($)	Module Factor (F_m)	System Factor (F_s)
25	25,000	90,000	160,000	3.600	1.778
250	150,000	350,000	450,000	2.333	1.286

In addition to the 20 analyses mentioned above, an independent analysis (Analysis 21) was conducted for the cost optimization. This analysis considered operational parameters such as a temperature of 75°C, a 6M KOH solution concentration, a separator porosity of 0.8, and a separator-electrode distance of 2 mm. The calculations were performed for a voltage range of 1.8 V to 2.5 V, and the resulting I-U curve is presented below. The output data obtained from Analysis 21 used in the EES program for cost optimization.

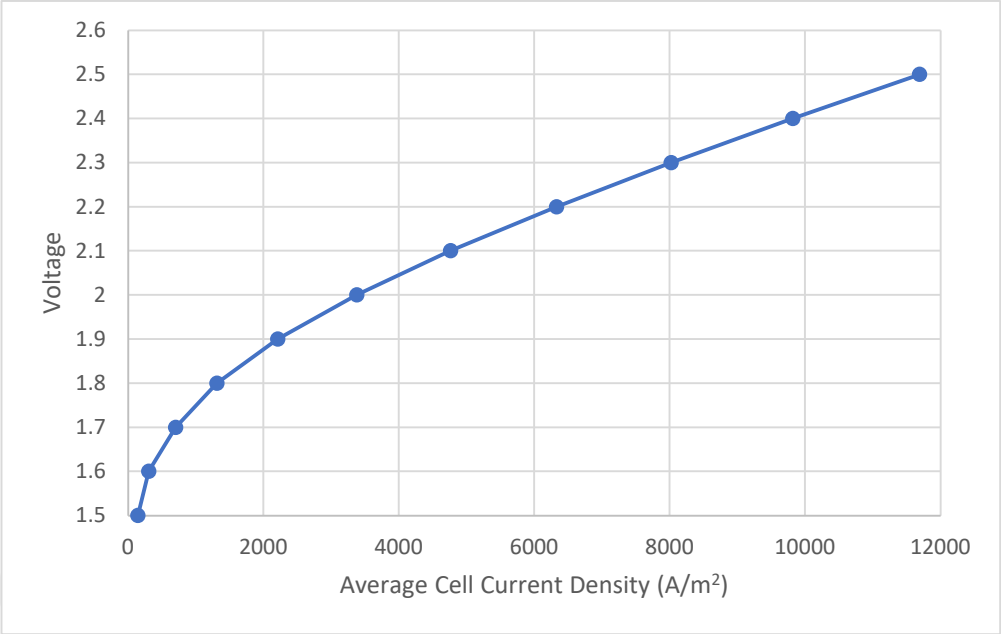

Figure 2.2 I-U Curve for 75 C-2 mm-6 M-0.8 seperator porosity and KOH Solution

The I-U curve data were used to derive a voltage-current function for total system power calculations, which was subsequently implemented in the EES program using Eq. 2.26. The current values obtained from the function correspond to a per-square-meter basis. To determine the total required area for achieving the desired system power, Eq. 2.27 was employed. The cost of the stack, which includes only cell manufacturing, was calculated using Eq. 2.28.

$$V_{cell} = -0{,}000000000293 * I_{cell}{}^2 + 0{,}0000627 * I_{cell} + 1{,}816 \quad (2.26)$$

$$A_{total} = (\dot{W_{total}}/(V_{cell} * I_{cell})) * 1000 \quad (2.27)$$

$$Cost_{stack} = A_{total} * 19200 \quad (2.28)$$

Market prices for 25 kW and 250 kW systems were obtained from current sources, including manufacturer quotes, industry-specific market reports, and publicly available pricing databases. For larger systems, these costs were interpolated using available unit prices. Based on the interpolated data, two critical factors were derived:

- System Factor (F_s) represents the costs associated with auxiliary systems (e.g., power sources, piping, control systems) surrounding the electrolyzer module. This factor incorporates the costs of infrastructure and integration requirements.

- Module Factor (F_m) relates to the scale of the electrolyzer module or its capacity. Smaller systems typically have higher unit costs due to limited economies of scale, reflecting the higher installation and production expenses for smaller modules.

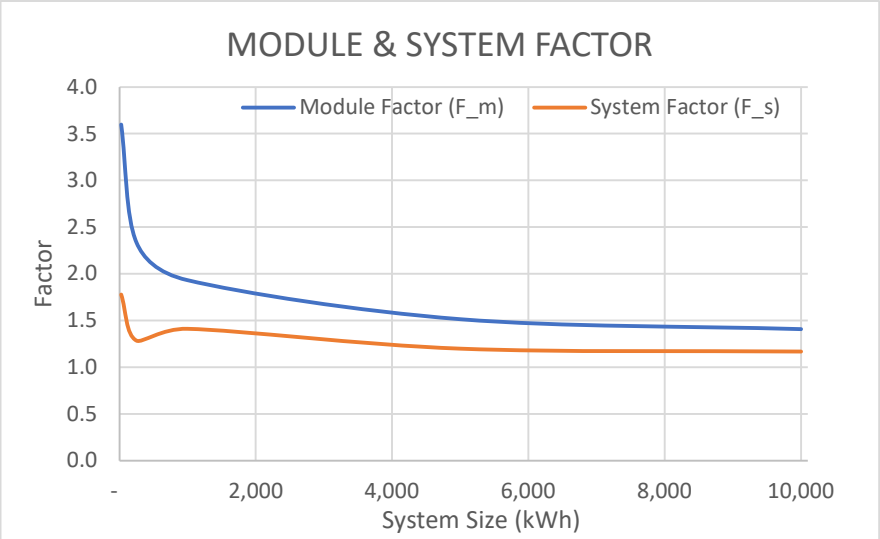

Figure 2.3 Module and System Factors as a Function of System Size

The figure illustrates the variation in the Module Factor and System Factor across different system sizes (kWh) for alkaline water electrolyzers. The data demonstrates a decreasing trend in both factors as the system size increases, indicating improved cost efficiency and scalability for larger systems. The Module Factor exhibits a sharper decline compared to the System Factor, reflecting the more significant economies of scale achieved at the module level.

These values are based on real-world market data, as presented in Table 2.3, ensuring the reliability of the trends shown. The alignment of the plotted data with actual market quotes highlights the credibility of the analysis.

The derived functions for these factors are expressed in Eq. 2.29 (F_s) and 2.30 (F_m), respectively. Additionally, the maintenance factor (F_{mn}), which accounts for repair labor and spare part costs, was set at 1.3 for this study. Capital expenditures (CapEx) calculations incorporated these factors using the following equation 2.31. Operational costs other than energy expenses were included within this framework.

$$F_s = 2{,}0642 * \dot{W}_{total}^{-0{,}063} \tag{2.29}$$

$$F_m = 5{,}7676 * \dot{W}_{total}^{-0{,}156} \tag{2.30}$$

$$CapEx = Cost_{stack} * F_s * F_m * F_{mn} \tag{2.31}$$

A 20-year operational lifespan was assumed for the system. Considering maintenance, repairs, and other operational downtimes, the capacity factor was adjusted to 85%. For the Levelized Cost of Electricity (LCOE) calculation, energy costs were analyzed based on different production sources (e.g., fossil fuels, renewables) and geographic variations in accessibility. As a result, LCOE were set at \$0.05/kWh and \$0.1/kWh for the calculations, reflecting typical values for renewable and fossil-based energy sources in various global regions. This range accounts for regional variability and provides a realistic basis for cost optimization modeling. Operational Expenditures (OpEx) was computed using Eq. 2.32.

$$OpEx = LCOE * \dot{W}_{total} * Life * Capacity * Annual\ Hours \tag{2.32}$$

The total cost, comprising CapEx and OpEx, formed the basis for calculating the levelized cost of hydrogen (LCOH). To perform this calculation:

1. Hydrogen production efficiency was determined using Eq. 2.33. Here, the constant 1.46 represents the theoretical maximum efficiency of converting electrical energy into hydrogen's chemical energy under standard conditions, accounting for the lower heating value (LHV) of hydrogen (33.3 kWh/kg) and the thermoneutral voltage of water splitting (1.23 V).

2. Hourly hydrogen production, based on system power, was calculated using Eq.2.34. Here, the constant 39.4 represents the higher heating value (HHV) of

hydrogen in kWh per kilogram, a standard metric used to correlate energy consumption with hydrogen production efficiency.

3. Cumulative hydrogen production over the system's lifespan was derived using Eq.2.35

4. LCOH calculations were performed using Eq.2.36, dividing the total cost by the total hydrogen production over the operational lifespan.

$$\eta_{H_2} = 1{,}46/V_{cell} \tag{2.33}$$

$$H_{2,per\ hour} = {\dot{W_{total}} * \eta_{H_2}}/{39.4} \tag{2.34}$$

$$H_{2,total} = H_{2,per\ hour} * Life * Capacity * Annual\ Hours \tag{2.35}$$

$$LCOH = {(CapEx + OpEx)}/{H_{2,total}} \tag{2.36}$$

The contributions of CapEx and OpEx to the total cost were analyzed separately using Eq. 2.37 and 2.38. Furthermore, the unit hydrogen production cost per kg contributions of CapEx and OpEx were clarified using Eq. 2.39 and 2.40, respectively.

$$CapEx_{cont} = CapEx/Total\ cost \tag{2.37}$$

$$OpEx_{cont} = OpEx/Total\ cost \tag{2.38}$$

$$CapEx_{per\ H_2} = CapEx/H_{2,total} \tag{2.39}$$

$$OpEx_{per\ H_2} = OpEx/H_{2,total} \tag{2.40}$$

This systematic approach provides a detailed framework for cost optimization in alkaline water electrolyzers and ensures that all relevant factors are comprehensively evaluated.

CHAPTER 3- RESULTS AND DISCUSSIONS

This chapter presents the results of the electrolysis analyses conducted using the COMSOL and discusses the effects of key operational parameters on the average cell current density and the cost optimization. Each parameter is examined systematically to isolate its influence on the electrolysis process, with detailed numerical results and comparative analyses provided. The findings are presented in the form of I-U graphs, supported by quantitative data to illustrate the relationship between operational parameters and system performance. These results offer a comprehensive understanding of the individual and combined effects of the analyzed parameters.

For the cost optimization, a systematic methodology was employed to evaluate the economic feasibility of various system configurations using the EES. This involved calculating CapEx and OpEx, followed by assessing the LCOH as the primary economic metric. Key parameters such as material costs, energy efficiency, and system scalability were integrated into the cost model to ensure a comprehensive analysis. Additionally, factors like the module factor (F_m), system factor (F_s), and maintenance factor (F_mn) were used to account for the influence of system size, auxiliary components, and long-term operational considerations. This approach enables a detailed understanding of how design and operational choices impact overall system economics.

3.1. COMSOL Analysis Results

The results of the COMSOL analyses are structured around the five key parameters studied: temperature, electrode-separator distance, separator porosity, electrolyte concentration, and electrolyte type. For each parameter, numerical simulations were performed by varying the parameter of interest while keeping the others constant. This approach ensures a focused evaluation of each parameter's role in determining the average cell current density. The following sections present the results for each parameter, starting with the effect of temperature.

In the following three figures, the electrolyte potential distributions, their gradients, and arrow surfaces are illustrated to analyze the effects of varying parameters on the performance of the electrolyzer. These visualizations demonstrate how changes in

these parameters influence the uniformity of potential distribution, the magnitude of potential drops, and the efficiency of ion transport within the cell.

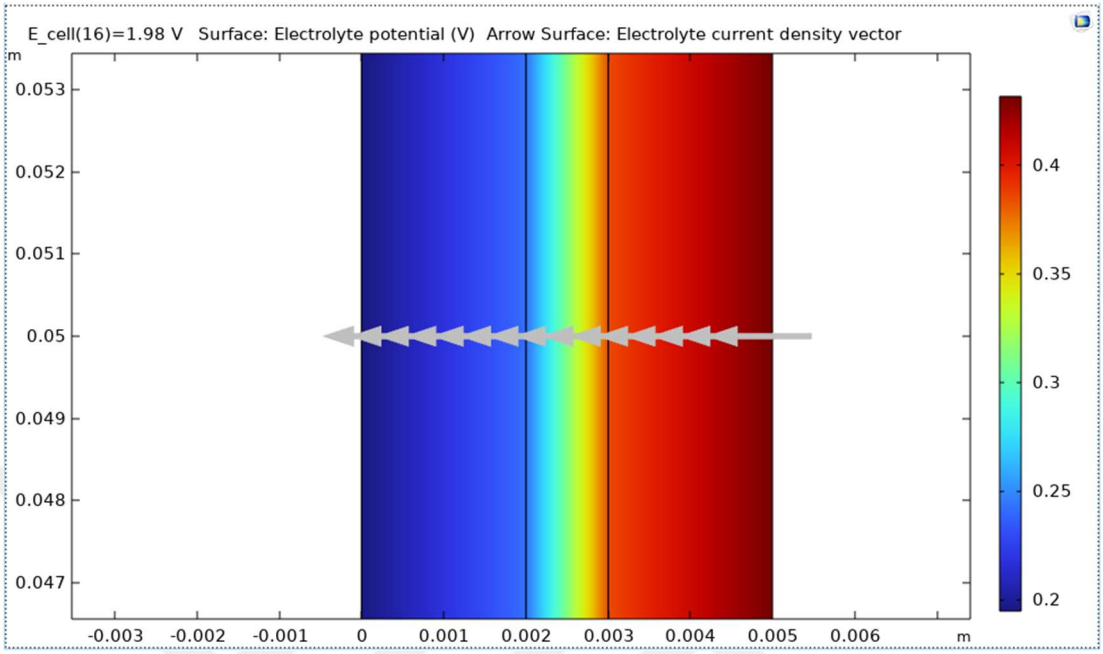

Figure 3.1 Electrolyte Potential Distribution and Current Density Vectors for Analysis 1

The figure represents the results of Analysis 1 given in Table 2.2, providing a visualization of the electrolyte potential distribution (V) and current density vectors within the electrolyzer cell under an applied voltage of 1.98 V. The color gradient, ranging from blue (low potential) to red (high potential), highlights the potential drop across the electrolyte. The arrows represent the electrolyte current density, indicating both the direction and magnitude of ion flow. Although the applied voltage changes, the gradient remains constant, while the absolute potential drop values vary accordingly.

Unlike conventional finite element models, this study employs a continuous computational domain without explicit meshing. Therefore, numerical discretization effects do not influence the solution. However, a numerical sensitivity analysis could be conducted by refining the computational grid to ensure solution stability and accuracy.

This type of visualization is critical for understanding the uniformity of potential distribution and ionic movement within the cell. Such analyses help identify potential

inefficiencies or irregularities in the cell, enabling further optimization of the system for enhanced performance.

The electrochemical behavior of the system is governed by Ohm's law, expressed below

$$I = \sigma * E \tag{3.1}$$

where I is the current density (A/m²), σ is the ionic conductivity (S/m), and E is the electric field (V/m)

Additionally, the potential distribution in the electrolyte follows Laplace's equation,

$$\nabla * (\sigma \nabla V) = 0 \tag{3.2}$$

where V is the electric potential (V), which ensures the conservation of charge within the system.

For this simulation, boundary conditions were defined to reflect realistic operating conditions. A constant potential difference of 1.98 V was applied across the electrodes to drive the electrochemical reaction. The lateral boundaries were assumed to have zero charge flux, meaning no leakage currents were present. Moreover, the electrolyte was considered homogeneous, with a uniform ionic conductivity throughout the domain.

To simplify the computational model and focus on the primary electrochemical interactions, several assumptions were made. First, the electrolyte was treated as a homogeneous and isotropic medium, meaning its conductivity remained uniform in all directions. Second, electrode kinetics and overpotential losses were not explicitly included in the model, assuming an idealized charge transfer process. Third, the temperature effects on conductivity and reaction rates were neglected, implying an isothermal system. Finally, fluid flow and bubble formation within the electrolyte were not considered, ensuring that the electric field and ion transport were not disturbed by additional hydrodynamic factors.

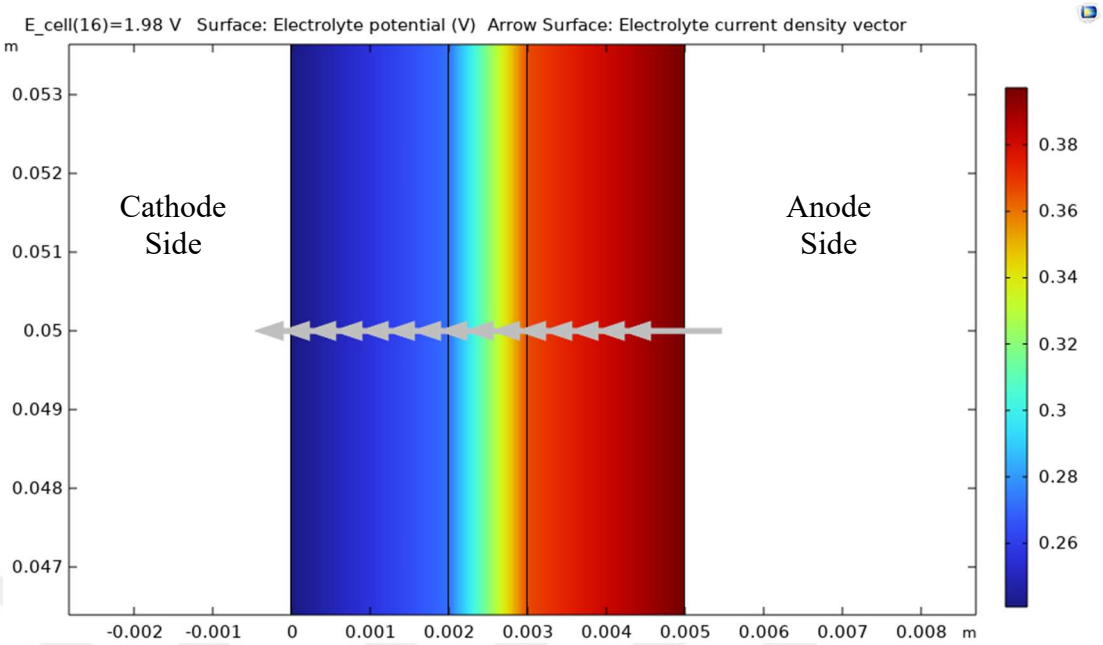

Figure 3.2 Electrolyte Potential Distribution and Current Density Vectors for Analysis 10

The figure above represents the results of Analysis 10 given in Table 2.2, visualizing the electrolyte potential distribution (V) and current density vectors within an electrolyzer cell under a cell voltage of 1.98 V. Changes in temperature do not significantly affect the gradient, as the color tones and intensities remain relatively stable, indicating that the electrolyte's potential distribution is largely unaffected by temperature variations under these conditions.

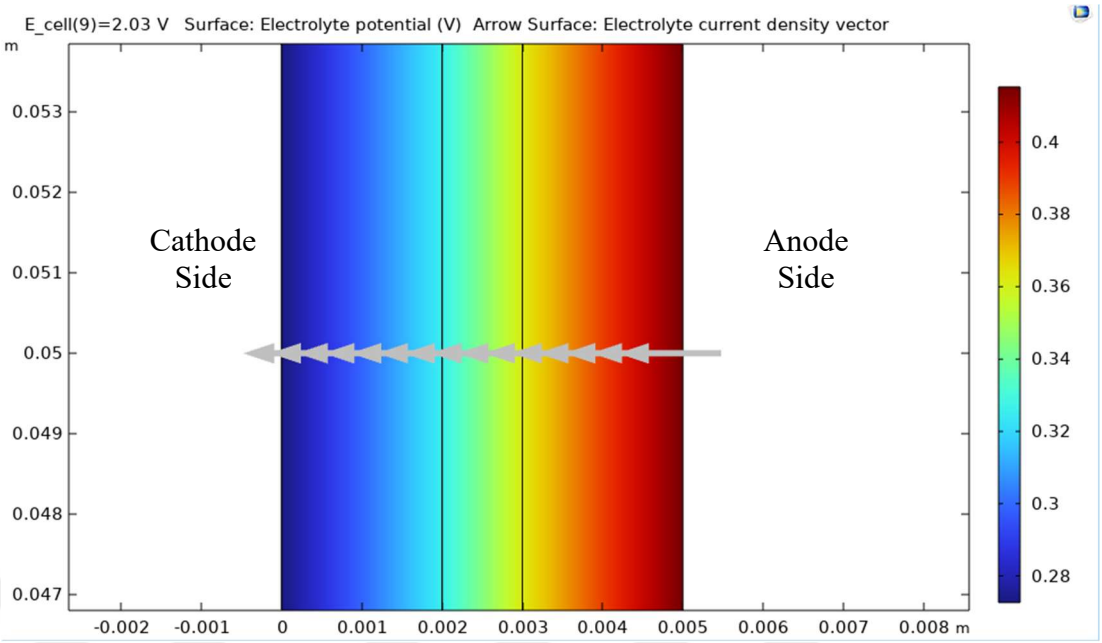

Figure 3.3 Electrolyte Potential Distribution and Current Density Vectors for Analysis used for Cost Optimization

The figure above represents the results of analysis used for cost optimization, visualizing the electrolyte potential distribution (V) and current density vectors within an electrolyzer cell under a cell voltage of 2.03 V. The increase in porosity leads to a noticeable reduction in the red region, indicating a decrease in the potential drop across the electrolyte. This suggests that increased porosity enhances ion flow and reduces ohmic losses, improving the efficiency of the electrolyzer under these conditions.

3.1.1. Effect of Temperature on Average Cell Current Density

Temperature has been identified as one of the most significant factors influencing the average cell current density in the electrolysis process. This is primarily because temperature affects both the electrochemical reaction kinetics and the ionic conductivity of the electrolyte. For instance, using KOH with a concentration of 6 M, a separator porosity of 0.3, and a distance of 2 mm, increasing the temperature from 25°C to 50°C leads to a notable increase in current density. At a potential of 1.88 V, the current density rises from 1058.2 A/m² to 1238.6 A/m², while at 1.98 V, it increases from 1470.7 A/m² to 1788.5 A/m². Similarly, when the temperature is

further elevated to 50°C and 75°C under the same conditions, the current densities at 1.88 V are 1325.1 A/m² and 1335.5 A/m², respectively. At 1.98 V, the corresponding current densities are 1982.2 A/m² and 2059.9 A/m².

In addition to KOH, the effects of temperature on average cell current density were also analyzed using NaOH as the electrolyte under similar conditions. For instance, at 25°C, a separator porosity of 0.3, and a distance of 2 mm, the current density at 1.88 V was 826.5 A/m², and at 1.98 V, it was 1119.1 A/m². When the temperature was increased to 50°C under the same conditions, the current density rose to 1035.1 A/m² at 1.88 V and 1455.5 A/m² at 1.98 V.

While both electrolytes exhibit a similar trend of increasing current density with temperature, the relative change differs between them. For KOH, increasing the temperature from 25°C to 50°C results in a 21.6% increase in current density, whereas for NaOH, the same temperature increase leads to a 30% difference in current density.

When examining the effects of temperature changes on current density at different separator porosity values, the current densities for a porosity of 0.3 at 25°C and 50°C at 1.98 V have already been provided. For a porosity of 0.4, these values are 1732.8 A/m² and 2074.3 A/m², respectively. While increasing the temperature from 25°C to 50°C increases the current density by 21.6% for a porosity of 0.3, the same temperature increase results in a 19.7% increase for a porosity of 0.4.

Temperature is a critical factor influencing current density, with significant improvements observed across different electrolytes and separator porosity values, highlighting its key role in optimizing electrolysis performance.

3.1.2 Effects of Electrode-Seperator Dist. on Avg. Cell Current Density

The changes in cell current density with variations in the electrode-separator distance were analyzed. For KOH at 25°C, 0.3 porosity, and a concentration of 6 M, the current density at 1.88 V decreases from 1058.2 A/m² to 854.4 A/m² when the distance increases from 2 mm to 4 mm. Similarly, at 1.98 V, the current density decreases from 1470.7 A/m² to 1160.6 A/m². When the temperature is increased to

50°C, the current density at 1.98 V decreases from 1788.5 A/m² to 1440.3 A/m² under the same conditions. The doubling of the distance at 25°C results in a 21% decrease in current density, while at 50°C, this decrease is 19.5%.

When NaOH is used instead of KOH, at 25°C and 1.98 V, increasing the distance from 2 mm to 4 mm decreases the current density from 1119.1 A/m² to 876.6 A/m². At 50°C, the current density decreases from 1455.5 A/m² to 1162.6 A/m² under the same conditions. For NaOH, the doubling of the distance at 25°C results in a 21.7% decrease in current density, while at 50°C, this decrease is 20%.

These results indicate that the change in electrolyte material has no significant effect on the impact of electrode-separator distance on cell current density, and this influence can be considered negligible.

When analyzed in terms of separator porosity, for KOH at 25°C, 6 M concentration, increasing the distance from 2 mm to 4 mm results in the current densities for 0.3 porosity at 1.98 V as provided above. When the porosity is increased to 0.4, the current density at 1.98 V decreases from 1732.8 A/m² to 1305 A/m². In this case, the decrease is 21% for 0.3 porosity and 24.7% for 0.4 porosity.

Increasing the electrode-separator distance significantly reduces current density, with the magnitude of the decrease slightly influenced by temperature and separator porosity, while the choice of electrolyte has negligible impact.

3.1.3. Effect of Concentration on Average Cell Current Density

When examining the effect of electrolyte concentration on current density, it was observed that for a KOH solution at 25°C,2 mm distance, and 0.3 porosity, the current density at 1.88 V was 1058.2 A/m², and at 1.98 V, it was 1470.7 A/m² for a concentration of 6 M. When the concentration was increased to 10 M, the current density at 1.98 V decreased to 1312.6 A/m². At 50°C, for a concentration of 6 M, the current density was 1788.5 A/m², while increasing the concentration to 10 M reduced it to 1697.5 A/m². The change in molarity at 25°C affects the current density by 10.7%, whereas at 50°C, this effect is reduced to 5.1%.

For KOH with 0.3 porosity, increasing the electrode-separator distance from 2 mm to 4 mm at 25°C resulted in current densities at 1.98 V of 1160.6 A/m² and 1032.6 A/m² for concentrations of 6 M and 10 M, respectively. At 50°C, the corresponding values were 1440.3 A/m² and 1364.0 A/m². Under these conditions, doubling the distance at 25°C caused a 11% reduction in current density due to the increase in electrolyte concentration, while at 50°C, the reduction was 5.3%.

Increasing the electrolyte concentration from 6 M to 10 M generally reduces current density, with the magnitude of the reduction being more pronounced at lower temperatures and smaller electrode-separator distances.

3.1.4. Effect of Separator Porosity on Average Cell Current Density

For the effect of seperator porosity, for KOH at 25°C, 2 mm distance, and a concentration of 6 M, increasing the separator porosity from 0.3 to 0.4 at 1.98 V results in the current density rising from 1470.7 A/m² to 1732.8 A/m². At 50°C, this increase is from 1788.5 A/m² to 2074.3 A/m². Similarly, at 75°C, 2 mm distance, and 6 M concentration, the current density at 1.98 V increases from 1982.2 A/m² to 2260.8 A/m² when the porosity is raised from 0.3 to 0.4. The effect of porosity on current density is 17.8% at 25°C, 16% at 50°C, and 14% at 75°C.

When NaOH is used under the same parameters, the current density at 25°C and 0.3 porosity is 1119.1 A/m², increasing to 1326.2 A/m² when the porosity is raised to 0.4. At 25°C, the increase in current density due to porosity is 17.8% for KOH, whereas for NaOH, this increase is 18.5%.

increasing separator porosity significantly enhances current density, with the effect being more pronounced at lower temperatures. The trend is consistent across both KOH and NaOH, with NaOH showing a slightly higher sensitivity to porosity changes.

3.1.5. Effect of Electrolyte Solution on Average Cell Current Density

When examining the effect of the electrolyte solution on current density, it was observed that at 25°C, 0.3 porosity, 2 mm distance, and 6 M concentration, the

current density at 1.98 V was 1470.7 A/m² for KOH and 1119.1 A/m² for NaOH. Under the same conditions at 50°C, the current density was 1788.5 A/m² for KOH and 1455.5 A/m² for NaOH. At 75°C, 0.3 porosity, 2 mm distance, and 6 M concentration, the current density at 1.98 V was 2059.9 A/m² for KOH and 1742.9 A/m² for NaOH.

The efficiency difference between KOH and NaOH decreases with increasing temperature, being 23.9% at 25°C, 18.6% at 50°C, and 15.4% at 75°C

3.1.6. Effect of Applied Voltage on Average Cell Current Density

Under conditions of 50°C, 2 mm electrode-separator distance, 0.3 porosity, and 6M concentration, the current density increases significantly with voltage for both KOH and NaOH electrolytes. For KOH solution, when voltage increases by 2.7% (from 1.88 V to 1.93 V), the current density rises by 21.4% (from 1238.6 A/m^2 to 1503.3 A/m^2), and for a 5.3% voltage increase (to 1.98 V), it increases by 44.4% (to 1788.5 A/m^2). In comparison, for NaOH solution under the same conditions, a 2.7% voltage increase leads to a 19.7% rise (from 1035.1 A/m^2 to 1238.7 A/m^2) in current density, while a 5.3% increase results in a 40.6% rise (to 1455.5 A/m^2). These trends highlight the higher conductivity and efficiency of KOH in promoting current density under identical operating conditions.

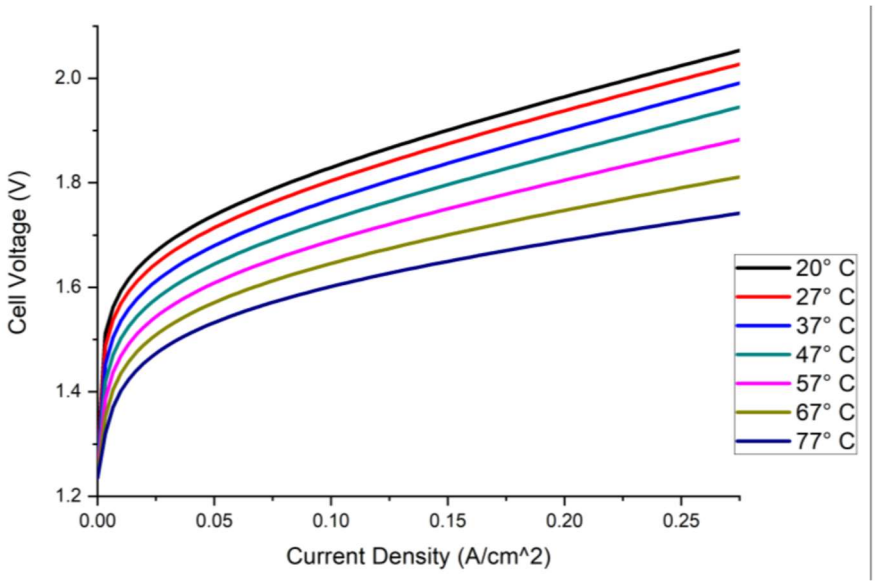

Figure 3.4 The I-U curve from the study by [22].

This graph obtained from [22] is used as a reference to validate the results obtained in this study. A comparison with the results obtained in this work shows a similar trend, indicating the reliability of the findings. The consistency between the two studies suggests that the methodology and modeling approach used in this research produce accurate results. Any minor deviations may be due to differences in analysis conditions.

Below are three figures summarizing the aforementioned results. These figures focus on the parameters that most significantly affect current density, and the combined effects of these parameters are presented in graphical form. Figure 3.5 illustrates the impact of temperature and separator porosity on current density for KOH solution. The effects of four different temperature values on current density at porosity levels of 0.3 and 0.4 are shown in Figure 3.5. Figure 3.6 combines the effects of electrode-separator distance and electrolyte concentration to create an I-U curve, while Figure 3.7 demonstrates the influence of KOH and NaOH on current density. Graphs for each of the 20 analyses listed in Table 2.2 are provided in Appendix A.

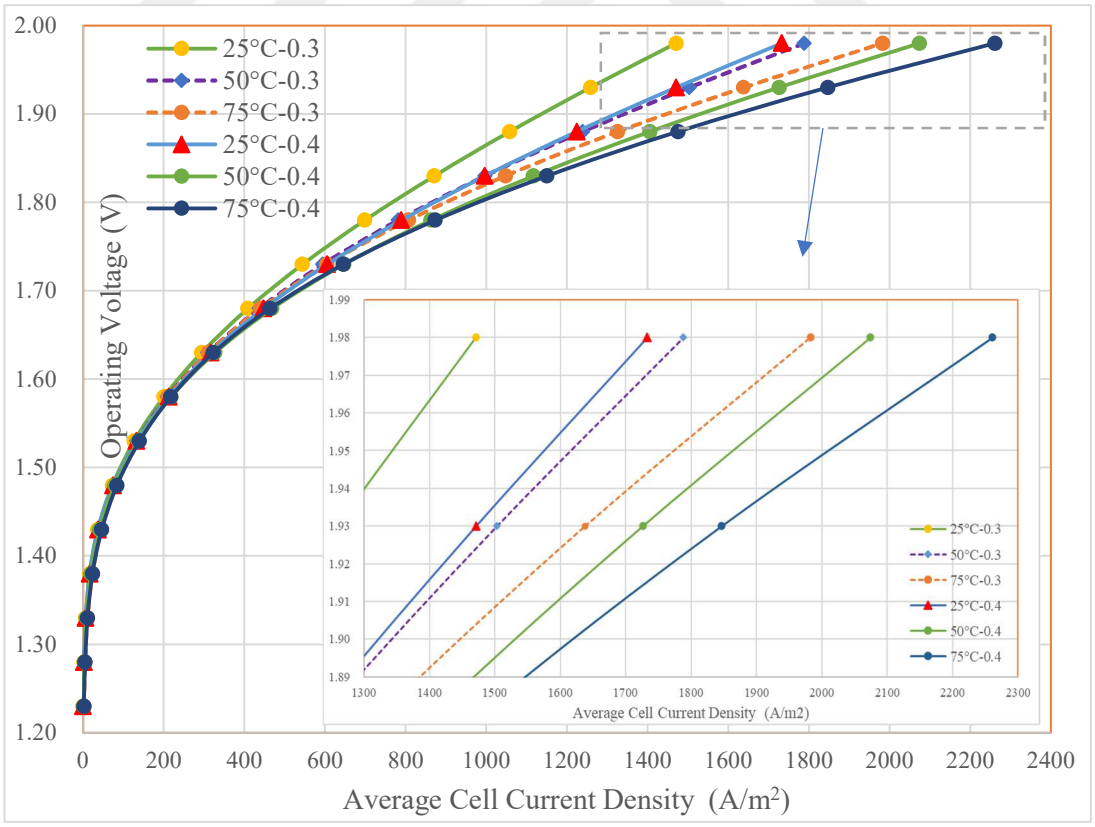

Figure 3.5 I-U Curve for Effect of Temperature and Separator Porosity

Figure 3.5 I-U Curve for Effect of Temperature and Separator Porosity

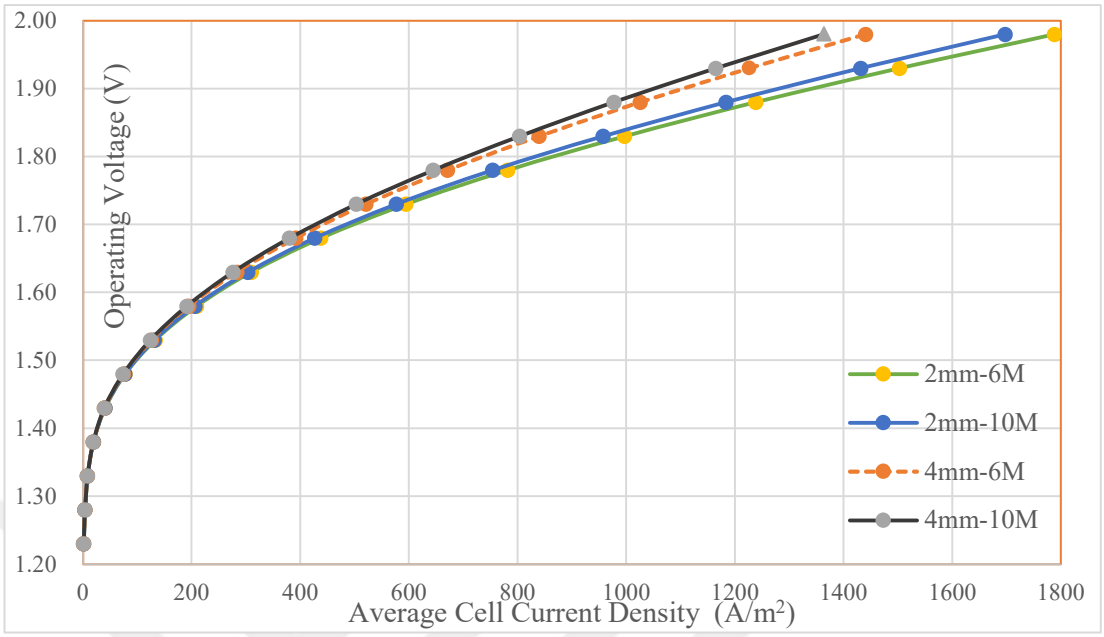

Figure 3.6 I-U Curve for Effect of Electrode-Separator Distance and Electrolyte Concentration

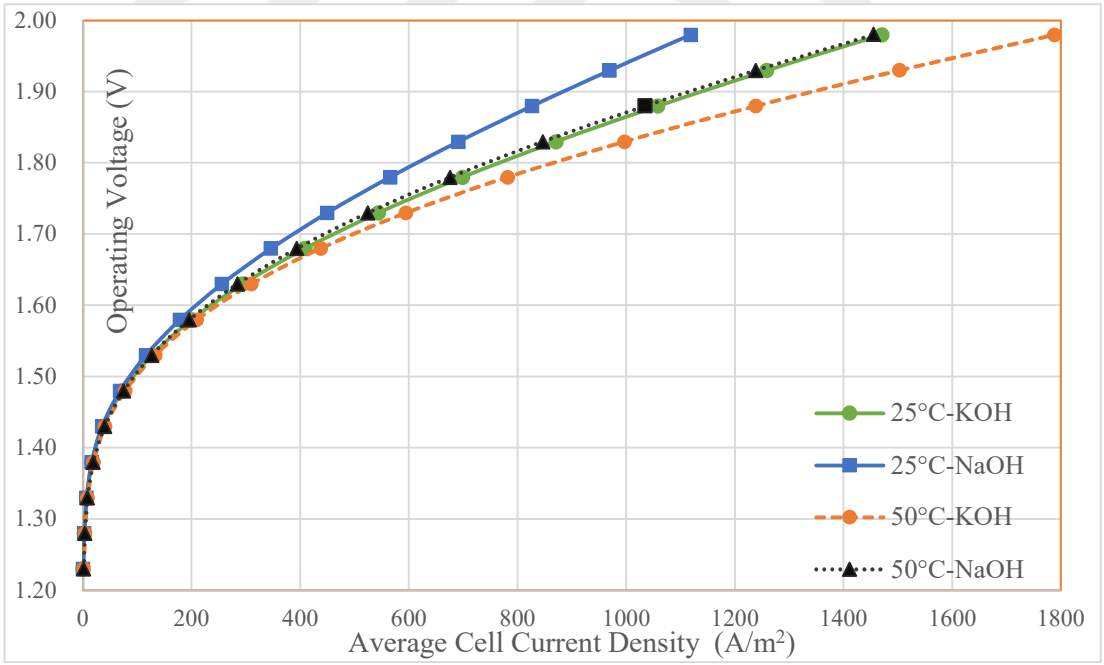

Figure 3.7 I-U Curve for Effect of Temperature and Electrolyte Solution

3.2. EES Analysis Results

In this study, cost optimization was performed using 1D modelling in COMSOL Multiphysics, providing a simplified yet effective approach to analyze the electrochemical performance and economic implications of alkaline water electrolyzers. The 1D model enabled the evaluation of key operational parameters, such as current density, voltage, and efficiency, which were subsequently integrated into the cost analysis framework to calculate the Levelized Cost of Hydrogen (LCOH).

The results from COMSOL modelling were transferred into the engineering equation solver (EES) environment to extend the analysis and systematically explore the impact of technical parameters on economic outcomes. This hybrid approach ensured that the cost optimization process combined accurate simulation data with flexible economic modeling, enabling the identification of operating conditions that minimize LCOH. By utilizing this methodology, the study demonstrates the practicality of 1D modelling-based analysis as a foundation for cost-effective hydrogen production and future design improvements.

Using the current-voltage formula derived from COMSOL data, calculations were performed in the EES program for systems with capacities of 25 kW, 100 kW, 1,000 kW, 5,000 kW and 10,000 kW. For these calculations, LCOE values of $ 0.05/kWh and $ 0.1/kWh were considered, and analyses were conducted for current densities of 10,000 A/m^2 and 20,000 A/m^2. The analysis focused on determining CapEx and OpEx values for cost optimization, while simultaneously calculating the total hydrogen produced by the system and deriving the LCOH values. A total of 20 analyses were conducted, incorporating these parameters. Non-cost-related analysis inputs and results are presented in Table 3.1, while cost-related analysis results are summarized in Table 3.2.

Table 3.1 shows the varying parameters such as current density, LCOE, voltage, and system efficiency, along with the corresponding total cell area and total hydrogen production. Table 3.2 details the cost components, including CapEx, OpEx, and their contributions to LCOH and total system cost.

Table 3.1 List of Analysis Cases and Results with Varying Parameters

No.	System Size (kWh)	Current Density (A/m^2)	LCOE ($/kWh)	Total Cell Area (m^2)	Voltage (V)	Fm	Fs	System eff.	Produced Total h_2 (tonne)
1	25	10000	0.05	1.036	2.414	3.49	1.68	0.605	57.2
2	25	20000	0.05	0.4233	2.953	3.49	1.68	0.494	46.7
3	25	10000	0.1	1.036	2.414	3.49	1.68	0.605	57.2
4	25	20000	0.1	0.4233	2.953	3.49	1.68	0.494	46.7
5	100	10000	0.05	4.143	2.414	2.81	1.54	0.605	228.6
6	100	20000	0.05	1.693	2.953	2.81	1.54	0.494	186.9
7	100	10000	0.11	4.143	2.414	2.81	1.54	0.605	228.6
8	100	20000	0.1	1.693	2.953	2.81	1.54	0.494	186.9
9	1,000	10000	0.05	41.43	2.414	1.96	1.34	0.605	1,869
10	1,000	20000	0.05	16.93	2.953	1.96	1.34	0.494	1,869
11	1,000	10000	0.1	41.43	2.414	1.96	1.34	0.605	2,286
12	1,000	20000	0.1	16.93	2.953	1.96	1.34	0.494	1,869
13	5,000	10000	0.05	207.2	2.414	1.53	1.21	0.605	11,430
14	5,000	20000	0.05	84.67	2.953	1.53	1.21	0.494	9,344
15	5,000	10000	0.1	207.2	2.414	1.53	1.21	0.605	11,430
16	5,000	20000	0.1	84.67	2.953	1.53	1.21	0.494	9,344
17	10,000	10000	0.05	414.3	2.414	1.37	1.15	0.605	22,860
18	10,000	20000	0.05	169.3	2.953	1.37	1.15	0.494	18,690
19	10,000	10000	0.1	414.3	2.414	1.37	1.15	0.605	22,860
20	10,000	20000	0.1	169.3	2.953	1.37	1.15	0.494	18,690

Table 3.2 List of Analysis Results for Cost Values

No.	Sys. Size (kWh)	Current Density (A/m^2)	LCOE ($/kWh)	Cap Ex ($M)	OpEx ($M)	LCOH ($/kg)	CapEx per kg ($)	OpEx per kg ($)	Total cost ($M)
1	25	10000	0.05	0.152	0.186	5.918	2.66	3.26	0.338
2	25	20000	0.05	0.062	0.186	5.315	1.33	3.98	0.248
3	25	10000	0.1	0.152	0.372	9.175	2.66	6.51	0.524
4	25	20000	0.1	0.062	0.372	9.299	1.33	7.97	0.434
5	100	10000	0.05	0.449	0.745	5.221	1.96	3.26	1.194
6	100	20000	0.05	0.184	0.745	4.966	0.98	3.98	0.928
7	100	10000	0.1	0.449	1.489	8.478	1.96	6.51	1.938
8	100	20000	0.1	0.184	1.489	8.951	0.98	7.97	1.673
9	1,000	10000	0.05	2.712	7.446	4.443	1.19	3.26	10.158
10	1,000	20000	0.05	1.108	7.446	4.577	0.59	3.98	8.554
11	1,000	10000	0.1	2.712	14.890	7.700	1.19	6.51	17.602
12	1,000	20000	0.1	1.108	14.890	8.562	0.59	7.97	15.998
13	5,000	10000	0.05	9.532	37.230	4.091	0.83	3.26	46.762
14	5,000	20000	0.05	3.896	37.230	4.401	0.42	3.98	41.126
15	5,000	10000	0.1	9.532	74.460	7.348	0.83	6.51	83.992
16	5,000	20000	0.1	3.896	74.460	8.385	0.42	7.97	78.356
17	10,000	10000	0.05	16.380	74.460	3.973	0.72	3.26	90.840
18	10,000	20000	0.05	6.695	74.460	4.342	0.36	3.98	81.155
19	10,000	10000	0.1	16.380	148.900	7.230	0.72	6.51	165.280
20	10,000	20000	0.1	6.695	148.900	8.327	0.36	7.97	155.595

For the 25 kW System with 10,000 A/m^2 and LCOE = \$0.05/kWh, the system requires a total cell area of 1.036 m^2 with an operational voltage of 2.414 V, achieving a system efficiency of 60.5%. This system produces 57.2 tonnes of

hydrogen over the system's lifetime and the CapEx and OpEx were calculated as $152,000 and $186,000, respectively, resulting in an LCOH of $5.918/kg. When the same system used but with doubled LCOE = $0.1/kWh, while the CapEx remains constant, the OpEx doubles to $372,000 due to the doubled electricity cost. Consequently, the LCOH rises to $9.175/kg. When the LCOE doubles, the LCOH increases by approximately 55.04% (from 5.918 to 9.175). For the 25 kW System 20,000 A/m^2 (doubling the current density) with LCOE = $0.05/kWh, with a higher current density, the required cell area decreases from 1.036 to 0.423 m^2 and the system efficiency drops to 49.4%. The LCOH is calculated as $5.315/kg. When the current density is doubled, the LCOH value decreases by approximately 10.19% (from 5.918 to 5.315). For the again 25 kW System with 20,000 A/m^2, but doubled LCOE is $0.1/kWh, the LCOH increases to $9.299/kg due to higher electricity costs. While, doubling the current density increases the LCOH by approximately 1.35% (from 9.175 to 9.299), doubling the LCOE increases the LCOH by approximately 74.96% (from 5.315 to 9.299).

For the 100 kW system with 10,000 A/m^2 and LCOE = $0.05/kWh, the system requires a total cell area of 4.143 m^2, achieving a system efficiency of 60.5%. This system produces 228.6 tonnes of hydrogen over its lifetime, with CapEx and OpEx calculated as $449,000 and $745,000, respectively, resulting in an LCOH of $5.221/kg. When the LCOE is doubled to $0.1/kWh, the OpEx doubles to $1,489,000, causing the LCOH to rise to $8.478/kg, an increase of 62.38%. Doubling the current density to 20,000 A/m^2 reduces the required cell area to 1.693 m^2, with the system efficiency dropping to 49.4%. The LCOH in this case is calculated as $4.966/kg, reflecting a decrease of 4.88%. However, when both the current density is doubled to 20,000 A/m^2 and LCOE increases to $0.1/kWh, the OpEx remains $1,489,000, and the LCOH further rises to $8.951/kg. This represents a 5.35% increase compared to the LCOH with the lower current density and a 80.21% increase compared to the baseline 10,000 A/m^2 LCOE = $0.05/kWh case.

For the 1000 kW system with 10,000 A/m^2 and LCOE = $0.05/kWh, the required total cell area is 41.43 $m^2$and a system efficiency of 60.5%. Over its lifetime, this system produces 1,869 tonnes of hydrogen, with CapEx and OpEx calculated as

$2.712 million and $7.446 million, respectively, resulting in an LCOH of $4.443/kg. When the LCOE is doubled to $0.1/kWh, the OpEx increases to $14.89 million, and the LCOH rises to $7.700/kg, representing an increase of 73.31%. Doubling the current density reduces the cell area to 16.93 m², with system efficiency dropping to 49.4%. The LCOH in this scenario increases slightly to $4.577/kg, reflecting a 3.02% rise. However, when both the current density is doubled, and the LCOE is increased to $0.1/kWh, the LCOH further increases to $8.562/kg, representing an 11.48% increase compared to the lower current density and an 86.97% increase compared to the baseline.

For the 5000 kW system with 10,000 A/m^2 and LCOE = $0.05/kWh, the system requires a total cell area of 207.2 m² with a system efficiency of 60.5%. This system produces 11,430 tonnes of hydrogen over its lifetime, with CapEx and OpEx calculated as $9.532 million and $37.23 million, respectively, resulting in an LCOH of $4.091/kg. Doubling the LCOE increases the OpEx to $74.46 million and the LCOH to $7.348/kg, representing a 79.61% increase. Doubling the current density reduces the required cell area to 84.67 m², with system efficiency dropping to 49.4%. The LCOH in this case rises to $4.401/kg, reflecting a 7.57% increase. When both the current density and LCOE are doubled, the LCOH increases to $8.385/kg, a rise of 11.19% compared to the lower current density and 90.54% compared to the baseline.

For the 10,000 kW system with 10,000 A/m^2 and LCOE = $0.05/kWh, the system requires a total cell area of 414.3 m² and a system efficiency of 60.5%. Over its lifetime, this system produces 22,860 tonnes of hydrogen, with CapEx and OpEx calculated as $16.38 million and $74.46 million, respectively, resulting in an LCOH of $3.973/kg. When the LCOE is doubled, the OpEx doubles to $148.9 million, increasing the LCOH to $7.230/kg, a rise of 81.98%. Doubling the current density reduces the cell area to 169.3 m², with system efficiency dropping to 49.4%. The LCOH increases slightly to $4.342/kg, representing a 9.29% rise. When both the current density and LCOE are doubled, the LCOH further increases to $8.327/kg, an increase of 14.97% compared to the lower current density and 91.71% compared to the baseline.

The following results summarize the observed changes in CapEx, OpEx, and LCOH when the current density is doubled (from 10,000 A/m² to 20,000 A/m²) and when the LCOE is doubled (from $0.05/kWh to $0.1/kWh). These analyses reveal the sensitivities of hydrogen production costs to operational and economic parameters across different system capacities.

While, Table 3.3 shows the changes observed when the current density is doubled, Table 3.4 shows the changes observed when the LCOE is doubled.

Table 3.3 List of Changes on CapEx with Doubled Current Density

System (kW)	CapEx Change ($M)	CapEx % Change	LCOH Change ($/kg)	LCOH % Change
25	-0.09	-59.21%	-0.603	-10.19%
100	-0.265	-59.02%	-0.255	-4.88%
1000	-1.604	-59.14%	0.134	3.02%
5000	-5.636	-59.13%	0.31	7.58%
10,000	-9.685	-59.13%	0.369	9.29%

Table 3.4 List of Changes on OpEx with Doubled LCOE

System (kW)	OpEx Change ($M)	OpEx % Change	LCOH Change ($/kg)	LCOH % Change
25	0.186	100%	3.257	55.04%
100	0.745	100%	3.257	62.38%
1000	7.446	100%	3.257	73.31%
5000	37.23	100%	3.257	79.61%
10,000	74.46	100%	3.257	81.98%

The tables 3.5 and 3.6 summarize the changes in total costs (CapEx + OpEx) and LCOH for various system capacities (25 kW to 10,000 kW) under two scenarios: (1) when the current density is doubled (from 10,000 A/m² to 20,000 A/m²), and (2) when the LCOE is doubled (from $0.05/kWh to $0.1/kWh). These results illustrate how operational and economic parameters influence both total costs and hydrogen production costs (LCOH). Doubling the Current Density results in a significant reduction in total costs across all systems, especially for smaller capacities. However, LCOH exhibits mixed behavior, decreasing for smaller systems but slightly

increasing for larger ones due to efficiency trade-offs. Doubling the LCOE leads to significant increases in both total costs and LCOH, with larger systems experiencing greater proportional and absolute impacts due to their higher energy consumption.

Table 3.5 List of Changes on Total Costs with Doubled Current Density

System (kW)	Total Cost ($M, 10k A/m², LCOE=0.05)	Total Cost ($M, 20k A/m², LCOE=0.05)	Change in Total Cost ($M)	Percentage Change (%)	LCOH ($/kg, 10k A/m²)	LCOH ($/kg, 20k A/m²)
25	0.338	0.248	-0.09	-26.63%	5.918	5.315
100	1.194	0.928	-0.266	-22.28%	5.221	4.966
1000	10.158	8.554	-1.604	-15.79%	4.443	4.577
5000	46.762	41.126	-5.636	-12.05%	4.091	4.401
10,000	90.84	81.155	-9.685	-10.66%	3.973	4.342

Table 3.6 List of Changes on Total Costs with Doubled LCOE

System (kW)	Total Cost ($M, LCOE = 0.05)	Total Cost ($M, LCOE = 0.1)	Change in Total Cost ($M)	Percentage Change (%)	LCOH ($/kg, LCOE = 0.05)	LCOH ($/kg, LCOE = 0.1)
25	0.338	0.524	0.186	55.03%	5.918	9.175
100	1.194	1.938	0.744	62.31%	5.221	8.478
1000	10.158	17.602	7.444	73.28%	4.443	7.7
5000	46.762	83.992	37.23	79.62%	4.091	7.348
10,000	90.84	165.28	74.44	81.95%	3.973	7.23

The following twelve graphs present the analyses and comparisons of solutions performed using EES software. These graphs examine key parameters of the hydrogen production system, such as levelized cost of hydrogen, energy consumption, production rate, and economic performance, to identify the optimal operating points for cost optimization. Each graph provides a detailed evaluation of different operating conditions and illustrates the impact of various parameters on system performance, offering valuable insights into achieving both efficiency and economic feasibility.

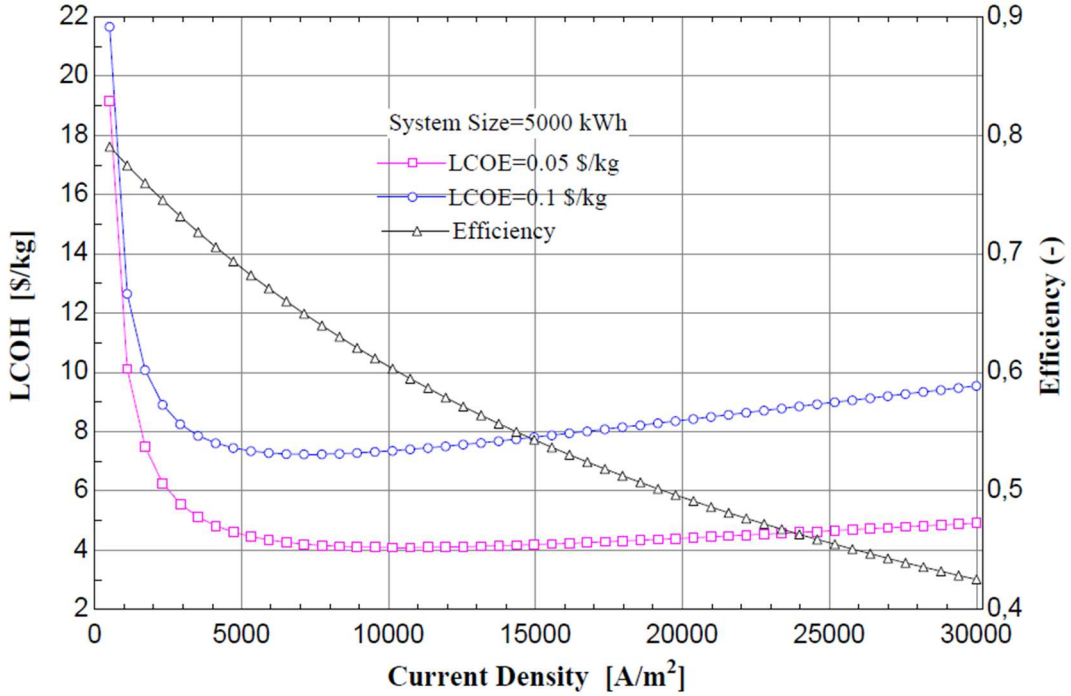

Figure 3.8 LCOH and Efficiency vs. Current Density Curve for Fixed System Size

The presented graph highlights the relationship between cell current density I_{cell}, Levelized Cost of Hydrogen (LCOH), and hydrogen production efficiency. As the current density increases, LCOH initially decreases due to improved utilization of system capacity and reduced relative fixed costs. However, beyond a certain point, the efficiency starts to decline significantly because of increased energy losses, such as ohmic resistance and overpotentials, leading to diminishing returns in cost reduction. The optimal operating range for the system appears to be between 8000-12000 A/m², where a balance between low LCOH and reasonable efficiency is achieved. In this range, LCOH values for low LCOE value are around 4$/kg. The analysis further demonstrates that electricity cost (LCOE) plays a critical role in determining the overall hydrogen production cost. For instance, systems operating with a lower LCOE of 0.05 $/kWh achieve significantly reduced LCOH compared to those with a higher LCOE of 0.1 $/kWh. This underscores the importance of optimizing both current density and electricity costs to ensure economically viable and energy-efficient hydrogen production.

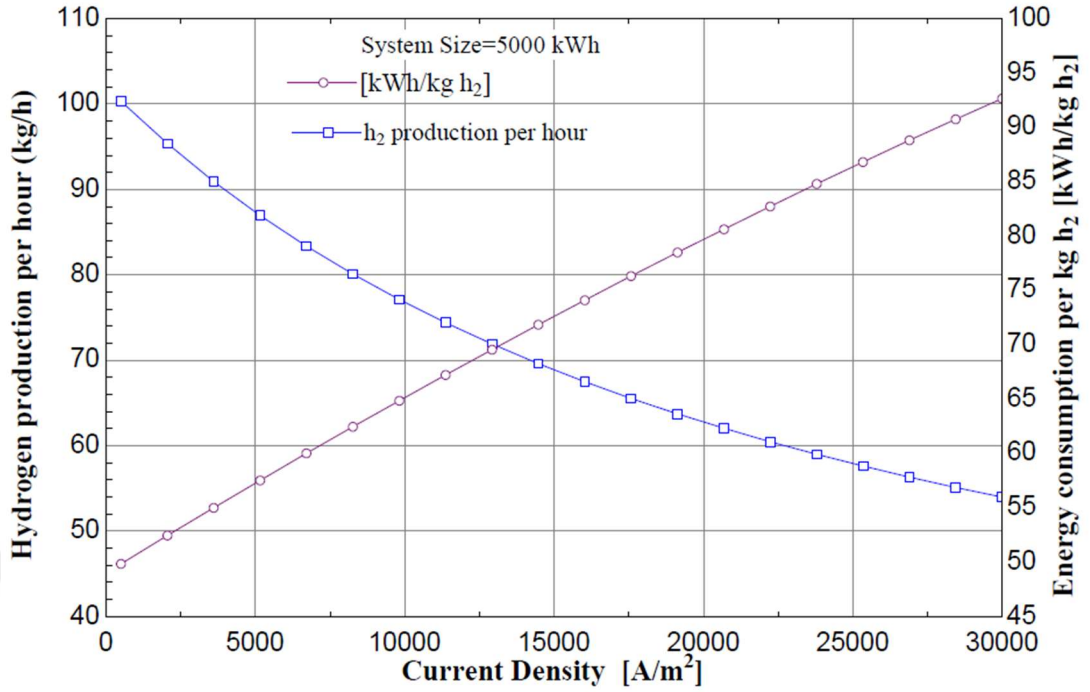

Figure 3.9 H_2 rate and Energy consumption vs. Current Density Curve for Fixed System Size

This graph illustrates the relationship between current density and two key parameters for a system size of 5000 kWh: hydrogen production rate and energy consumption per kilogram of hydrogen. As the current density increases, the hydrogen production rate (blue line) initially rises, reflecting the enhanced production capacity due to higher current input. However, after a certain point, the hydrogen production rate begins to stabilize and eventually decreases slightly, likely due to inefficiencies arising from increased ohmic losses and reduced system efficiency at very high current densities. Conversely, the energy consumption per kilogram of hydrogen (pink line) increases linearly with current density. This trend indicates that operating at higher current densities requires more energy per unit of hydrogen produced, which could significantly impact operational costs.

The graph highlights the trade-off between production capacity and energy efficiency. While higher current densities may increase short-term production, they come at the cost of greater energy consumption per kilogram of hydrogen. Therefore, identifying an optimal current density that balances hydrogen production rate and energy efficiency is critical for cost-effective and sustainable system operation.

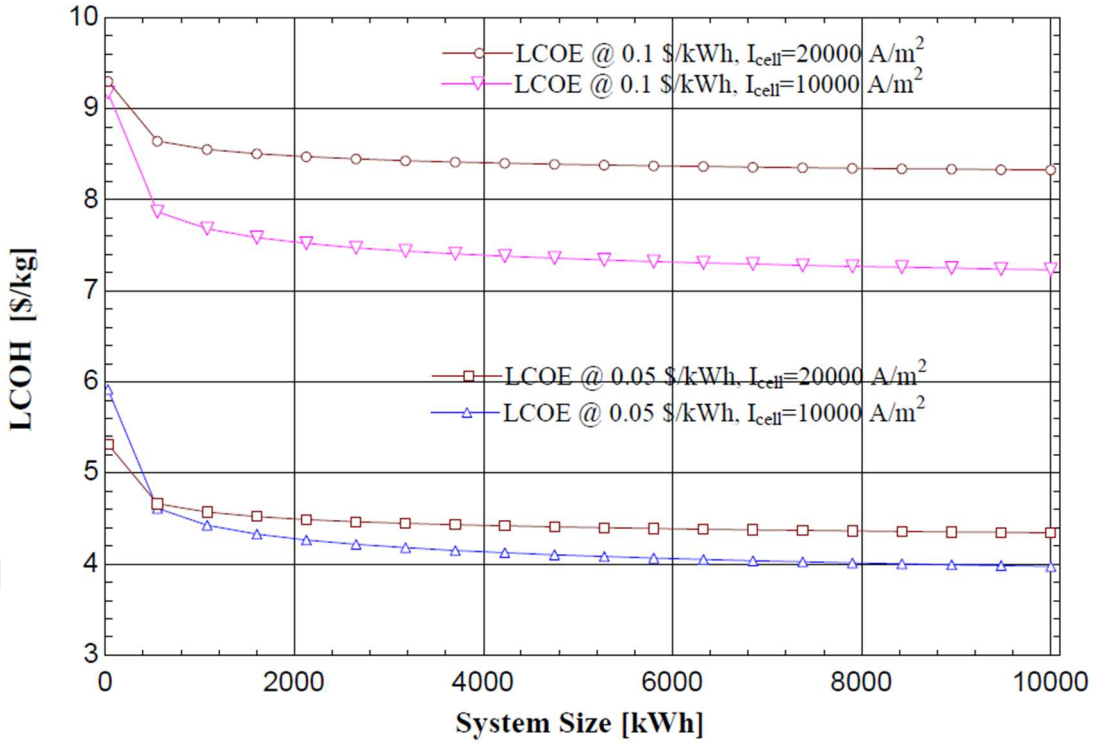

Figure 3.10 LCOH vs. System Size Curve for Different Current Densities and LCOE

The graph depicts the variation of Levelized Cost of Hydrogen (LCOH) as a function of system size under different operating conditions, specifically two electricity cost scenarios (LCOE = 0.05 $/kWh and 0.1 $/kWh) and two current densities 10,000 A/m^2 and 20,000 A/m^2). The results show that LCOH decreases with increasing system size due to economies of scale, although this reduction stabilizes beyond approximately 2000–4000 kWh, indicating diminishing returns. Systems with a lower LCOE consistently exhibit significantly reduced LCOH, highlighting the critical role of electricity costs in hydrogen production. Additionally, higher current densities (20,000 A/m^2) result in marginally higher LCOH due to efficiency losses associated with increased ohmic resistance. This analysis underscores the importance of optimizing system size, electricity cost, and current density to achieve economically viable hydrogen production.

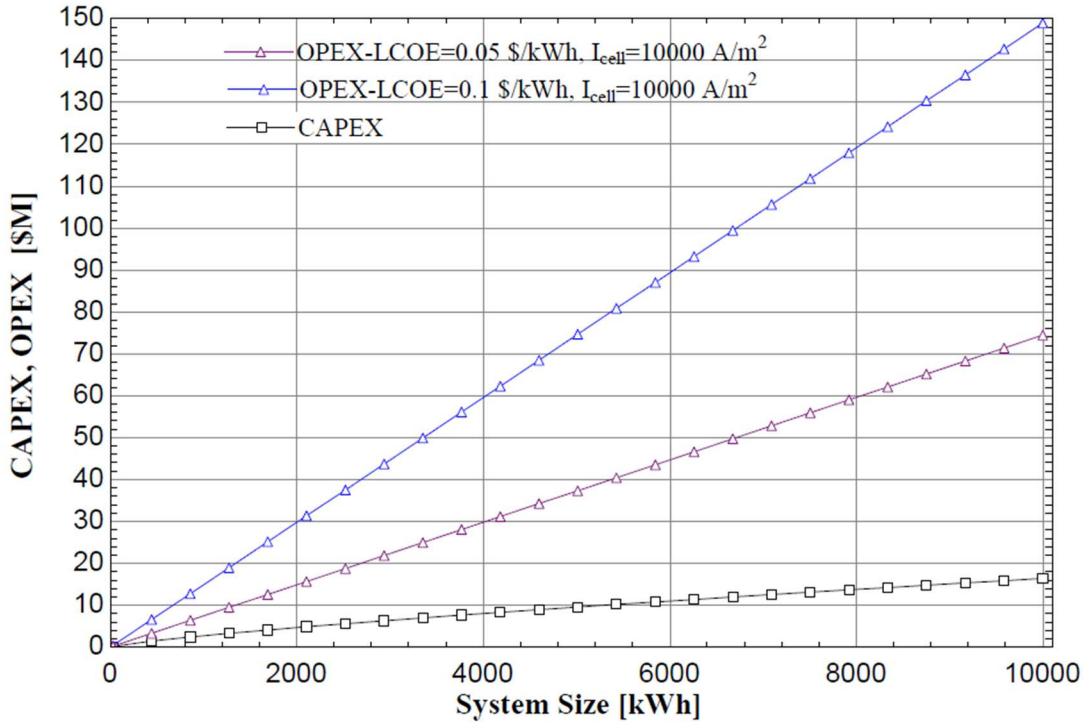

Figure 3.11 CapEx and OpEx vs. System Size Curve for Different Current Densities and LCOE

The graph presents the relationship between system size (kWh), capital expenditures (CapEx), and operational expenditures (OpEx) for two electricity cost scenarios: LCOE = 0.05 $/kWh and LCOE = 0.1 $/kWh, at a constant current density (10,000 A/m^2). CapEx remains relatively constant and increases linearly with system size, but its contribution is significantly lower compared to OpEx. On the other hand, OpEx shows a steep linear increase as the system size grows, with higher values observed at LCOE = 0.1 $/kWh due to the increased cost of electricity. In contrast, at LCOE = 0.05 $/kWh, OpEx values are substantially lower, reflecting the critical impact of electricity costs on operational expenses. This analysis highlights that while CapEx is relatively stable and predictable, reducing LCOE is essential for minimizing long-term operational costs, making electricity cost the dominant factor in determining the economic feasibility of hydrogen production systems.

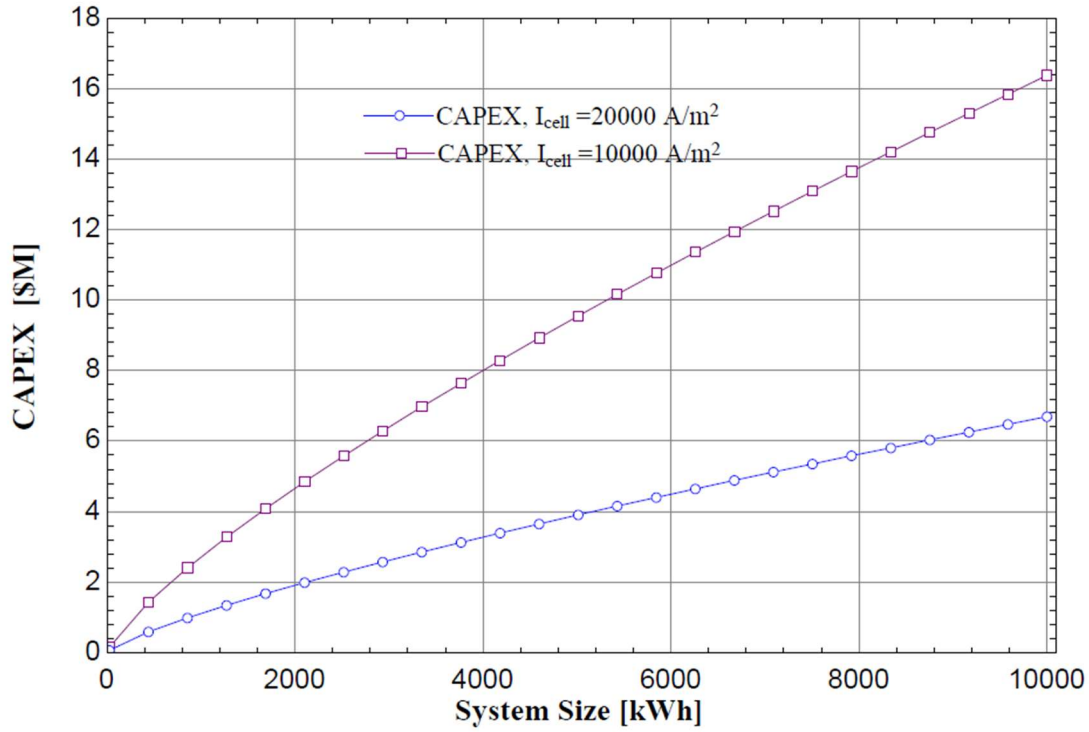

Figure 3.12 CapEx vs. System Size Curve for Different Current Densities

The graph illustrates the relationship between system size (kWh) and capital expenditures (CapEx) at two current densities: 10,000 A/m^2 and 20,000 A/m^2. CapEx increases linearly with system size for both scenarios, but the magnitude of CapEx is significantly higher for the lower current density (10,000 A/m^2) compared to the higher current density (20,000 A/m^2). This trend highlights the impact of current density on system design and cost, as lower current densities require larger electrode areas, thereby increasing the capital investment.

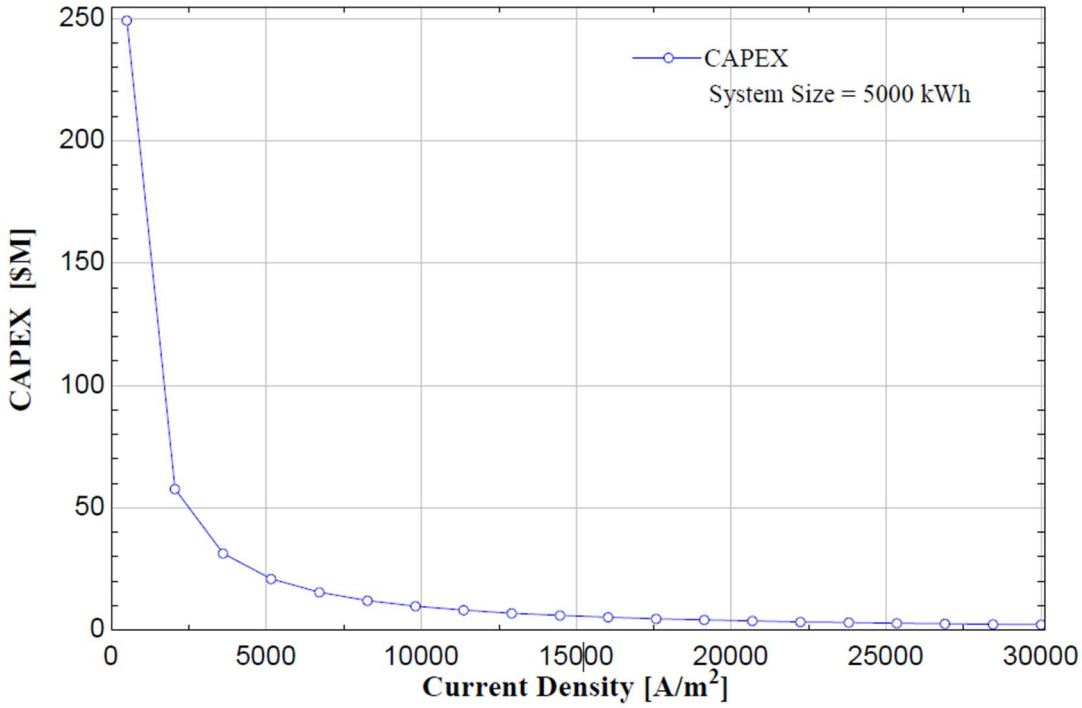

Figure 3.13 CapEx vs. Current Density Curve for Fixed System Size

The graph shows the relationship between current density and capital expenditures (CapEx) for a system size of 5000 kWh. CapEx decreases sharply as the current density increases, especially in the lower range of current density values (0–5000 A/m^2). Beyond approximately 10,000 A/m^2, the rate of decrease slows significantly, and CapEx begins to stabilize at relatively low levels.

This trend highlights the inverse relationship between current density and electrode area requirements. At low current densities, larger electrode areas are needed to accommodate the reduced current, resulting in higher capital costs. Conversely, higher current densities reduce the required electrode area, leading to significant CapEx reductions. However, increasing current density beyond a certain point may introduce trade-offs, such as higher operational costs and reduced efficiency due to increased resistive losses.

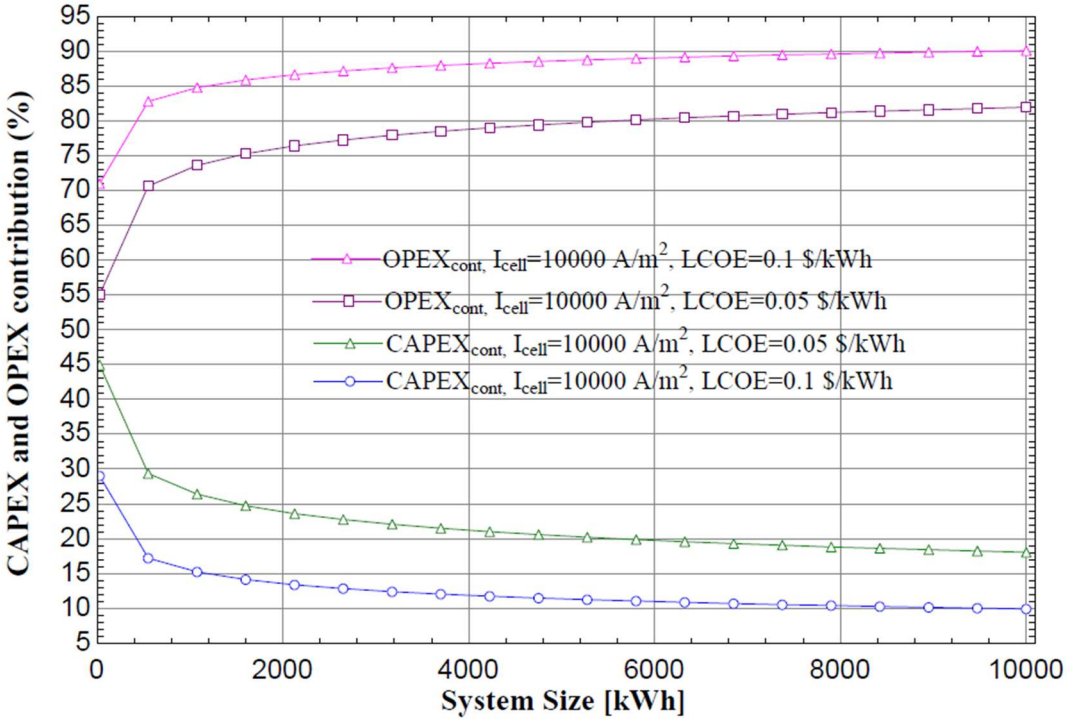

Figure 3.14 CapEx and OpEx contribution vs System Size Curve for Different LCOE

The graph illustrates the percentage contributions of CapEx and OpEx to the total cost of hydrogen production as a function of system size, under different LCOE scenarios (LCOE=0.1 $/kWh and 0.05 $/kWh) at a constant current density (10,000 A/m^2). The results reveal that OpEx dominates the total cost, particularly at higher LCOE values (0.1 $/kWh), where it accounts for up to 90% of the total cost, stabilizing as system size increases. At lower LCOE values (0.05 $/kWh), OpEx remains the largest cost component, contributing approximately 75–80% for large-scale systems. Conversely, CapEx has a significantly lower contribution, decreasing with system size and stabilizing around 10–25% depending on the LCOE. These trends highlight the critical role of electricity costs in hydrogen production economics, with OpEx being the dominant factor, particularly for large systems. The findings emphasize the need for reducing LCOE to achieve cost-effective hydrogen production, as CapEx plays a diminishing role in total costs at larger scales.

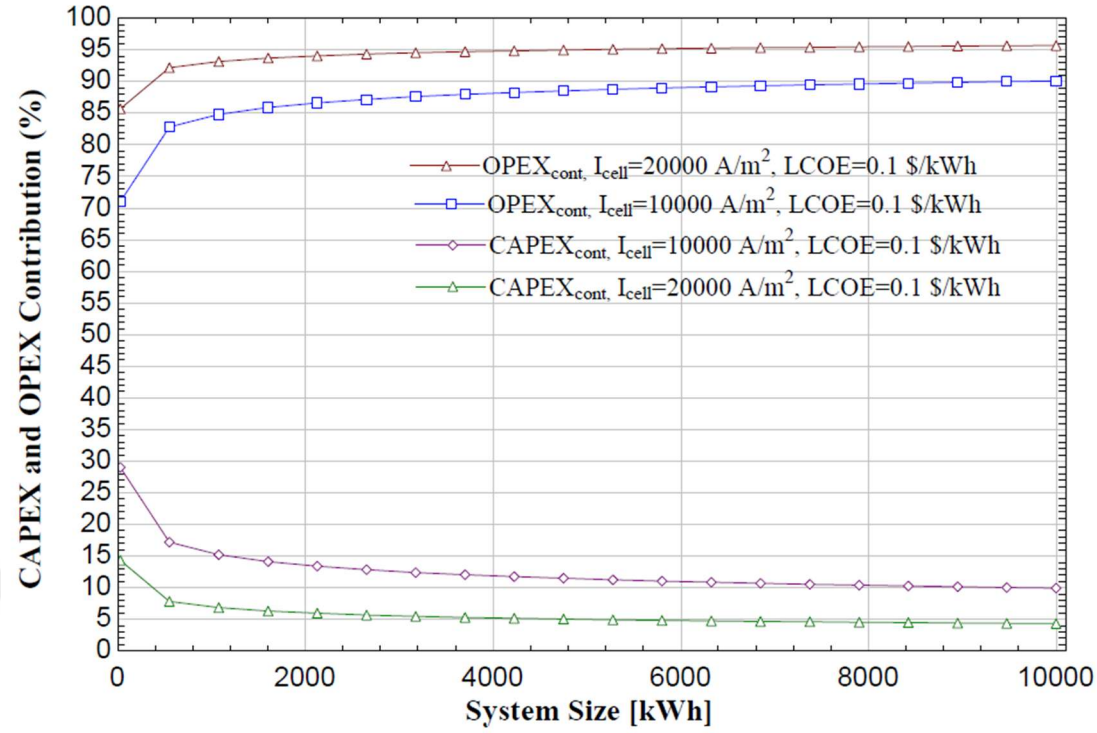

Figure 3.15 CapEx and OpEx contribution vs System Size Curve for Different Current Densities

This graph, in conjunction with the previous one, provides a comprehensive perspective on the contributions of CapEx and OpEx to the total cost of hydrogen production, considering variations in both current density and LCOE. As observed, OpEx remains the dominant cost factor across all system sizes, with its contribution exceeding 95% at higher current densities (20,000 A/m^2) and stabilizing slightly lower for I_{cell}=10,000 A/m^2. Lower LCOE values (0.05 $/kWh) in the previous graph demonstrate a significant reduction in OpEx, reinforcing the critical role of electricity prices in hydrogen production economics. CapEx, in contrast, diminishes in importance as system size increases, with its contribution dropping below 5% at I_{cell}=20,000 A/m^2 and stabilizing at approximately 10% for I_{cell}=10,000 A/m^2. Higher current densities reduce CapEx significantly due to smaller electrode areas required, but slightly increase OpEx due to efficiency losses. When considering LCOE, systems operating at 0.05 $/kWh (as shown previously) exhibit better cost distribution, with OpEx and CapEx contributions more balanced compared to systems at 0.1 $/kWh. These findings underscore the necessity of optimizing both current density and electricity cost to achieve a balance between CapEx and OpEx, ensuring scalable and economically viable hydrogen production systems.

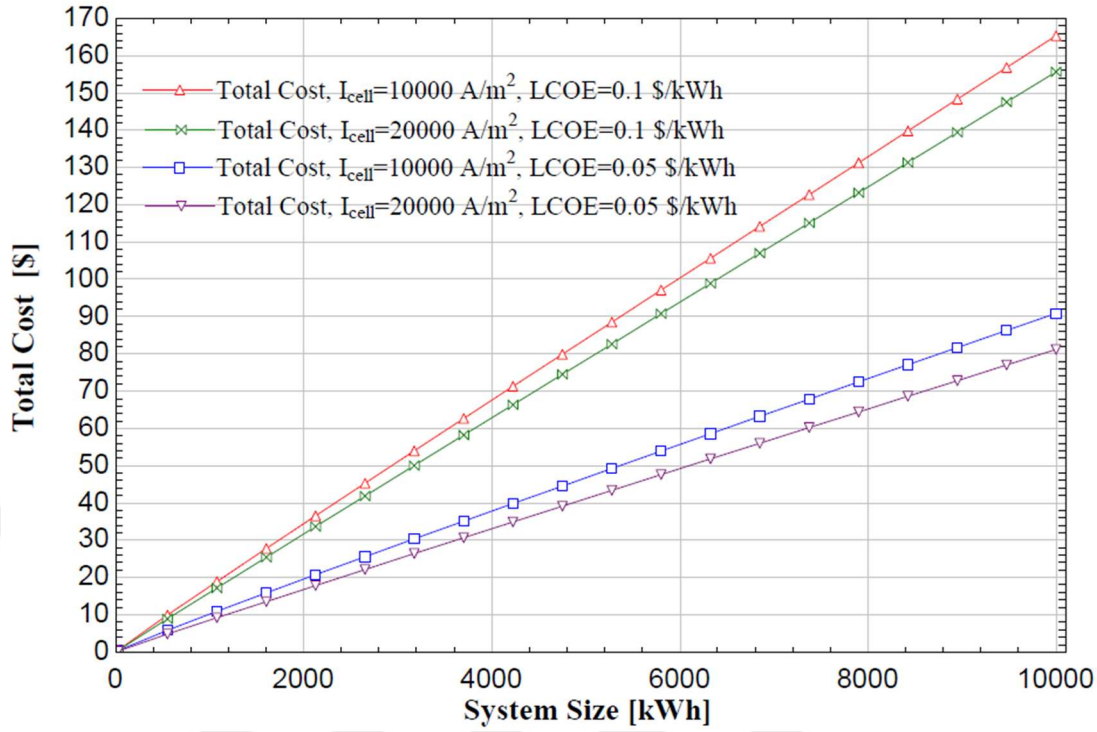

Figure 3.16 Total Cost vs System Size Curve for Different Current Densities and LCOE

This graph presents the total cost of hydrogen production as a function of system size (kWh), considering different combinations of current densities (10,000 A/m^2 and 20,000 A/m^2) and electricity costs (0.1 $/kWh and 0.05 $/kWh). The results indicate a linear increase in total cost with system size across all scenarios, with the magnitude of the cost primarily influenced by the LCOE and, to a lesser extent, by the current density.

At higher LCOE values (0.1 $/kWh), the total cost is significantly higher, with the 10,000 A/m^2 current density configuration showing the highest costs due to its larger CapEx contribution. Conversely, systems with lower LCOE values (0.05 $/kWh) exhibit substantially lower total costs, highlighting the critical role of electricity prices in reducing overall hydrogen production expenses. Within the same LCOE scenarios, higher current densities (20,000 A/m^2) result in lower total costs compared to 10,000 A/m^2 current density, primarily due to reduced CapEx requirements.

This comparison underscores the importance of optimizing both LCOE and current density to minimize the total cost of hydrogen production. Lower electricity prices

and higher current densities prove to be effective strategies for achieving economic scalability in hydrogen production systems.

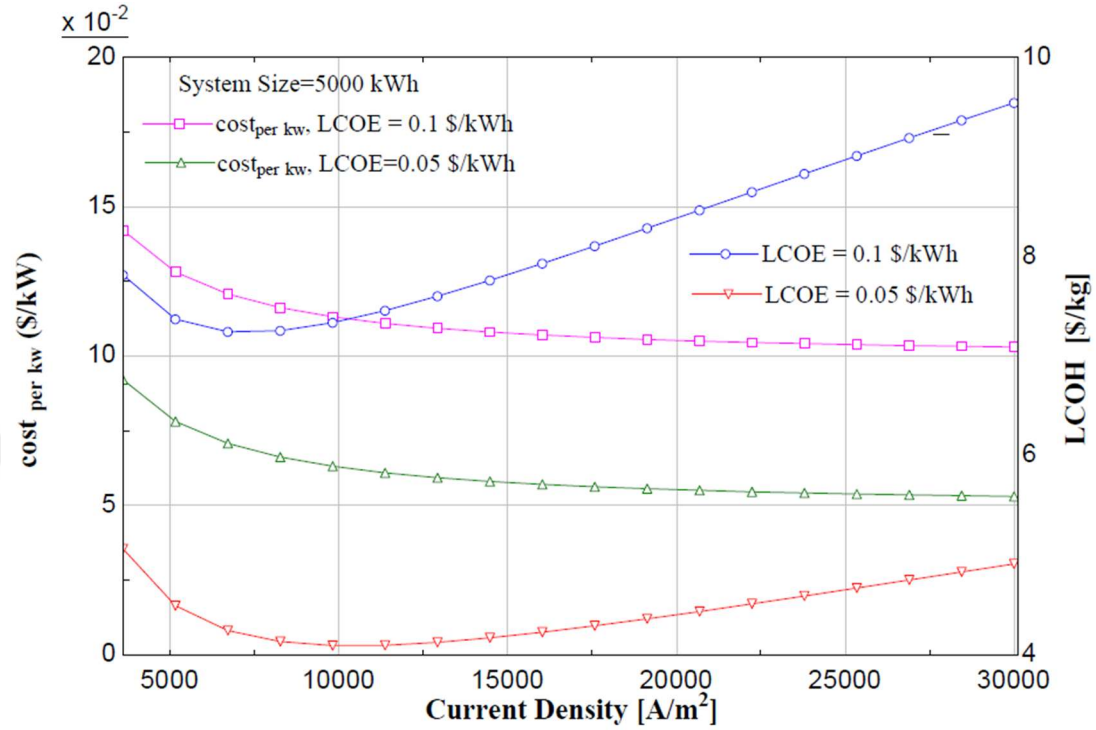

Figure 3.17 Cost per energy consumption and LCOH vs Current Density Curve for Different LCOE

The graph evaluates the cost per unit energy consumption (cost per kw) and (LCOH) under varying current densities and LCOE scenarios. The cost per unit energy consumption provides an economic efficiency metric by analyzing the total system cost relative to the energy consumed.

In the case of low LCOE , the cost per kw starts at a higher value, decreases with increasing current density, and stabilizes around the range of 8,000 – 13,000 A/m^2, where the system achieves its optimal cost efficiency. Conversely, for high LCOE, the cost per kw begins at a higher value and, after a slight decrease, increases again beyond 10,000 A/m^2, indicating the significant impact of higher electricity costs on operational expenses.

The LCOH trends align with LCOE variations. For LCOE=0.05 $/kWh, the LCOH remains relatively low and stable as current density increases. However, under LCOE=0.1 $/kWh, the LCOH exhibits a linear increase with increasing current

density, emphasizing the direct influence of electricity costs on total production costs.

In summary, this graph highlights the critical role of the cost per unit energy consumption metric in evaluating system design and optimizing energy costs. Operating under lower LCOE values and within an optimal current density range (8,000–13000 A/m^2) minimizes both cost per kw and LCOH, ensuring sustainable and economically feasible hydrogen production. This analysis underscores the necessity of reducing LCOE and optimizing current density for cost-effective system performance.

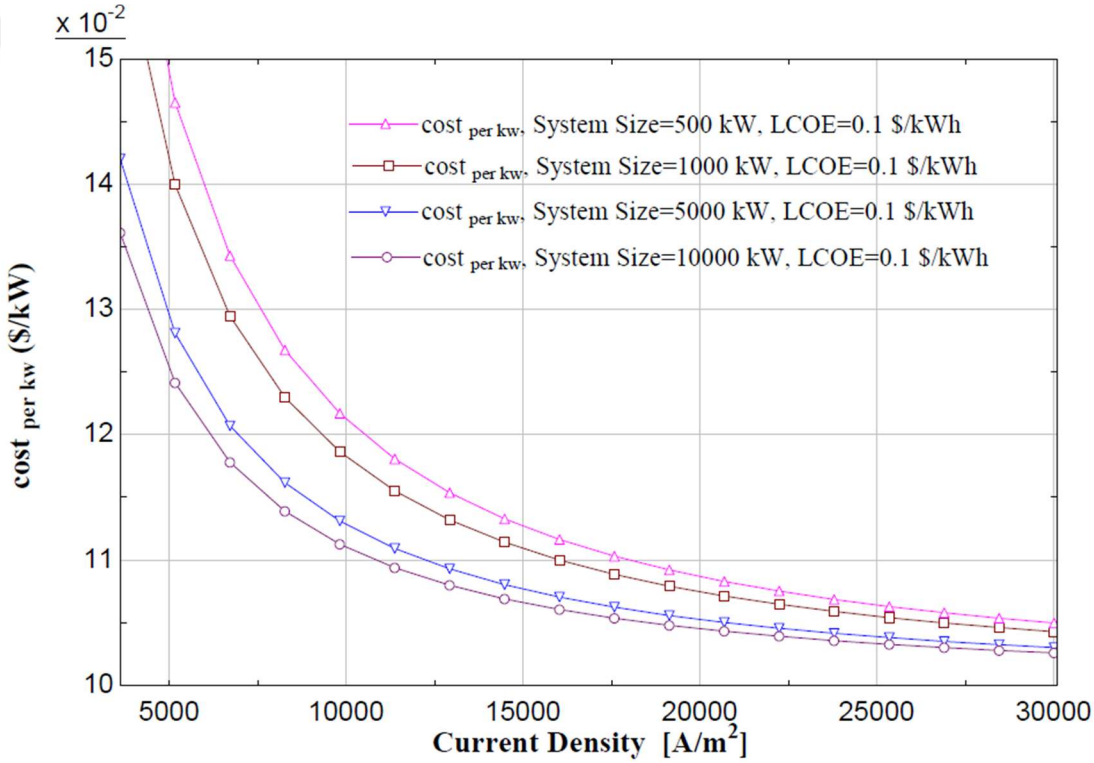

Figure 3.18 Cost per energy consumption vs Current Density Curve for Different System Size

The graph illustrates the relationship between cost per unit energy consumption (cost per kw) and current density for different system sizes (500 kW, 1000 kW, 5000 kW, and 10,000 kW) under a fixed LCOE of 0.1 $/kWh. As current density increases, cost per kw decreases significantly across all system sizes due to reduced electrode area requirements, which lower CapEx. This cost reduction stabilizes beyond 10,000–15,000 A/m^2, marking the optimal current density range where energy

consumption costs are minimized. Larger system sizes exhibit consistently lower cost per kw due to economies of scale, highlighting their cost-effectiveness compared to smaller systems. These results emphasize the importance of optimizing current density and leveraging system size to achieve economically sustainable hydrogen production, with larger systems and an optimal current density range offering the most significant cost advantages.

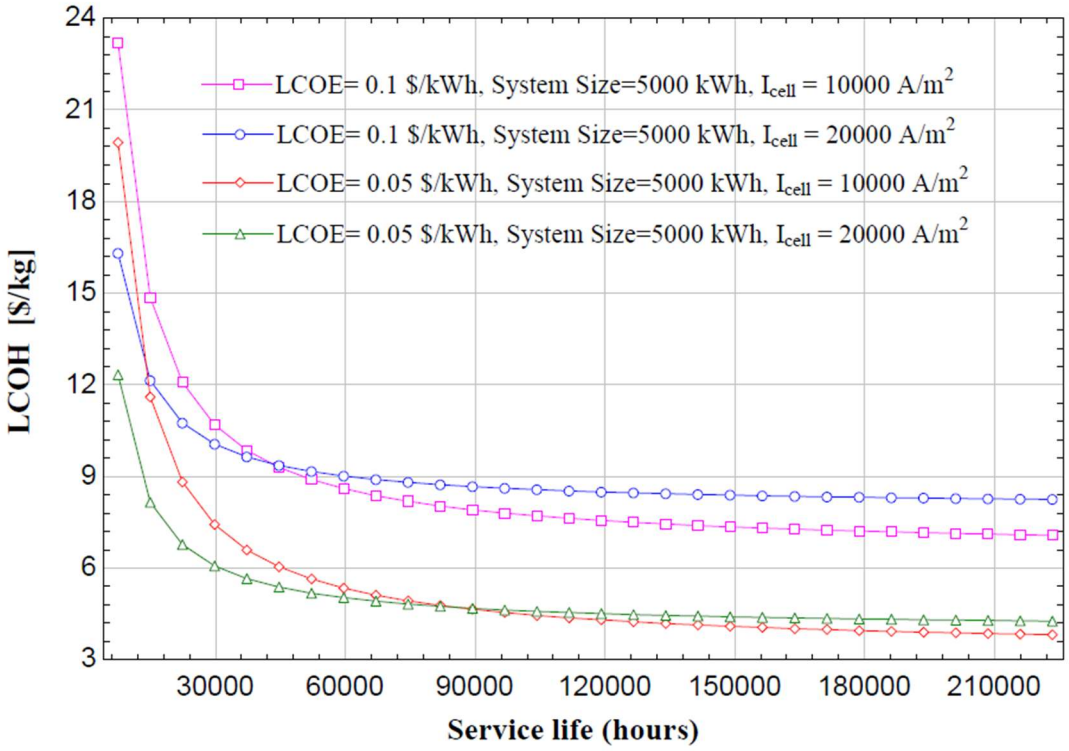

Figure 3.19 LCOH vs Service Life Curve for Different System Size, Current Density and LCOE

The graph illustrates the relationship between LCOH, and service life (hours) for different LCOE values (0.1 $/kWh and 0.05 $/kWh) and current densities (10,000 A/m^2 and 20,000 A/m^2) for a fixed system size of 5000 kW. While standard calculations are based on a 20-year service life (148,920 hours, with the 85% capacity factor), this analysis extends the evaluation to 30 years (223,380 hours) to assess long-term performance. The results show that LCOH decreases sharply as the service life increases up to 20 years, primarily due to the amortization of CapEx. Beyond 20 years, the reduction rate slows significantly, indicating diminishing returns from extended operation. Systems with lower LCOE (0.05 $/kWh) and higher current densities (20,000 A/m^2) consistently achieve lower LCOH values, stabilizing

around 4–5 $/kg, compared to 9–10 $/kg for higher LCOE (0.1 $/kWh). This indicates that systems designed for low-cost electricity and optimized current density remain economically viable even with extended service lives, provided durability requirements are met.

The findings from this study highlight the critical relationships between key operational parameters, such as current density, system size, and electricity costs, and their impact on the Levelized Cost of Hydrogen (LCOH). In particular, the comparative analysis of different LCOE scenarios and current densities has provided valuable insights into the economic optimization of hydrogen production. The following bar charts summarize the key results, illustrating the trends in LCOH under varying conditions, including system size, current density, and electricity costs. These visualizations serve to reinforce the detailed discussions presented in the preceding sections and provide a comprehensive overview of the cost optimization potential for industrial-scale alkaline electrolyzers.

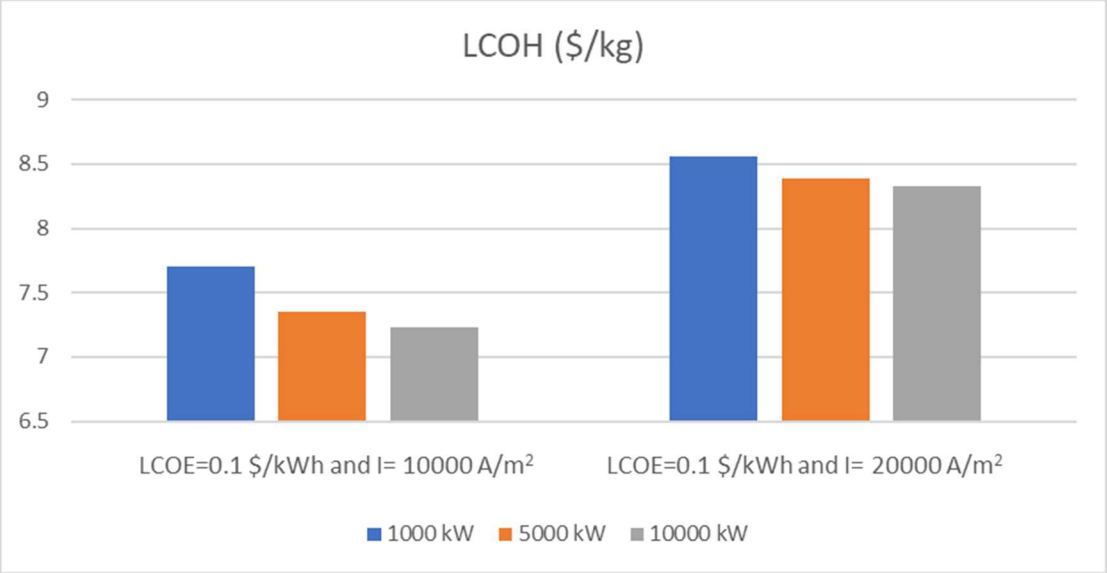

Figure 3.20 Impact of System Size and Current Density on LCOH

This chart compares the Levelized Cost of Hydrogen (LCOH) for different system sizes (1000 kWh, 5000 kWh, and 10,000 kWh) under two operating conditions: a current density of 10,000 A/m² and 20,000 A/m², with an electricity cost of $0.1/kWh.

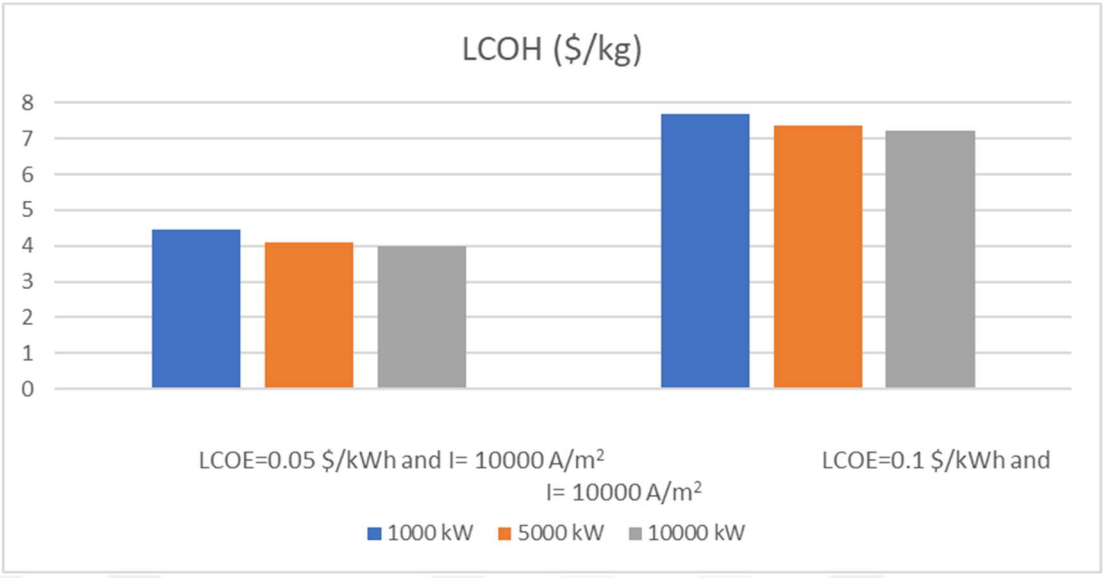

Figure 3.21 Influence of System Size and LCOE on LCOH

This chart presents the Levelized Cost of Hydrogen (LCOH) for varying system sizes (1000 kWh, 5000 kWh, and 10,000 kWh) under two electricity cost scenarios: $0.05/kWh and $0.1/kWh, with a current density of 10,000 A/m². The results indicate that for both electricity cost scenarios, an increase in system size leads to a reduction in LCOH due to the economies of scale. The graph underscores the importance of reducing electricity costs to achieve cost-effective hydrogen production, particularly for smaller system sizes where the relative impact of electricity costs is more pronounced. Additionally, scaling up the system size proves beneficial in minimizing the overall hydrogen production cost.

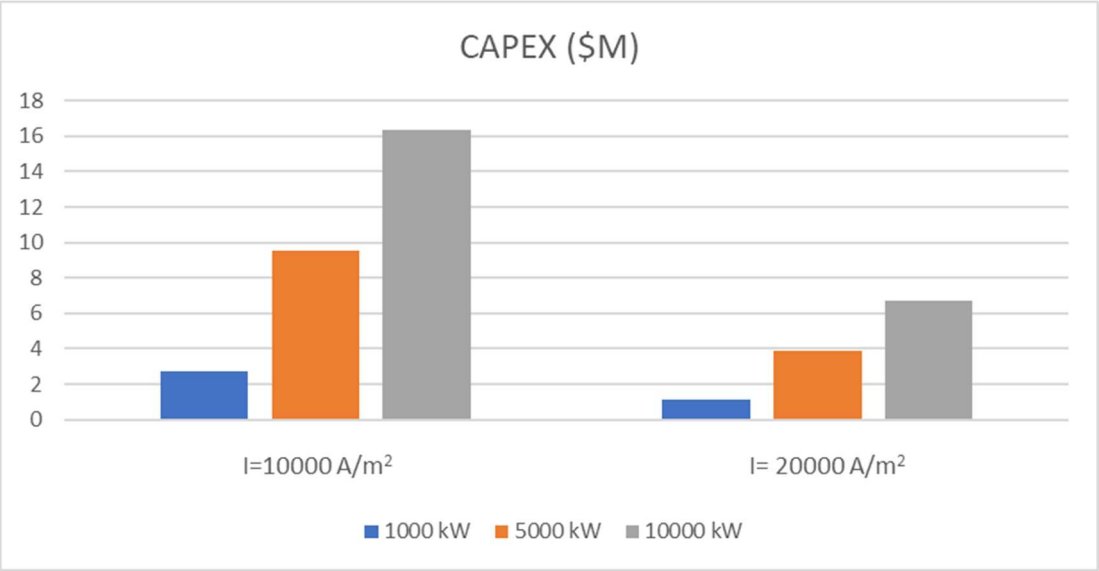

Figure 3.22 Impact of System Size and Current Density on CAPEX

Above chart illustrates the capital expenditure (CAPEX) for varying system sizes (1000 kWh, 5000 kWh, and 10,000 kWh) under two current density scenarios: 10,000 A/m² and 20,000 A/m². This graph emphasizes the substantial influence of system size on CAPEX, highlighting the trade-offs involved in scaling up hydrogen production. While higher current densities may reduce some capital costs, they can introduce operational challenges, necessitating careful optimization to balance CAPEX and overall system efficiency.

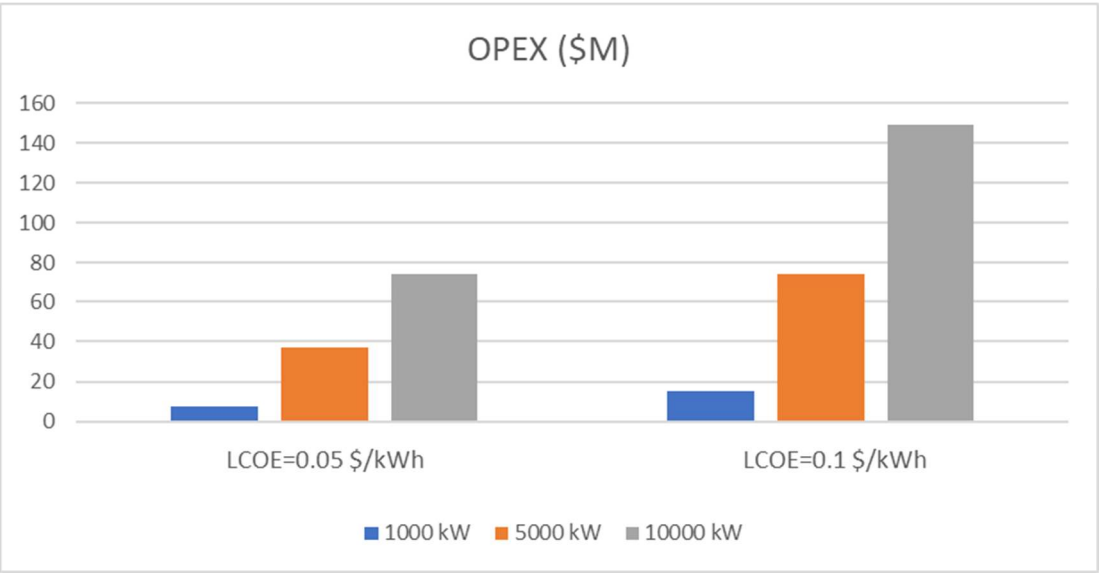

Figure 3.23 Effect of System Size and LCOE on OPEX

This chart shows the operational expenditure (OPEX) for varying system sizes (1000 kWh, 5000 kWh, and 10,000 kWh) under two electricity cost scenarios: $0.05/kWh and $0.1/kWh. The results highlight that OPEX increases significantly with both system size and electricity cost. This graph underscores the critical impact of electricity costs on OPEX in hydrogen production systems. These results emphasize the necessity of optimizing electricity procurement strategies to minimize overall production costs.

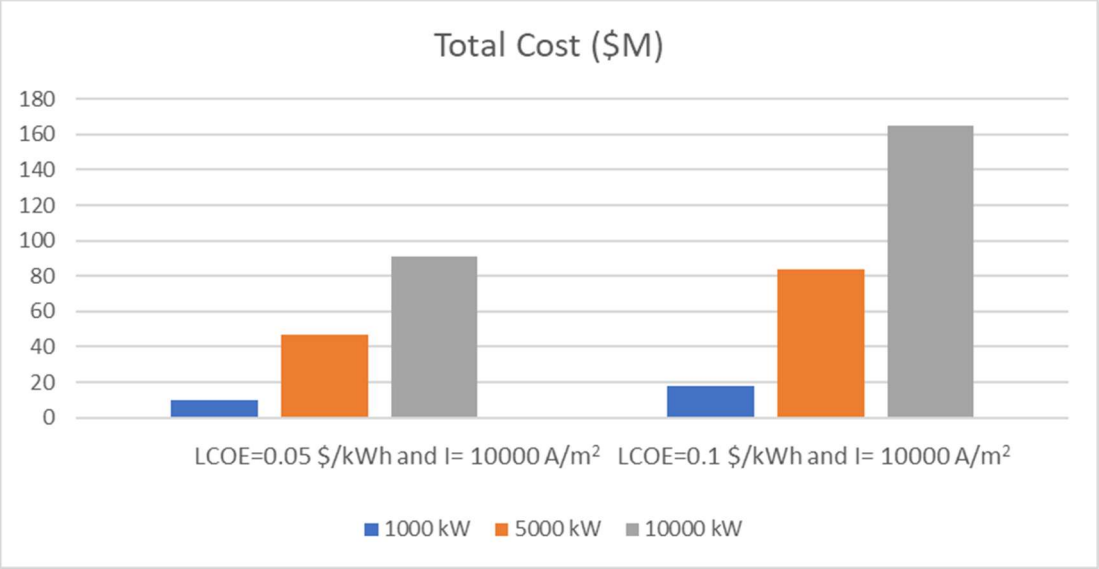

Figure 3.24 Impact of System Size and LCOE on Total Cost

The chart above illustrates the total cost of hydrogen production for varying system sizes (1000 kWh, 5000 kWh, and 10,000 kWh) under two electricity cost scenarios: $0.05/kWh and $0.1/kWh, with a current density of 10,000 A/m². The results show a significant increase in total cost with both system size and electricity cost. This graph highlights the compounded effect of system scaling and electricity price on overall production costs. While larger systems provide higher hydrogen output, the associated increase in both operational and capital expenditures drives up the total cost, especially under higher electricity price scenarios.

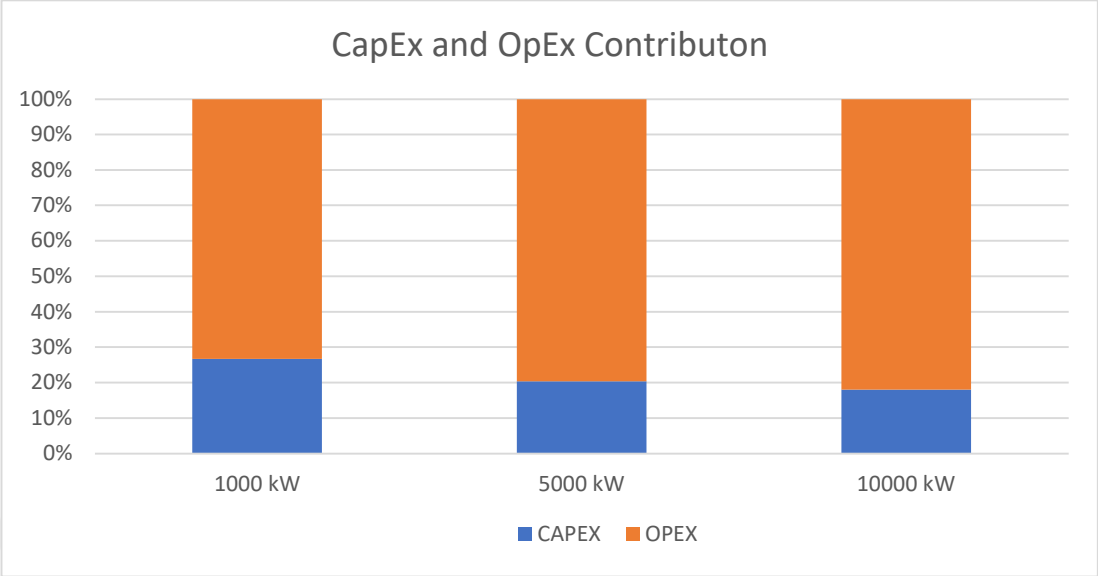

Figure 3.25 CapEx and OpEx Contributions to LCOH at Different System Sizes

This chart illustrates the contributions of CapEx and OpEx to the Levelized Cost of Hydrogen (LCOH) for varying system sizes, ranging from 1000 kWh to 10,000 kWh, under operating conditions of 10,000 A/m² and an electricity cost of $ 0.05/kWh.

CHAPTER 4- CONCLUSIONS AND RECOMMONDATIONS

4.1. Conclusions

This study integrates electrochemical modeling in COMSOL Multiphysics with cost optimization in the Engineering Equation Solver (EES) to comprehensively evaluate the performance and cost-effectiveness of alkaline water electrolyzers. Through systematic analysis, 20 different simulations were conducted in COMSOL by varying key parameters such as temperature, electrode-separator distance, separator porosity, and electrolyte concentration and solution. The results of these simulations were used to generate current-voltage (I-V) curves, providing a detailed understanding of how each parameter influences system performance.

Among the analyzed parameters, temperature and porosity were identified as having the most significant impact on system performance. For instance, increased temperature enhanced reaction rates and reduced energy consumption, while higher porosity improved ion flow and minimized ohmic resistance. These findings emphasize the critical role of these parameters in optimizing electrolyzer efficiency.

The simulation results from COMSOL were subsequently used as inputs for cost optimization calculations in EES. Real-world market data were utilized to calculate model and system factors, which served as a foundation for system scaling studies. Additionally, analyses were conducted for two different current densities and two distinct Levelized Cost of Electricity (LCOE) values across varying system capacities. These analyses provided the necessary data to calculate the Levelized Cost of Hydrogen (LCOH). The findings demonstrated that optimizing these parameters is essential for improving both performance and economic feasibility.

Key findings of this study include:

- Impact of Temperature and Porosity: Among all parameters, temperature and porosity exhibited the most significant influence on system performance, with direct effects on energy efficiency and current density.

- LCOE Sensitivity: The analyses revealed that LCOE is the dominant factor affecting LCOH, with lower electricity costs (e.g., $0.05/kWh) significantly reducing hydrogen production costs, particularly in large-scale systems.
- System Scaling and Optimization: Scaling studies based on real market data highlighted the trade-offs between capital and operational expenditures, emphasizing the need for system-specific designs to minimize overall costs.

This study provides a robust framework for evaluating alkaline water electrolyzers, offering valuable insights for system selection and optimization during the project development phase. By combining advanced electrochemical modeling with economic analyses, it establishes a pathway for designing systems that achieve the lowest possible LCOH under realistic market conditions.

4.2. Recommondations

Based on the findings of this study, several recommendations are proposed to further improve the performance and cost-effectiveness of alkaline water electrolyzers:

- Material Innovation:
    - Research and develop advanced electrode and separator materials to enhance conductivity and durability while reducing costs.
    - Explore non-precious metal catalysts and composite materials to improve energy efficiency and decrease capital expenditure (CapEx).
- Further Optimization of Temperature at High Pressures:
    - Conduct in-depth studies to determine the combined effects of temperature and high pressures on system performance. Investigate how elevated pressures influence reaction rates, energy efficiency, and hydrogen production capacity to identify optimal operating ranges for various conditions.
    - Develop control strategies to dynamically adjust these parameters for real-time performance optimization.
- Integration with Renewable Energy Sources:
    - Investigate the direct integration of electrolyzers with renewable energy sources (solar, wind) to address electricity cost variability.

  - Assess the use of hybrid systems or energy storage solutions to stabilize operations during fluctuations in power supply.
- Lifecycle and Sustainability Assessments:
  - Perform comprehensive lifecycle analyses to evaluate the environmental impact, recyclability, and resource efficiency of electrolyzer components.
- Scaling Studies for Industrial Applications:
  - Validate the findings of this study through large-scale experimental and simulation-based analyses to assess the economic and technical viability of industrial-scale systems..
- Policy and Market Integration:
  - Explore the impact of government incentives and market regulations on the adoption of alkaline electrolyzers, aligning design and cost optimizations with future policy frameworks.

REFERENCES

[1] Megia, P. J. & Vizcaino, A. J. & Calles, J. A. & Carrero, A. , “Hydrogen Production Technologies: From Fossil Fuels toward Renewable Sources. A Mini Review” Energy and Fuels,. American Chemical Society, 2021.

[2] Brockway, P. E. & Owen, A. & Brand-Correa, L. I. & Hardt, L. , “Estimation of Global Final-Stage Energy-Return-on-Investment for Fossil Fuels with Comparison to Renewable Energy Sources” Nat. Energy, 4 (7), 612–621, 2019.

[3] Shindell, D. & Smith, C. J. , “Climate and Air-Quality Benefits of a Realistic Phase-out of Fossil Fuels” Nature, 573 (7774), 408–411, 2019.

[4] Chun, Y. N. & Yang, Y. C. & Yoshikawa, K. , “Hydrogen Generation from Biogas Reforming Using a Gliding Arc Plasma-Catalyst Reformer” Catal. Today, 148 (3–4), 283–289, 2009.

[5] Nikolaidis, P. & Poullikkas, A. , “A Comparative Overview of Hydrogen Production Processes” Renew. Sustain. Energy Rev.,. Elsevier Ltd 2017.

[6] Ursúa, A. & Gandía, L. M. & Sanchis, P. , “Hydrogen Production from Water Electrolysis: Current Status and Future Trends” Proc. IEEE, 100, 410–426. Institute of Electrical and Electronics Engineers Inc., 2012.

[7] Muazzam, Y. & Yousaf, M. & Zaman, M. & Elkamel, A. & Mahmood, A. & Rizwan, M. & Adnan, M. , “Thermo-Economic Analysis of Integrated Hydrogen, Methanol and Dimethyl Ether Production Using Water Electrolyzed Hydrogen” Resources, 11 (10), 2022.

[8] Rashid, M. M. & Mesfer, M. K. Al & Naseem, H. & Danish, M. , “Hydrogen Production by Water Electrolysis: A Review of Alkaline Water Electrolysis, PEM Water Electrolysis and High Temperature Water Electrolysis” Int. J. Eng. Adv. Technol., no. 3, 2249–8958, 2015.

[9] Martinez Lopez, V. A. & Ziar, H. & Haverkort, J. W. & Zeman, M. & Isabella, O. , “Dynamic Operation of Water Electrolyzers: A Review for Applications in

Photovoltaic Systems Integration" Renew. Sustain. Energy Rev., 182 (August), 113407, 2023.

[10] El-Emam, R. S. & Özcan, H. , "Comprehensive Review on the Techno-Economics of Sustainable Large-Scale Clean Hydrogen Production" J. Clean. Prod., Elsevier Ltd 2019.

[11] Gambou, F. & Guilbert, D. & Zasadzinski, M. & & Rafaralahy, H. , "A Comprehensive Survey of Alkaline Electrolyzer Modeling: Electrical Domain and Specific Electrolyte Conductivity" Energies, MDPI 2022.

[12] Zoulias, E. & Varkaraki, E. & Lymberopoulos, N. & Christodoulou, C. N. & Karagiorgis, G. N. , "A Review On Water Electrolysis", *Tcjst*, *4*(2), 41-71, 2004

[13] Grigoriev, S. A. & Fateev, V. N. & Bessarabov, D. G. & & Millet, P. , "Current Status, Research Trends, and Challenges in Water Electrolysis Science and Technology" Int. J. Hydrogen Energy, 45 (49), 26036–58, 2020.

[14] Kreutert, W. & Hofmannz, H. , "Electrolysis: The Important Energy Transformer In A World Of Sustainable Energy" Int. Jour. of Hydrog. Energy,. Vol. 23(8), 661-666, 1998.

[15] Mei, W. & Sun, L. & Zhao, Y. "Overview of Hydrogen Energy and General Aspects of Water Electrolysis." Green Hydrogen Production by Water Electrolysis, CRC Press, 1-26, 2025.

[16] Santos, D. M. F. & Sequeira, C. A. C. & Figueiredo, J. L. , "Hydrogen Production By Alkaline Water Electrolysis" Quim. Nov., 36, 1176-1193, 2013.

[17] Harrison, K. & Levene, J.I. , "Electrolysis of Water" Solar hydrogen generation: toward a renewable energy future, 41-63, 2008.

[18] Shiva Kumar, S. & Lim, H. , "An Overview of Water Electrolysis Technologies for Green Hydrogen Production" Energy Reports, 8, 13793-13813, 2022.

[19] David, M. & Ocampo-Martínez, C. & & Sánchez-Peña, R. , “Advances in Alkaline Water Electrolyzers: A Review” J. Energy Storage, 23, 392-403, 2019.

[20] Horri, B. A. & Ozcan, H. , “Green Hydrogen Production by Water Electrolysis: Current Status and Challenges” Curr. Opin. Green Sustain. Chem., 47, 100932, 2024.

[21] Ulleberg, Ø. , “Modeling of Advanced Alkaline Electrolyzers: A System Simulation Approach” Int. J. Hydrogen Energy, 28(1), 21-33, 2003.

[22] Niroula, S. & Chaudhary, C. & Subedi, A. & Thapa, B. S. , “Parametric Modelling and Optimization of Alkaline Electrolyzer for the Production of Green Hydrogen” IOP Conf. Ser. Mater. Sci. Eng., 1279 (1), 012005, 2023.

[23] Rodríguez, J. & Palmas, S. & Sánchez-Molina, M. & Amores, E. & Mais, L. & & Campana, R. , “Simple and Precise Approach for Determination of Ohmic Contribution of Diaphragms in Alkaline Water Electrolysis” Membranes, 9(10), 129, 2019.

[24] Haug, P. & Kreitz, B. & Koj, M. & Turek, T. , “Process Modelling of an Alkaline Water Electrolyzer” Int. J. Hydrogen Energy, 42 (24), 15689–15707, 2017.

[25] Sánchez, M. & Amores, E. & Rodríguez, L. & Clemente-Jul, C. , “Semi-Empirical Model and Experimental Validation for the Performance Evaluation of a 15 KW Alkaline Water Electrolyzer” Int. J. Hydrogen Energy, 43 (45), 20332–20345, 2018.

[26] Sánchez, M. & Amores, E. & Abad, D. & Rodríguez, L. & Clemente-Jul, C. , “Aspen Plus Model of an Alkaline Electrolysis System for Hydrogen Production” Int. J. Hydrogen Energy, 45 (7), 3916–29, 2020.

[27] Brauns, J. & Turek, T. , “Alkaline Water Electrolysis Powered by Renewable Energy: A Review” Processes, 8(2), 248, 2020.

[28] Zeng, K. & Zhang, D. , “Recent Progress in Alkaline Water Electrolysis for Hydrogen Production and Applications” Prog. Energy Combust. Sci., 36 (3), 307-326, 2010.

[29] Rodríguez, J. & Amores, E. , “CFD Modeling and Experimental Validation of an Alkaline Water Electrolysis Cell for Hydrogen Production” Processes, 8 (12), 1–17, 2020.

[30] Gandía, L. M. & Arzamendi, G. & & Diéguez, P. M. , “Renewable Hydrogen Energy: An Overview” Renew. Hydrog. Technol. Prod. Purification, Storage, Appl. Saf., 1–17, 2013.

[31] Kelly, N. A. , “Hydrogen Production by Water Electrolysis” Adv. Hydrog. Prod. Storage Distrib., 159–185, 2014.

[32] Rashad, A. & Elmaihy, A. , “Theoretical and Experimental Performance of Oxy-Hydrogen Generators” Arab. J. Sci. Eng., 43 (3), 1279–1289, 2018.

[33] Millet, P. & Grigoriev, S. , “Water Electrolysis Technologies” Renew. Hydrog. Technol. Prod. Purification, Storage, Appl. Saf., 19–41, 2013.

[34] Smolinka, T. & Bergmann, H. & Garche, J. & Kusnezoff, M. , “The History of Water Electrolysis from Its Beginnings to the Present” Electrochemical Power Sources: Fundamentals, Systems, and Applications; Elsevier, 83-164, 2021.

[35] Hug, W. & Bussmann, H. & & Brinner, A. , “Intermittent Operation And Operation Modeling Of An Alkaline Electrolyzer” Int. J. Hydrog. Energy, 18(12), 973-977, 1993.

[36] Hug, W. & Divisek, J. & Mergel, J. & Seeger, W. & Steeb, H. (1992). “Highly efficient advanced alkaline electrolyzer for solar operation” Int. J. Hydrog Energy, *17*(9), 699-705, 1992

[37] Ulleberg, Ø. & Morner, S. O. , “Trnsys Simulation Models For Solar-Hydrogen Systems” Solar Energy, 59(4-6), 271-279, 1997.

[38] Kothari, R. & Buddhi, D. & & Sawhney, R. L. , “Studies on the Effect of Temperature of the Electrolytes on the Rate of Production of Hydrogen” Int. J. Hydrogen Energy, 30 (3), 261–263, 2005.

[39] Roy, A. & Watson, S. & & Infield, D. , “Comparison of Electrical Energy Efficiency of Atmospheric and High-Pressure Electrolysers” Int. J. Hydrogen Energy, 31 (14), 1964–1979, 2006.

[40] Gandía, L. M. & Oroz, R. & Ursúa, A. & Sanchis, P. & & Diéguez, P. M. , “Renewable Hydrogen Production: Performance of an Alkaline Water Electrolyzer Working under Emulated Wind Conditions” Energy and Fuels, 21 (3), 1699–1706, 2007.

[41] Diéguez, P. M. & Ursúa, A. & Sanchis, P. & Sopena, C. & Guelbenzu, E. & Gandía, L. M. , “Thermal Performance of a Commercial Alkaline Water Electrolyzer: Experimental Study and Mathematical Modeling” Int. J. Hydrogen Energy, 33 (24), 7338–7354, 2008.

[42] Artuso, P. & Gammon, R. & Orecchini, F. & Watson, S. J. , “Alkaline Electrolysers: Model and Real Data Analysis” Int. J. Hydrogen Energy, 36 (13), 7956–62, 2011.

[43] Ursúa, A. & Sanchis, P. , “Static-Dynamic Modelling of the Electrical Behaviour of a Commercial Advanced Alkaline Water Electrolyser” Int. J. Hydrogen Energy, 37 (24), 18598–18614, 2012.

[44] Hammoudi, M. & Henao, C. & Agbossou, K. & Dubé, Y. & Doumbia, M. L. , “New Multi-Physics Approach for Modelling and Design of Alkaline Electrolyzers” Int. J. Hydrogen Energy, 37 (19), 13895–13913, 2012.

[45] Ursúa, A. & San Martín, I. & Barrios, E. L. & & Sanchis, P. , “Stand-Alone Operation of an Alkaline Water Electrolyser Fed by Wind and Photovoltaic Systems” Int. J. Hydrogen Energy, 38 (35), 14952–14967, 2013.

[46] Mori, M. & Mržljak, T. & Drobnič, B. & & Sekavčnik, M. , “Integral Characteristics of Hydrogen Production in Alkaline Electrolysers” Stroj. Vestnik/Journal Mech. Eng., 59 (10), 585–594, 2013.

[47] Manabe, A. & Kashiwase, M. & Hashimoto, T. & Hayashida, T. & Kato, A. & Hirao, K. & Shimomura, I. & Nagashima, I. , “Basic Study of Alkaline Water Electrolysis” Electrochim. Acta, 100, 249–256 2013.

[48] Phillips, R. & Dunnill, C. W. , “Zero Gap Alkaline Electrolysis Cell Design for Renewable Energy Storage as Hydrogen Gas” RSC Adv., 6(102), 100643-100651, 2016.

[49] Douglas, T. G. & Cruden, A. & Infield, D. , “Development of an Ambient Temperature Alkaline Electrolyser for Dynamic Operation with Renewable Energy Sources” Int. J. Hydrogen Energy, 38 (2), 723–739, 2013.

[50] Amores, E. & Rodríguez, J. & & Carreras, C. , “Influence of Operation Parameters in the Modeling of Alkaline Water Electrolyzers for Hydrogen Production” Int. J. Hydrogen Energy, 39 (25) , 13063–13078, 2014.

[51] Tijani, A. S. & Yusup, N. A. B. & & Rahim, A. H. A. , “Mathematical Modelling and Simulation Analysis of Advanced Alkaline Electrolyzer System for Hydrogen Production” Procedia Technol., 15, 798–806 2014.

[52] Zouhri, K. & Lee, S. Y. , “Evaluation and Optimization of the Alkaline Water Electrolysis Ohmic Polarization: Exergy Study” Int. J. Hydrogen Energy, 41 (18), 7253–7263, 2016.

[53] Chen, Y. & Mojica, F. & Li, G. & & Chuang, P. Y. A. , “Experimental Study and Analytical Modeling of an Alkaline Water Electrolysis Cell” Int. J. Energy Res., 41 (14), 2365–2373, 2017.

[54] Kuckshinrichs, W. & Koj, J. C. , “Levelized Cost of Energy from Private and Social Perspectives: The Case of Improved Alkaline Water Electrolysis” J. Clean. Prod., 203, 619–632, 2018.

[55] Lee, B. & Lee, H. & Cho, H. S. & Cho, W. C. & Kim, C. H. & Lim, H. , “Projected Economic Outlook and Scenario Analysis for H2 Production by Alkaline Water Electrolysis on the Basis of the Unit Electricity Price, the Learning Rate, and the Automation Level” Sustain. Energy Fuels, 3 (7), 1799–1807, 2019.

[56] Reksten, A. H. & Thomassen, M. S. & Møller-Holst, S. & Sundseth, K. , “Projecting the Future Cost of PEM and Alkaline Water Electrolysers; a CAPEX Model Including Electrolyser Plant Size and Technology Development” Int. J. Hydrogen Energy, 47 (90), 38106–38113, 2022.

[57] Zun, M. T. & McLellan, B. C. , “Cost Projection of Global Green Hydrogen Production Scenarios” Hydrog., 4 (4), 932–960, 2023.

[58] Sadiq, M. & Alshehhi, R. J. & Urs, R. R. & Mayyas, A. T. , “Techno-Economic Analysis of Green-H2@Scale Production” Renew. Energy, 219, 119362, 2023.

[59] McPhy. McLyzer range: 200 to 3200 Nm^3/h at 30 bar. Retrieved January 2, 2025, from https://mcphy.com/en/equipment-services/electrolyzers/large/. 2023, June.

[60] Sunfire-HyLink Alkaline. Sunfire-HyLink Alkaline. Retrieved January 2, 2025, from https://sunfire.de/en/products/pressurized-alkaline-electrolyzers-AWE. 2024, October.

[61] HygreenEnergy. Alkaline Electrolyzers. Retrieved January 3, 2025, from https://www.hygreenenergy.com/electrolyzers/alkaline

[62] Thyssenkrupp Nucera. Green hydrogen: Alkaline water electrolysis solutions. Retrieved January 3, 2025, from https://www.thyssenkrupp-nucera.com/green-hydrogen (October 29, 2024).

[63] Shen, M. & Bennett, N. & Ding, Y. & Scott, K. , “A Concise Model for Evaluating Water Electrolysis” Int. J. Hydrogen Energy, 36 (22), 14335–14341, 2011.

[64] See, D. M. & White, R. E. , “Temperature and Concentration Dependence of the Specific Conductivity of Concentrated Solutions of Potassium Hydroxide” Journal of Chem. & Eng. Data, 42(6), 1266-1268, 1997.

[65] Gilliam, R. J. & Graydon, J. W. & Kirk, D. W. & & Thorpe, S. J. , “A Review of Specific Conductivities of Potassium Hydroxide Solutions for Various Concentrations and Temperatures” Int. J. Hydrogen Energy, 32 (3), 359–364, 2007.

[66] Bideau, D. Le & Mandin, P. & Benbouzid, M. & Kim, M. & Sellier, M. , “Review of Necessary Thermophysical Properties and Their Sensivities with Temperature and Electrolyte Mass Fractions for Alkaline Water Electrolysis Multiphysics Modelling” Int. J. Hydrogen Energy, 44(10), 4553-4569, 2019.

[67] COMSOL. (2023). Fuel Cell & Electrolyzer Module: Alkaline Electrolyzer. COMSOL Multiphysics 6.1 Application Library. Retrieved from https://www.comsol.com/model/alkaline-electrolyzer-99281

[68] COMSOL AB. (2023). *Electrochemistry Module User's Guide* (Version 6.2). COMSOL. Retrieved from https://doc.comsol.com/6.2/doc/com.comsol.help.echem/ElectrochemistryModuleUsersGuide.pdf

APPENDICES

Appendix A – I-U Curves for Parameter Effects on Current Density

The graphs presented in this section are derived from COMSOL data. These graphs represent the results of 20 individual analyses performed to evaluate the impact of varying parameters on the system's performance. The data from these graphs have been consolidated and interpreted in the Results section to provide a comprehensive understanding of the findings.

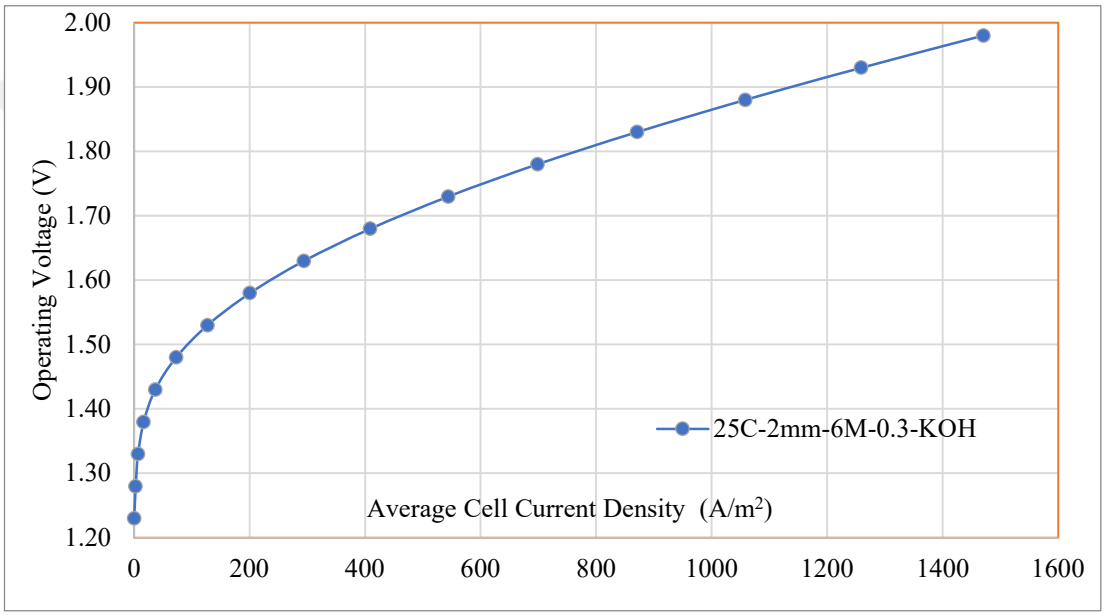

Figure A.1 I-U Curve for 25 C-2 mm-6 M-0.3 seperator porosity and KOH Solution

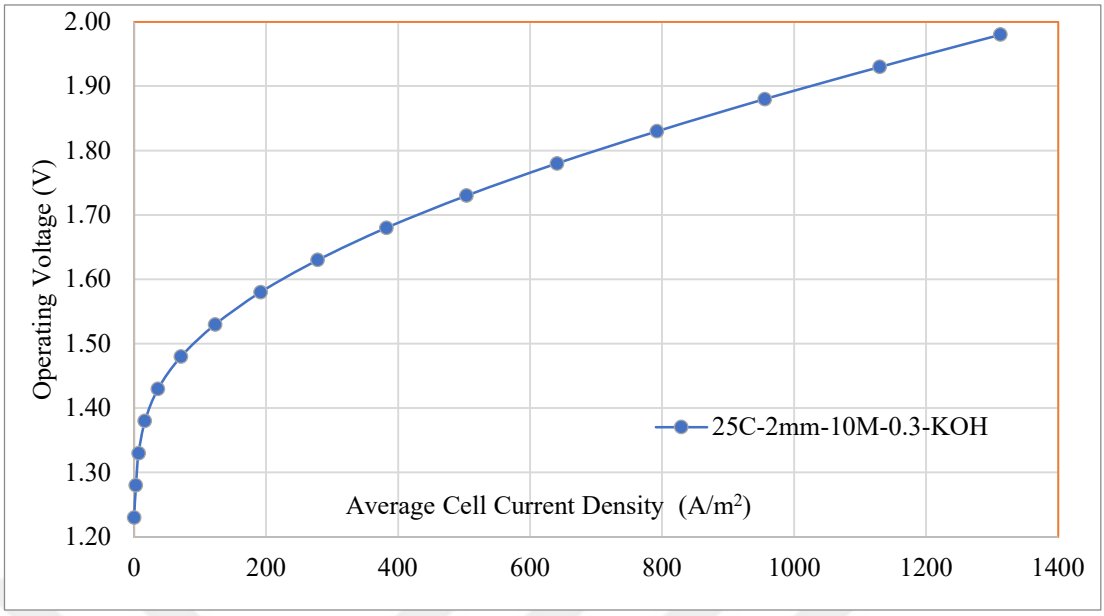

Figure A.2 I-U Curve for 25 C-2 mm-10 M-0.3 seperator porosity and KOH Solution

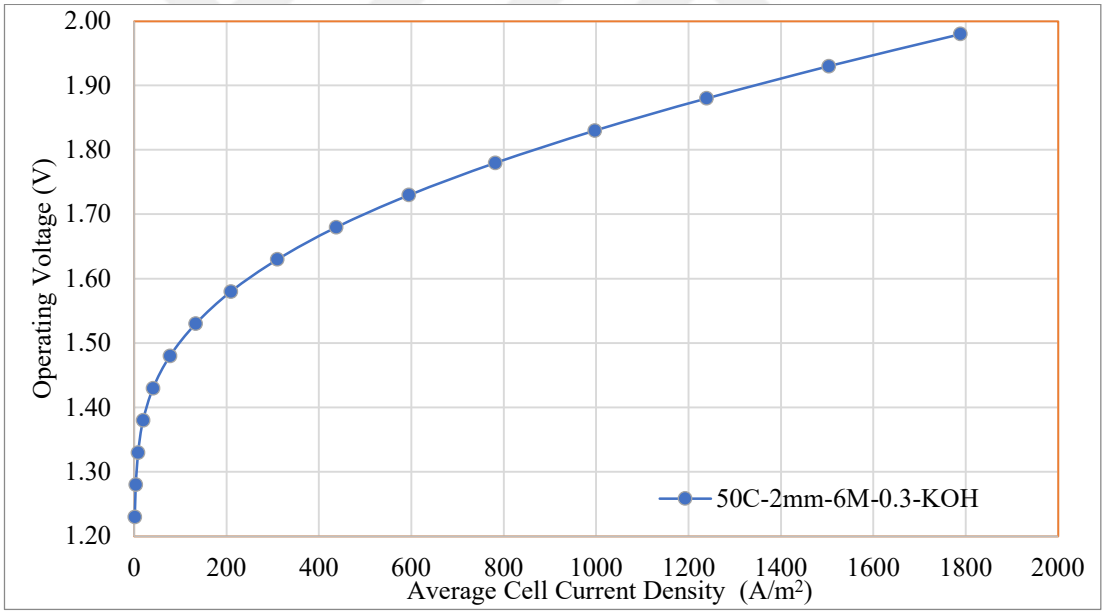

Figure A.3 I-U Curve for 50 C-2 mm-6 M-0.3 seperator porosity and KOH Solution

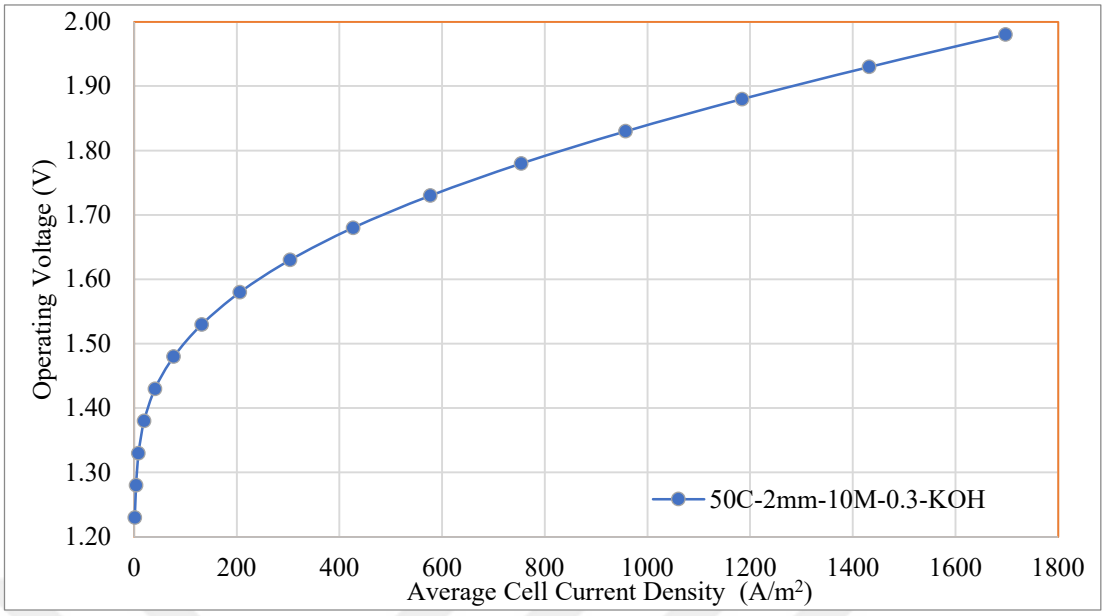

Figure A.4 I-U Curve for 50 C-2 mm-10 M-0.3 seperator porosity and KOH Solution

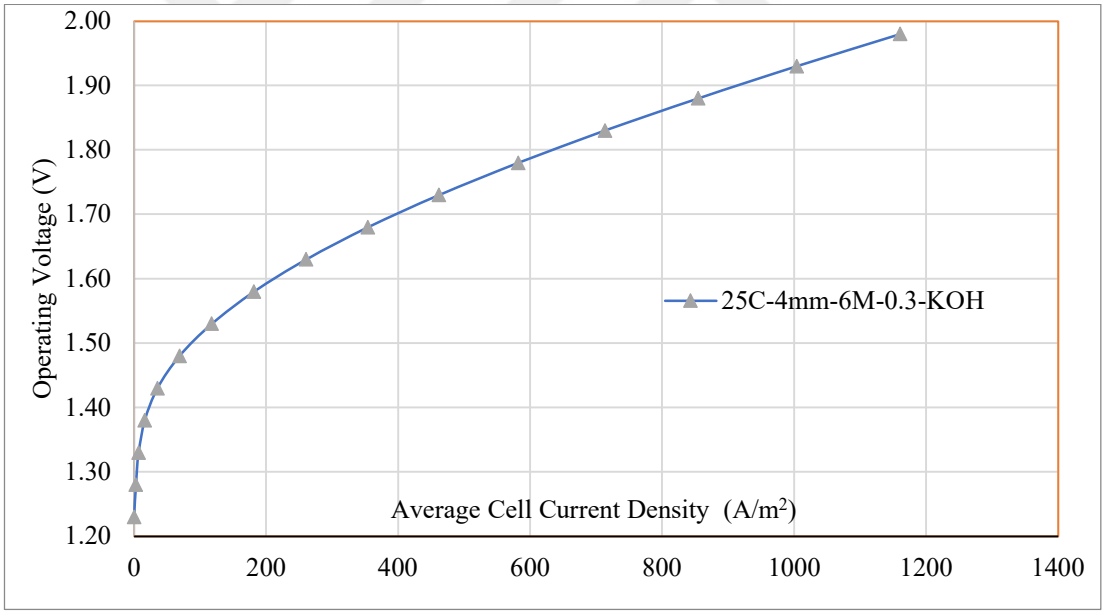

Figure A.5 I-U Curve for 25 C-4 mm-6 M-0.3 seperator porosity and KOH Solution

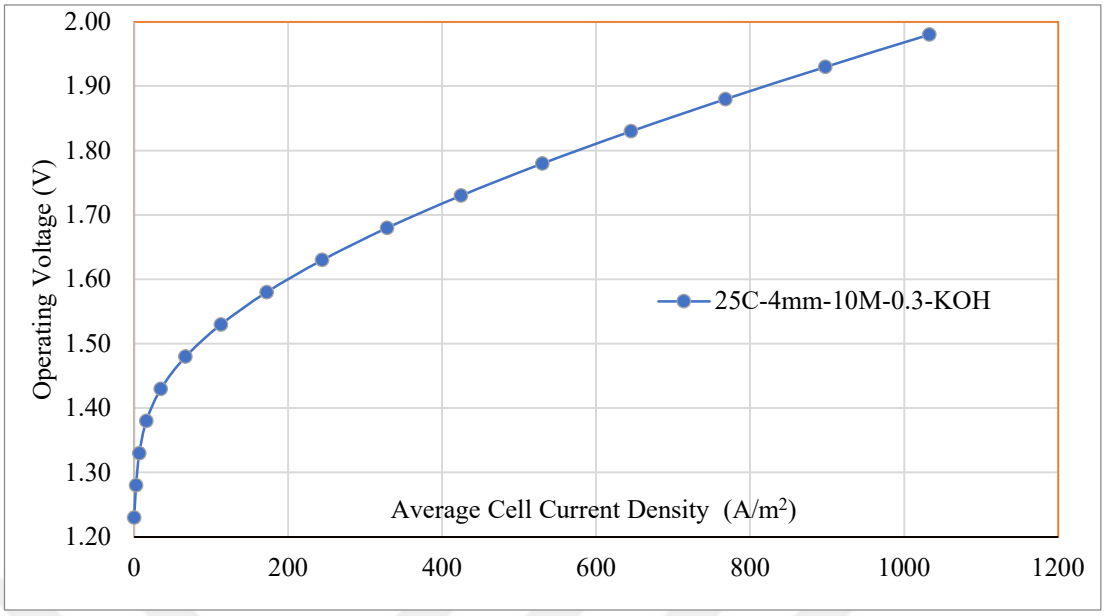

Figure A.6 I-U Curve for 25 C-4 mm-10 M-0.3 seperator porosity and KOH Solution

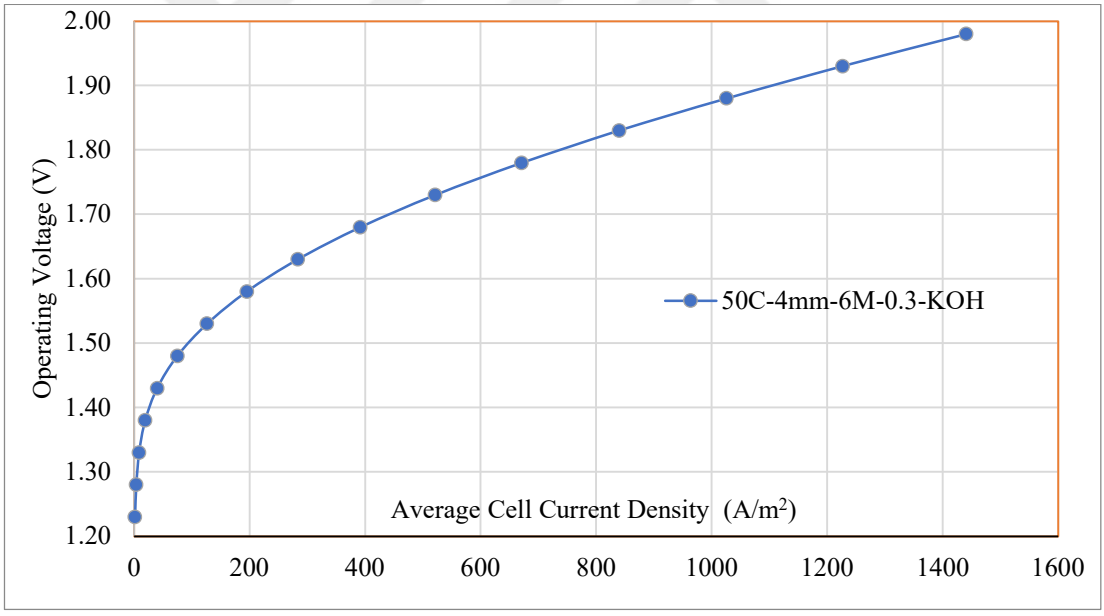

Figure A.7 I-U Curve for 50 C-4 mm-6 M-0.3 seperator porosity and KOH Solution

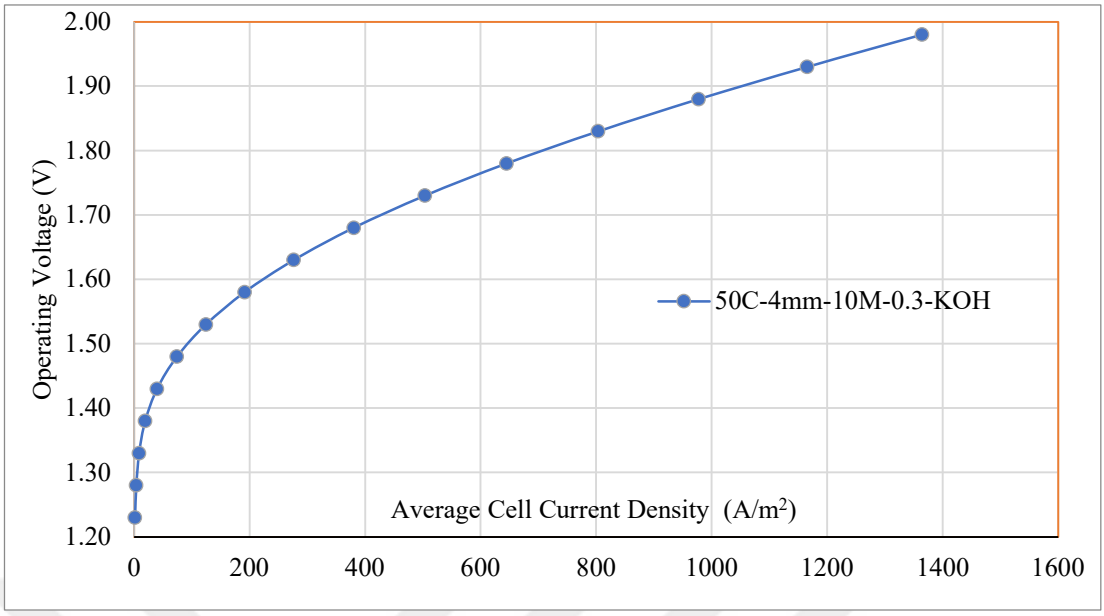

Figure A.8 I-U Curve for 50 C-4 mm-10 M-0.3 seperator porosity and KOH Solution

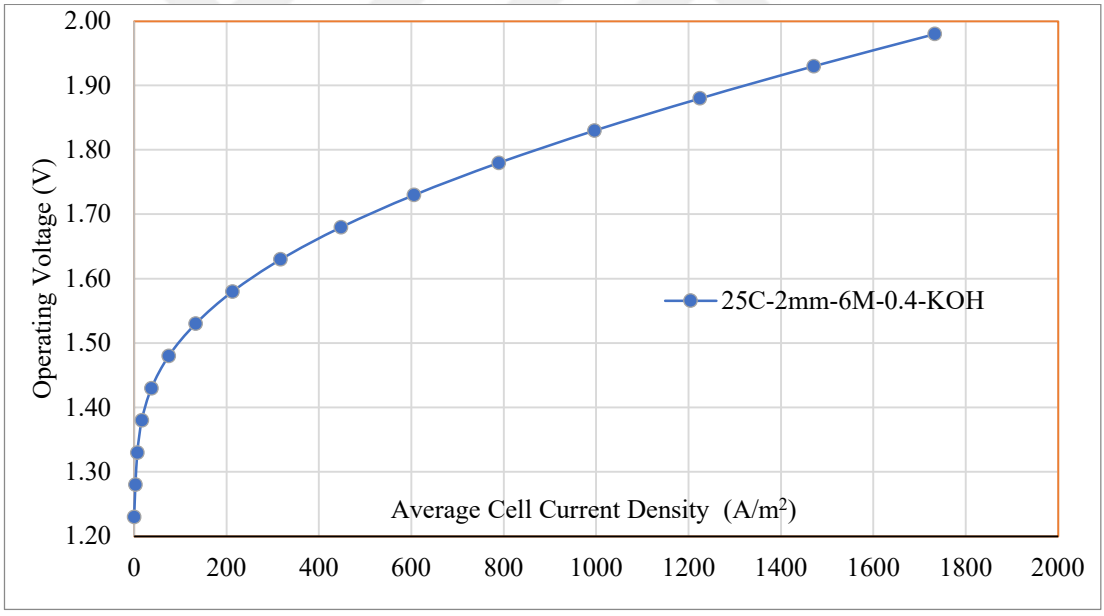

Figure A.9 I-U Curve for 25 C-2 mm-6 M-0.4 seperator porosity and KOH Solution

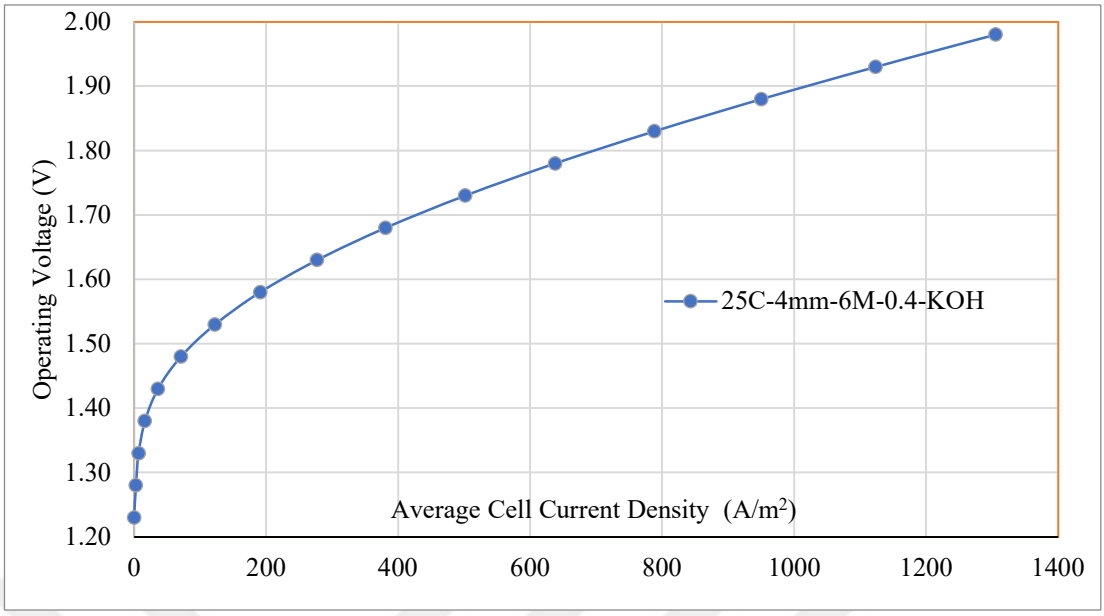

Figure A.10 I-U Curve for 25 C-4 mm-6 M-0.4 seperator porosity and KOH Solution

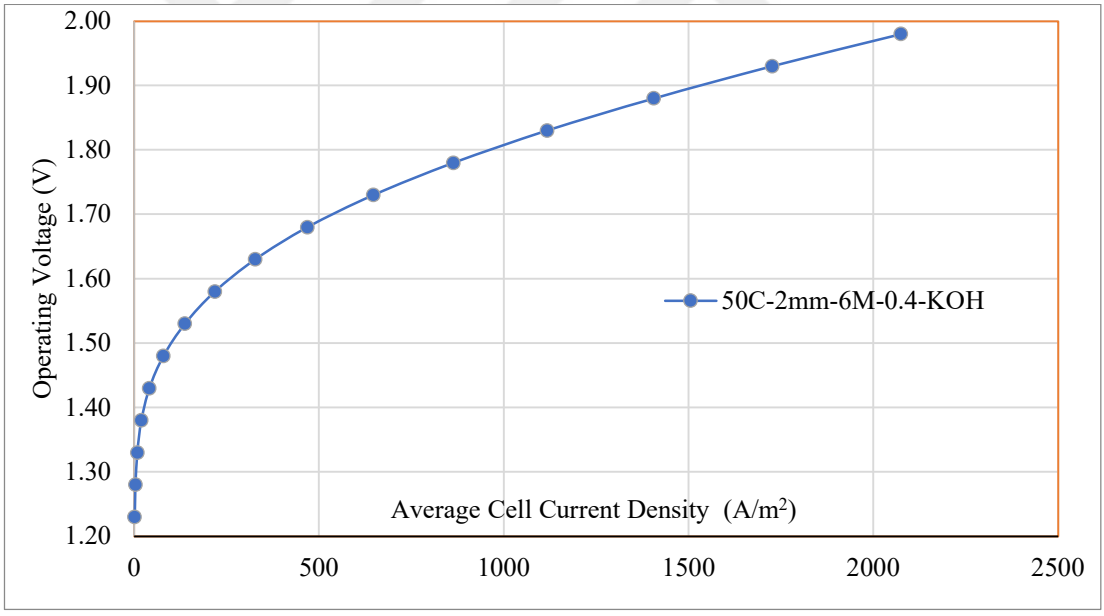

Figure A.11 I-U Curve for 50 C-2 mm-6 M-0.4 seperator porosity and KOH Solution

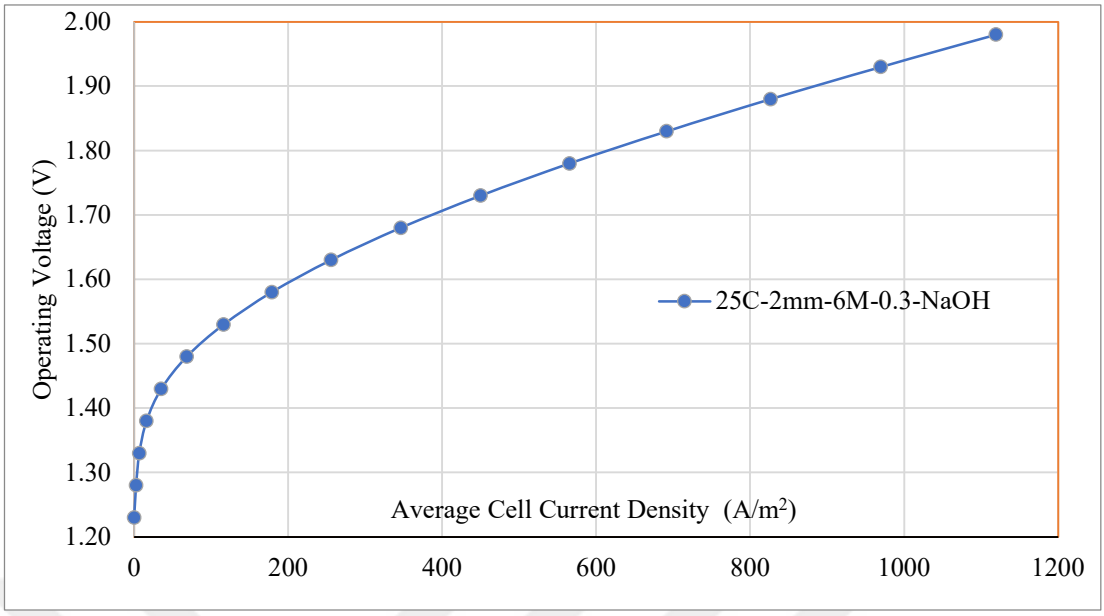

Figure A.12 I-U Curve for 25 C-2 mm-6 M-0.3 seperator porosity and NaOH Solution

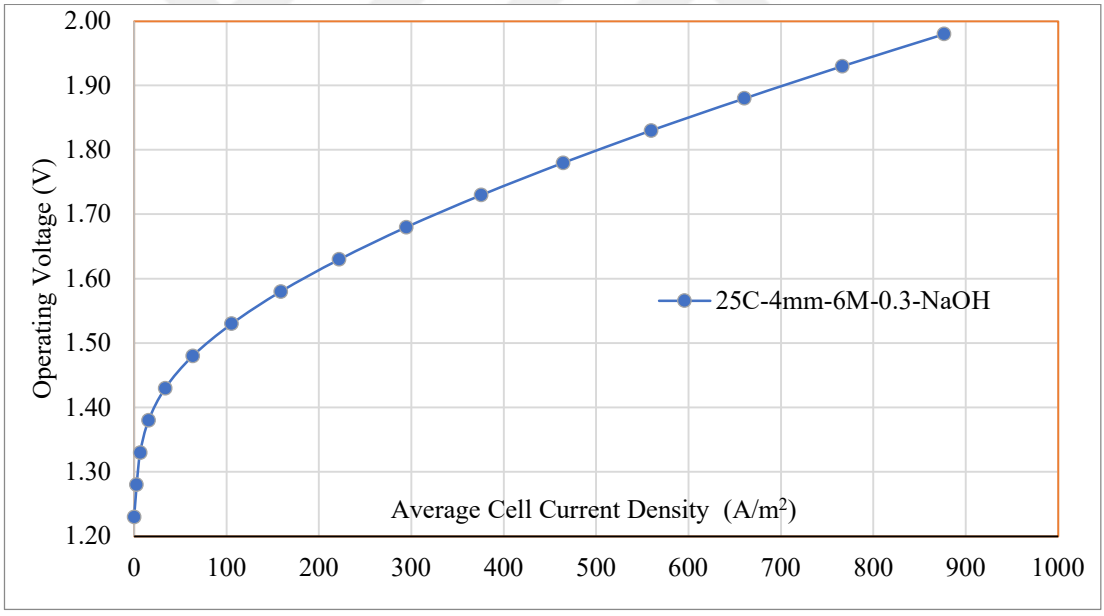

Figure A.13 I-U Curve for 25 C-4 mm-6 M-0.3 seperator porosity and NaOH Solution

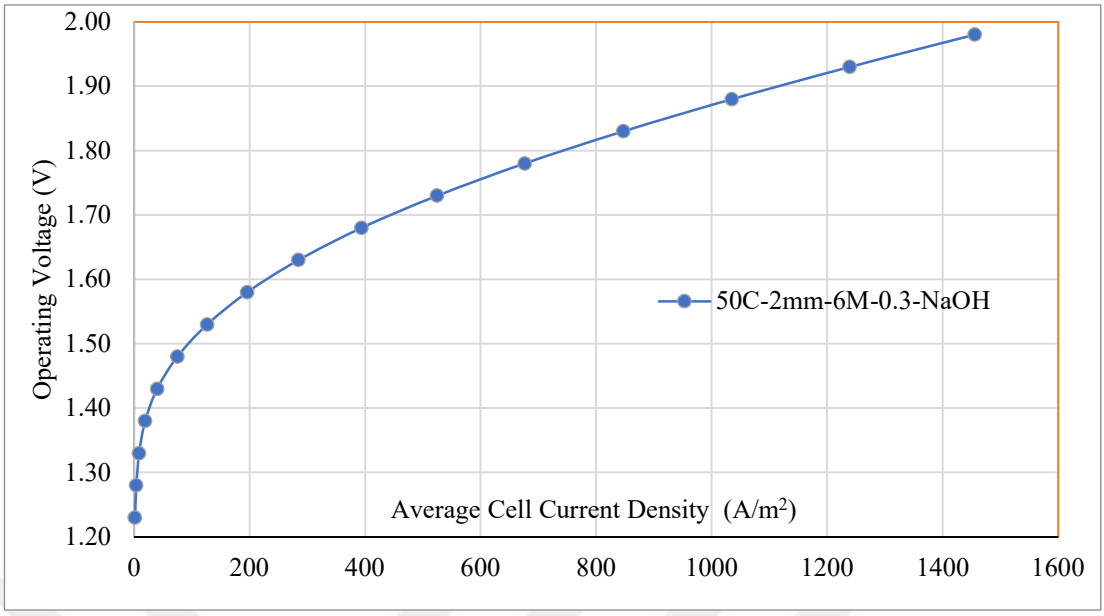

Figure A.14 I-U Curve for 50 C-2 mm-6 M-0.3 seperator porosity and NaOH Solution

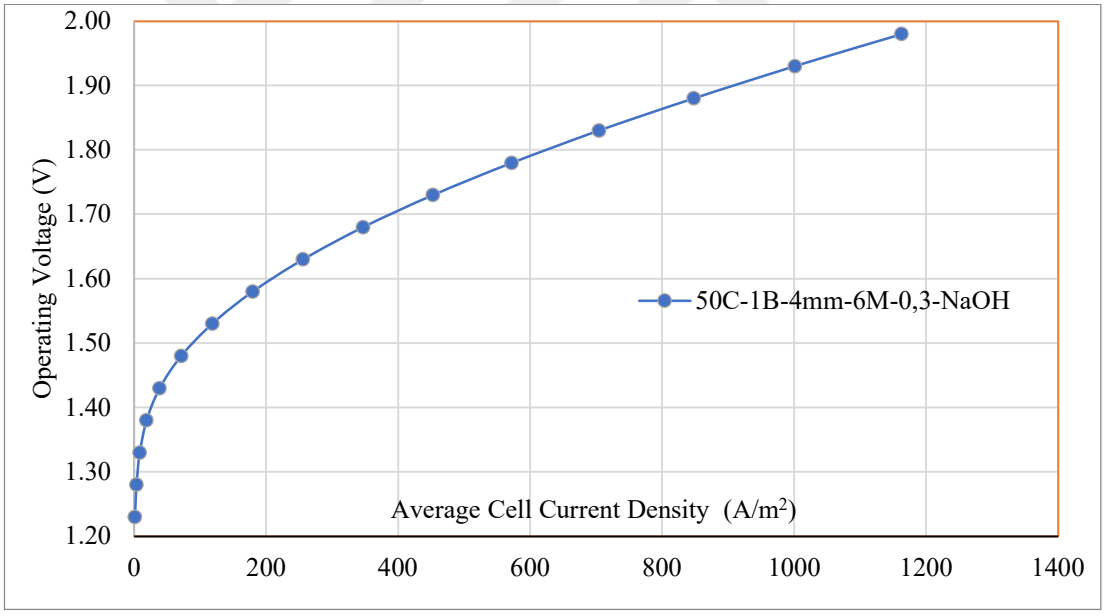

Figure A.15 I-U Curve for 50 C-4 mm-6 M-0.3 seperator porosity and NaOH Solution

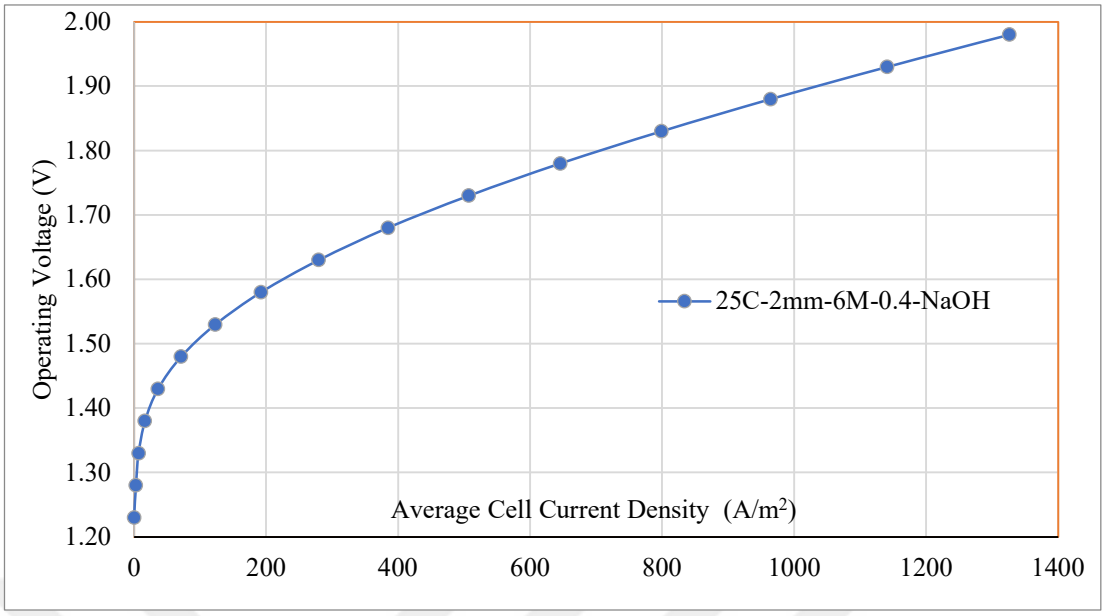

Figure A.16 I-U Curve for 25 C-2 mm-6 M-0.4 seperator porosity and NaOH Solution

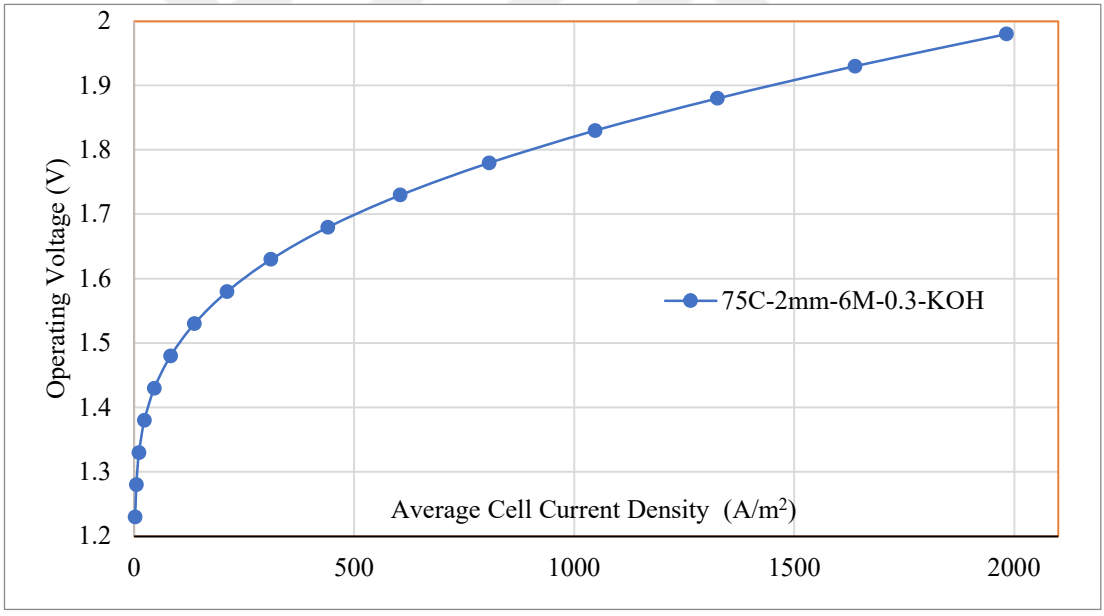

Figure A.17 I-U Curve for 75 C-2 mm-6 M-0.3 seperator porosity and KOH Solution

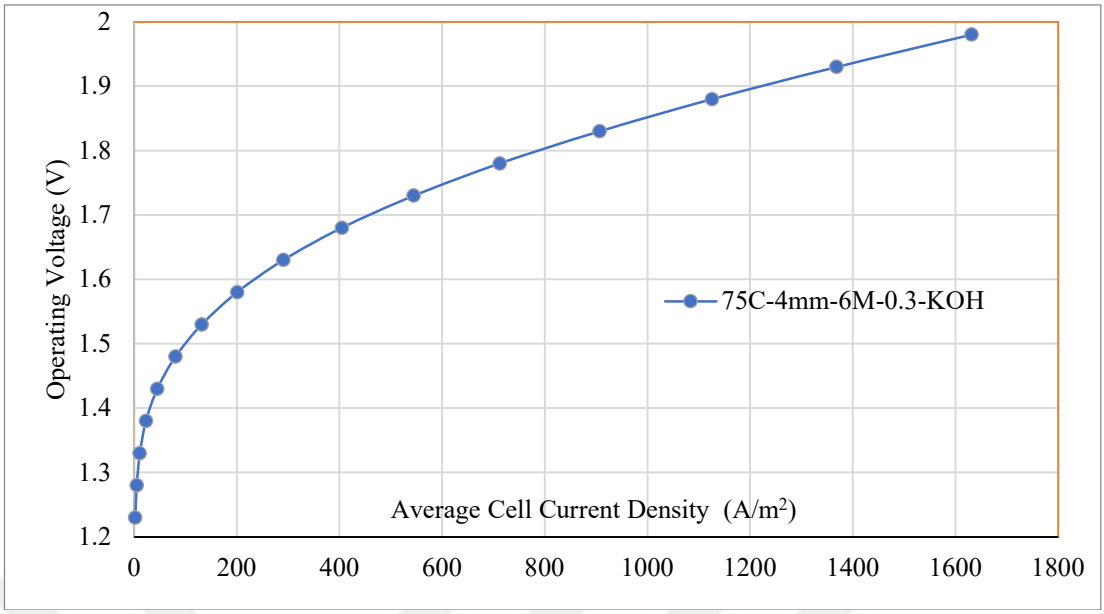

Figure A.18 I-U Curve for 75 C-4 mm-6 M-0.3 seperator porosity and KOH Solution

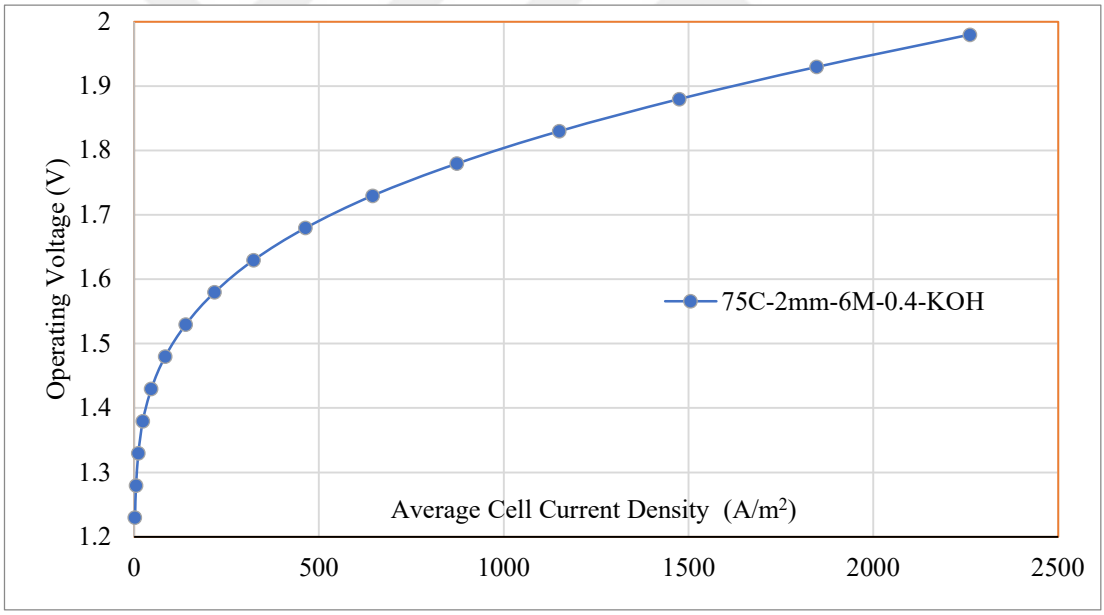

Figure A.19 I-U Curve for 75 C-2 mm-6 M-0.4 seperator porosity and KOH Solution

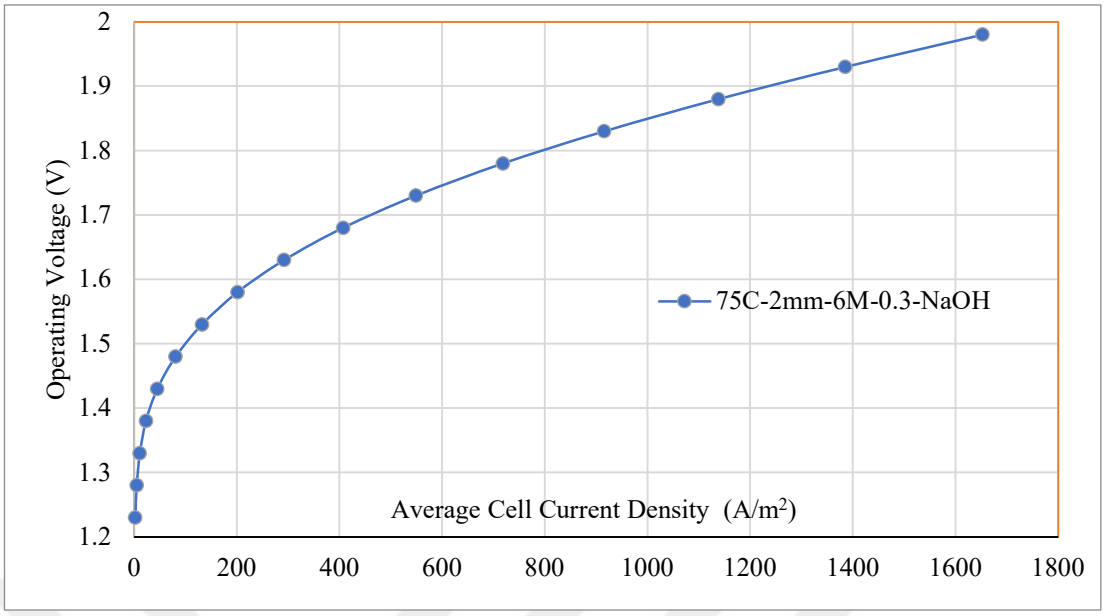

Figure A.20 I-U Curve for 75 C-2 mm-6 M-0.3 seperator porosity and NaOH Solution